

University of Windsor

Scholarship at UWindor

Electronic Theses and Dissertations

Theses, Dissertations, and Major Papers

2008

The Analysis and Control of Distortion in Carbonitrided and Nitrocarburized Plain Carbon Steels

Victoria Campagna
University of Windsor

Follow this and additional works at: <https://scholar.uwindsor.ca/etd>

Recommended Citation

Campagna, Victoria, "The Analysis and Control of Distortion in Carbonitrided and Nitrocarburized Plain Carbon Steels" (2008). *Electronic Theses and Dissertations*. 8024.
<https://scholar.uwindsor.ca/etd/8024>

This online database contains the full-text of PhD dissertations and Masters' theses of University of Windsor students from 1954 forward. These documents are made available for personal study and research purposes only, in accordance with the Canadian Copyright Act and the Creative Commons license—CC BY-NC-ND (Attribution, Non-Commercial, No Derivative Works). Under this license, works must always be attributed to the copyright holder (original author), cannot be used for any commercial purposes, and may not be altered. Any other use would require the permission of the copyright holder. Students may inquire about withdrawing their dissertation and/or thesis from this database. For additional inquiries, please contact the repository administrator via email (scholarship@uwindsor.ca) or by telephone at 519-253-3000ext. 3208.

**The Analysis and Control of Distortion in Carbonitrided and Nitrocarburized
Plain Carbon Steels**

by
Victoria Campagna

A Thesis
Submitted to the Faculty of Graduate Studies
through Materials Engineering
in Partial Fulfillment of the Requirements for
the Degree of Master of Applied Science at the
University of Windsor

Windsor, Ontario, Canada

2008

© 2008 Victoria Campagna



Library and
Archives Canada

Bibliothèque et
Archives Canada

Published Heritage
Branch

Direction du
Patrimoine de l'édition

395 Wellington Street
Ottawa ON K1A 0N4
Canada

395, rue Wellington
Ottawa ON K1A 0N4
Canada

Your file *Votre référence*
ISBN: 978-0-494-47074-9
Our file *Notre référence*
ISBN: 978-0-494-47074-9

NOTICE:

The author has granted a non-exclusive license allowing Library and Archives Canada to reproduce, publish, archive, preserve, conserve, communicate to the public by telecommunication or on the Internet, loan, distribute and sell theses worldwide, for commercial or non-commercial purposes, in microform, paper, electronic and/or any other formats.

The author retains copyright ownership and moral rights in this thesis. Neither the thesis nor substantial extracts from it may be printed or otherwise reproduced without the author's permission.

AVIS:

L'auteur a accordé une licence non exclusive permettant à la Bibliothèque et Archives Canada de reproduire, publier, archiver, sauvegarder, conserver, transmettre au public par télécommunication ou par l'Internet, prêter, distribuer et vendre des thèses partout dans le monde, à des fins commerciales ou autres, sur support microforme, papier, électronique et/ou autres formats.

L'auteur conserve la propriété du droit d'auteur et des droits moraux qui protègent cette thèse. Ni la thèse ni des extraits substantiels de celle-ci ne doivent être imprimés ou autrement reproduits sans son autorisation.

In compliance with the Canadian Privacy Act some supporting forms may have been removed from this thesis.

Conformément à la loi canadienne sur la protection de la vie privée, quelques formulaires secondaires ont été enlevés de cette thèse.

While these forms may be included in the document page count, their removal does not represent any loss of content from the thesis.

Bien que ces formulaires aient inclus dans la pagination, il n'y aura aucun contenu manquant.

■ ■ ■
Canada

The Analysis and Control of Distortion in Carbonitrided and Nitrocarburized
Plain Carbon Steels

by

Victoria Campagna

APPROVED BY:

Dr. S. Holger Eichorn
Department of Chemistry and Biochemistry

Dr. X. Nie
Department of Mechanical, Automotive, & Materials Engineering

Dr. D.O. Northwood, Co-Advisor
Department of Mechanical, Automotive, & Materials Engineering

Dr. R.J. Bowers, Co-Advisor
Department of Mechanical, Automotive, & Materials Engineering

Dr. H. Hu, Chair of Defense
Department of Mechanical, Automotive, & Materials Engineering

8 October 2008

CO-AUTHORSHIP DECLARATION

I hereby declare that this thesis incorporates material that is the result of a joint research undertaken in collaboration with Dr. Xichen Sun and Peter Bauerle from the Chassis and Powertrain Materials Engineering Department of Chrysler LLC under the supervision of professors Derek O. Northwood and Randy J. Bowers. The research collaboration is covered in Chapters 4, 5, and 6 of the thesis. In all cases, the key ideas, primary contributions, experimental designs, data analysis and interpretation, were performed by the author, and the contributions of the co-authors was in the capacity of supervision of the research in the form of technical advice and suggestions.

I am aware of the University of Windsor Senate Policy on Authorship and I certify that I have properly acknowledged the contributions of other researchers to my thesis, and have obtained permission from each of the co-authors to include the above materials in my thesis.

I certify that, with the above qualification, this thesis, and the research to which it refers, is the product of my own work.

DECLARATION OF PREVIOUS PUBLICATIONS

This thesis includes four original papers that have been previously published/submitted for publication in peer reviewed journals, as follows:

1. V. Campagna, R. Bowers, D.O. Northwood, X. Sun, and P. Bauerle, The Nitrocarburizing of Plain Carbon Steel Automotive Components, Proceedings of the 24th ASM Heat Treating Society Conference, 17-19 September 2007, COBO Center, Detroit, MI, U.S.A., ASM International, Materials Park, Ohio U.S.A., 2007, pp. 239-244.
2. V. Campagna, R. Bowers, D.O. Northwood, X. Sun, and P. Bauerle, Distortion and Residual Stresses in Nitrocarburized and Carbonitrided SAE 1010 Plain Carbon Steel, SP 2192: Experiments in Automotive Engineering, Paper No. 2008-01-1421, SAE International, Warrendale, Pennsylvania U.S.A., 2008, pp. 69-75.
3. V. Campagna, R. Bowers, D.O. Northwood, X. Sun, and P. Bauerle, A Comparison of Carbonitriding and Nitrocarburising on the Size and Shape Distortion of Plain Carbon SAE 1010 Steel. Submitted on 31 October 2007 for publication in Materials Forum.
4. V. Campagna, D.O. Northwood, R. Bowers, X. Sun, and P. Bauerle, The Analysis and Control of Distortion in Carbonitrided and Nitrocarburized Thin-Shelled Plain Carbon Steel Automotive Powertrain Components. Submitted on 24 April 2008 for publication in the Journal of ASTM International.

I certify that I have obtained permission from the copyright owners to include the above published materials in my thesis. I certify that the above material describes work completed during my registration as a graduate student at the University of Windsor.

I declare that, to the best my knowledge, my thesis does not infringe upon anyone's copyright nor violate any proprietary rights and that any ideas, techniques, quotations, or any other material from the work of other people included in my thesis, published or otherwise, are fully acknowledged in accordance with the standard referencing practices. Furthermore, to the extent that I have included copyrighted material that surpasses the bounds of fair dealing within the meaning of the Canada Copyright Act, I certify that I have obtained permission from the copyright owners to include such materials in my thesis.

I declare that this is a true copy of my thesis, including any final revisions, as approved by my thesis committee and the Graduate Studies office, and that this thesis has not been submitted for a higher degree to any other University or Institution.

ABSTRACT

The main objective of this study was to compare the carbonitriding and gaseous ferritic nitrocarburizing processes. The driving force behind this research was to be able to use these results to determine the potential of ferritic nitrocarburizing as a suitable replacement to the carbonitriding process currently being used to impart a hard, wear resistant case on the surface of SAE 1010 steel torque converter pistons.

The carbonitriding and ferritic nitrocarburizing processes were evaluated with respect to physical, mechanical, and metallurgical properties. The processes were compared quantitatively using distortion, retained austenite, and residual stress values, and qualitatively through optical and scanning electron microscopy. All test specimens were machined from low carbon steel and heat treated according to specified schedules. While the carbonitrided conditions were similar to those of the current production schedule, conditions for the nitrocarburized test specimens incorporated a range of processing times and temperatures.

The results from this study support the use of gaseous ferritic nitrocarburizing as a means of reducing size and shape distortion in the torque converter pistons. Not only were distortion values lower after heat treatment, but the lack of retained austenite within the steel decreases the likelihood of further distortion associated with the delayed transformation of austenite to martensite. Although these findings do support the use of the nitrocarburizing process, the presence of tensile stresses measured at the surface of the pistons warrant the need for additional wear testing. Until such tests are performed, a change in process to gaseous ferritic nitrocarburizing cannot be endorsed.

To my very first editor,

My Mother

ACKNOWLEDGEMENTS

First and foremost, I would like to extend my most sincere thanks to my advisors Dr. Derek O. Northwood and Dr. Randy J. Bowers. It is through their example that I have learned many invaluable research and workplace skills. Their enthusiasm has made the last two years a truly enjoyable learning experience.

I would also like to extend my thanks to Dr. Xichen Sun and Peter Bauerle from Chrysler LLC, who provided technical suggestions and support throughout this project,. Dr. Sun was instrumental in coordinating the tests performed at the Chrysler Technology Center, Woodworth, Inc., and Proto Manufacturing Ltd. The laboratory assistance of Mr. J. Robinson is also much appreciated.

This research project would not have been possible if not for the significant contributions and financial support provided by the Chassis and Powertrain Materials Engineering Department of Chrysler LLC, Woodworth, Inc., the Natural Sciences and Engineering Research Council of Canada (NSERC), and the Ontario Graduate Scholarship Program (OGS).

TABLE OF CONTENTS

CO-AUTHORSHIP DECLARATION.....	III
DECLARATION OF PREVIOUS PUBLICATIONS.....	III
ABSTRACT.....	IV
DEDICATION.....	V
ACKNOWLEDGEMENTS.....	VI
LIST OF TABLES.....	X
LIST OF FIGURES.....	XII
LIST OF ABBREVIATIONS.....	XVII
I. INTRODUCTION.....	1
II. LITERATURE REVIEW.....	3
2.1 AUTOMOTIVE TORQUE CONVERTER PISTONS.....	3
2.1.1 FUNCTION.....	3
2.1.2 FABRICATION.....	3
2.1.3 LOW CARBON STEEL AND THE IMPORTANCE OF SURFACE HEAT TREATMENT.....	7
2.2 SURFACE HARDENING OF STEEL.....	7
2.2.1 CARBONITRIDING.....	7
2.2.2 GASEOUS FERRITIC NITROCARBURIZING.....	9
<i>Formation of the Compound Layer.....</i>	<i>10</i>
<i>Braunite.....</i>	<i>10</i>
<i>Distortion in Nitrocarburized Steel.....</i>	<i>12</i>
2.3 DISTORTION.....	12
2.3.1 SIZE DISTORTION.....	13
2.3.2 SHAPE DISTORTION.....	14
2.3.3 ISSUES WITH DISTORTION IN MANUFACTURING.....	15
2.3.4 CORRECTING DISTORTION THROUGH METAL GRINDING.....	15
2.3.5 MEASUREMENT OF DISTORTION.....	16
2.4 RETAINED AUSTENITE.....	18
2.4.1. EFFECTS OF RETAINED AUSTENITE.....	20
<i>Positive Attributes of Retained Austenite [40].....</i>	<i>20</i>
<i>Negative Attributes of Retained Austenite [2, 17, 40, 44].....</i>	<i>20</i>
2.4.2 MINIMIZING RETAINED AUSTENITE.....	20
<i>Cryogenic Treatments.....</i>	<i>20</i>
<i>Reducing Retained Austenite in Carbonitrided Steels.....</i>	<i>21</i>
2.4.3 MEASUREMENT OF RETAINED AUSTENITE USING X-RAY DIFFRACTION.....	22
2.5 RESIDUAL STRESS.....	24
<i>Thermal Stresses.....</i>	<i>24</i>
<i>Transformation Stresses.....</i>	<i>25</i>
2.5.1 RESIDUAL STRESSES IN SURFACE HARDENED STEELS.....	25
<i>Residual Stresses in Carbonitrided Steels.....</i>	<i>25</i>
<i>Residual Stresses in Nitrocarburized Steels.....</i>	<i>26</i>
2.5.2 MEASUREMENT OF RESIDUAL STRESSES.....	26
III. EXPERIMENTAL DETAILS.....	30
3.1 OVERVIEW.....	30
3.2 TEST SPECIMENS.....	31
<i>Navy C-rings.....</i>	<i>31</i>
<i>Torque Converter Pistons.....</i>	<i>31</i>

3.3 HEAT TREATMENT DETAILS	33
<i>Navy C-rings</i>	33
<i>Torque Converter Pistons</i>	34
3.4 DIMENSIONAL MEASUREMENTS AND CALCULATION OF DISTORTION	35
<i>Navy C-rings</i>	35
<i>Torque Converter Pistons</i>	40
3.5 RETAINED AUSTENITE MEASUREMENT	43
<i>Navy C-rings</i>	43
<i>Torque Converter Pistons</i>	44
3.6 RESIDUAL STRESS MEASUREMENT.....	44
<i>Navy C-rings</i>	44
<i>Torque Converter Pistons</i>	45
3.7 DETERMINATION OF SURFACE GROWTH DIRECTION IN NITROCARBURIZED SAE 1010 STEEL	45
3.8 METALLOGRAPHIC PROCEDURE	46
<i>Navy C-rings</i>	47
<i>Torque Converter Pistons</i>	47
<i>Coupons</i>	47
IV. EFFECT OF HEAT TREATMENT ON SIZE AND SHAPE DISTORTIONS	48
4.1 NAVY C-RINGS	48
<i>Size Distortion</i>	48
<i>Shape Distortion</i>	53
4.2 TORQUE CONVERTER PISTONS	55
<i>Size Distortion</i>	56
<i>Shape Distortion</i>	59
4.3 HYPOTHESIS TESTING OF SIZE AND SHAPE DISTORTION	63
4.4 UNDERSTANDING SIZE AND SHAPE DISTORTION	63
V. EFFECT OF HEAT TREATMENT ON RETAINED AUSTENITE AND RESIDUAL STRESS .65	
5.1 RETAINED AUSTENITE.....	65
5.1.1 NAVY C-RINGS	65
5.1.2 TORQUE CONVERTER PISTONS	67
5.1.3 UNDERSTANDING THE PRESENCE OF RETAINED AUSTENITE IN SURFACE TREATED STEELS	69
5.2 RESIDUAL STRESS	70
5.2.1 NAVY C-RINGS	71
<i>Surface Residual Stresses</i>	71
<i>Residual Stress Profiles</i>	71
5.2.2 TORQUE CONVERTER PISTONS	73
<i>Surface Residual Stresses</i>	73
<i>Residual Stress Profiles</i>	75
5.2.3 RELATIONSHIP BETWEEN RETAINED AUSTENITE CONTENT AND RESIDUAL STRESS VALUES	77
VI EFFECT OF HEAT TREATMENT ON THE CASE AND CORE MICROSTRUCTURES OF PLAIN CARBON STEEL	78
6.1 CASE AND CORE MICROGRAPHS.....	78
<i>Carbonitriding</i>	78
<i>Nitrocarburizing</i>	79
6.2 GROWTH DIRECTION IN NITROCARBURIZED STEEL.....	83
VII. CONCLUSIONS AND RECOMMENDATIONS FOR FUTURE WORK.....	85
7.1 CONCLUSIONS	85
7.2 SUMMARY OF CONCLUSIONS.....	88
7.3 RECOMMENDATIONS FOR FUTURE WORK.....	88
<i>Recommendations to Improve the Accuracy</i>	88

<i>Recommendations for Future Work</i>	89
APPENDIX A	90
NAVY C-RING SIZE DISTORTION (OD, ID, GAP WIDTH AND THICKNESS).....	90
NAVY C-RING SHAPE DISTORTION (FLATNESS, CYLINDRICITY, AND ROUNDNESS)	95
TORQUE CONVERTER PISTON SIZE DISTORTION (OD, ID)	98
TORQUE CONVERTER PISTON SHAPE DISTORTION (TOTAL FLATNESS, FLATNESS TAPER).....	102
APPENDIX B	104
SAMPLE HYPOTHESIS TEST	104
<i>Flatness Distortion (PC versus PN₅₁₀)</i>	104
REFERENCES	105
PUBLICATIONS AND PRESENTATIONS	112
PUBLICATIONS.....	112
PRESENTATIONS	112
VITA AUCTORIS	114

LIST OF TABLES

Chapter 2

Table 2.1 Size changes associated with microstructural changes in carbon steels from austenite to martensite [17].....	13
--	----

Chapter 3

Table 3.1 Chemical composition of AISI 1019/1021 steel.....	31
---	----

Table 3.2 Nominal chemical composition of AISI 1010 steel [12].....	32
---	----

Table 3.3 Specimen identification and heat treatment details for the Navy C-rings and torque converter pistons.....	34
---	----

Chapter 4

Table 4.1 Average size distortion values (diameter, gap width, and thickness) for the Navy C-ring specimens resulting from the carbonitriding and nitrocarburizing processes. See Appendix A for full results.	50
---	----

Table 4.2 Average shape distortion values (flatness, cylindricity, and roundness) for the Navy C-ring specimens resulting from the carbonitriding and nitrocarburizing processes. See Appendix A for full results.	53
---	----

Table 4.3a Average size distortion values (OD and ID) of the torque converter pistons resulting from the carbonitriding and nitrocarburizing processes. Sample sizes for the carbonitrided and nitrocarburized pistons are three and ten, respectively. See Appendix A for full results.....	57
--	----

Table 4.3b Average size distortion values (OD and ID) of the torque converter pistons resulting from the carbonitriding and nitrocarburizing processes. Sample sizes for the carbonitrided and nitrocarburized pistons are equal.	57
--	----

Table 4.4a Average shape distortion values (total flatness and taper) of the torque converter pistons induced by carbonitriding and nitrocarburizing. Sample sizes for the carbonitrided and nitrocarburized pistons are three and ten, respectively. See Appendix A for full results.....	60
--	----

Table 4.4b Average shape distortion values (total flatness and taper) of the torque converter pistons induced by carbonitriding and nitrocarburizing. Sample sizes for the carbonitrided and nitrocarburized pistons are equal.	60
--	----

Chapter 5

Table 5.1 Retained austenite content in the Navy C-ring specimens. Measurements were made at the 'bottom' position of the C-ring inward through the case to a depth of approximately 1.5 mm. Error in the results: $\pm 2\%$	66
Table 5.2 Retained austenite content in the torque converter pistons. Measurements were made from the lockup surface inward through the case to a depth of approx. 1.5 mm....	68
Table 5.3 Surface residual stress values for the Navy C-rings and torque converter pistons.	71
Table 5.4 Residual stresses measurements for the Navy C-ring specimens. Measurements were made from the 'bottom' position of the C-ring inward through the case to a depth of approximately 2.5 mm. (a) NCR-C10 (b) NCR-N2.	72
Table 5.5 Surface residual stress values for the torque converter pistons from group PN ₅₁₀	74
Table 5.6 Residual stress values for the torque converter pistons. Measurements were made from the lockup surface inward through the case to a depth of approximately 2 mm.	75

LIST OF FIGURES

Chapter 2

- Figure 2.1 Top view of the torque converter piston and spring retainer ring. (a) Torque converter piston; nominal OD of 261.3 mm; (b) spring retainer ring..... 4
- Figure 2.2 Schematic diagram of an automotive transmission highlighting the major components of the torque converter assembly including the stator, impeller, turbine, spring retainer ring, and torque converter piston. *Courtesy of Chrysler LLC, Auburn Hills, Michigan U.S.A.*..... 4
- Figure 2.3 Five stage stamping operation of a torque converter piston. (a) Piston blank, (b) piston at stamping stage 1, (c) at stamping stage 2, (d) at stamping stage 3, (e) at stamping stage 4, and (f) at stamping stage 5..... 5
- Figure 2.4 Torque converter piston assembly (left) showing the attachment of the piston and spring retainer ring using rivets (right). 6
- Figure 2.5 Comparison between the carbonitriding and nitrocarburizing processes [18]. . 9
- Figure 2.6 Braunitite (St 37, nitrided at 640 °C for 16 h) [22]. 11
- Figure 2.7 Size and shape distortion in hardening [26]. 14
- Figure 2.8 Schematic of material ground from a distorted gear tooth after case hardening treatment [9, 32]. 15
- Figure 2.9 Grind burn on the lockup surface of a carbonitrided torque converter piston. Defect can be detected visually (left) and through use of a coordinate measuring machine (CMM) flatness scan of the surface (right). 16
- Figure 2.10 Navy C-rings. (a) Example of a Navy C-ring test specimen used in a quench distortion study. (b) Modified Navy C-ring distortion test specimen [9, 39]. 17
- Figure 2.11 Retained austenite in quenched Fe-C alloys at room temperature as function of carbon content [4]. 19
- Figure 2.12 Martensitic start (Ms) and martensitic finish (Mf) temperatures versus carbon content in unalloyed steels [45]. 21
- Figure 2.13 Illustration of the Bragg relation [33, 54]. 27
- Figure 2.14 Definition of the axis and the direction of measurement [59,60]. 28

Chapter 2

Figure 3.1 Testing methodology.....	30
Figure 3.2 Navy C-ring test specimen; dimensions and measurement positions [37].....	32
Figure 3.3 Nitriding/nitrocarburizing furnace. This furnace was used in the heat treatment of the nitrocarburized Navy C-rings and torque converter pistons from groups NCR-N and PN, respectively. Furnace dimensions measure 8 ft x 8 ft x 33 ft. <i>Figure courtesy of Woodworth Inc., Detroit, Michigan U.S.A.</i>	33
Figure 3.4 PRISMO coordinate measuring machine (CMM).....	36
Figure 3.5 Example of a flatness form plot obtained using a CMM; specimen NCR-C6 after heat treatment. Points “A” and “B” are the points of maximum and minimum deviation away from surface “1-2-3-4”, respectively.	37
Figure 3.6 Example of a roundness form plot; specimen NCR-C1 after heat treatment. Plots for R-1, R-2, and R-3 are shown. Points “A” and “B” are the points of maximum deviation toward and away from circle ID-1, respectively. Points “C” and “D” are the points of maximum deviation toward and away from circle ID-2, respectively. Points “E” and “F” are the points of maximum deviation toward and away from circle ID-3, respectively. The three circles (ID-1, ID-2, and ID-3) have equal diameters, but have been scaled to avoid overlapping of the measured profiles.	38
Figure 3.7 Example of a cylindricity form plot; specimen NCR-C1 after heat treatment. Points “A” and “B” are the points of maximum deviation toward and away from the centre of three circles along the OD of the C-ring. The three circles have equal diameters, but have been scaled to avoid overlapping of the measured profiles.	39
Figure 3.8 Torque converter piston measurement positions.....	40
Figure 3.9 Example of a total flatness form plot obtained using a CMM; specimen PC-3 after heat treatment. Total flatness represents the maximum and minimum points of deviation along the lockup surface, measured at six separate diameters. Points “A” and “B” are the points of maximum and minimum deviation away from surface “1-2-3-4”, respectively.	41
Figure 3.10 Example of a flatness taper form plot obtained using a CMM; specimen PN605-1 after heat treatment. The flatness taper represents the maximum and minimum points of deviation measured along the $\pm Y$ and $\pm X$ directions of the lockup surface. Points “A” and “B” are the points of maximum and minimum deviation away from surface “1-2-3-4”, respectively.	42

Figure 3.11 Test set-up for the measurement of retained austenite and residual stresses for the (a) Navy C-ring specimens (b) Torque converter pistons.....	43
Figure 3.12 Schematic diagram of the SAE 1010 steel coupon. To prevent the formation of the compound layer, a layer of Nitrostop was applied prior to heat treatment.....	45
Figure 3.13 Metallographic observation of the microstructures was made using a scanning electron microscope (left) and light optical microscope (right).	46

Chapter 4

Figure 4.1 Average diameter (OD and ID) distortion for the Navy C-ring specimens induced by carbonitriding and nitrocarburizing.....	51
Figure 4.2 Average gap width distortion for the Navy C-ring specimens induced by carbonitriding and nitrocarburizing.	51
Figure 4.3 Average thickness distortion values for the Navy C-ring specimens induced by carbonitriding and nitrocarburizing. (a) Thickness distortion calculated by averaging all NCR-N values. (b) Thickness distortion calculated excluding NCR-N5.	52
Figure 4.4 Average change in flatness values for the carbonitrided and nitrocarburized Navy C-ring specimens.....	54
Figure 4.5 Average change in roundness values (R-1, R-2, and R-3) for the carbonitrided and nitrocarburized Navy C-ring specimens.....	54
Figure 4.6 Average change in cylindricity values for the carbonitrided and nitrocarburized Navy C-ring specimens.	55
Figure 4.7 Average diameter distortion (OD and ID) for the carbonitrided and nitrocarburized torque converter pistons. (a) Values from Table 4.3a; all nitrocarburized pistons. (b) Values from Table 4.3b; a random sampling of three pistons from each PN group.	58
Figure 4.8 Average change in total flatness values for the carbonitrided and nitrocarburized torque converter pistons. (a) Values from Table 4.4a; all nitrocarburized pistons. (b) Values from Table 4.4b; a random sampling of three pistons from each PN group.	61
Figure 4.9 The average change in flatness taper values for the carbonitrided and nitrocarburized torque converter pistons. (a) Values from Table 4.4a; all nitrocarburized pistons. (b) Values from Table 4.4b; a random sampling of three pistons from each PN group.	62

Chapter 5

- Figure 5.1 Retained austenite profiles of the carbonitrided and nitrocarburized Navy C-ring specimens, NCR-C10 and NCR-N2, respectively..... 66
- Figure 5.2a Retained austenite profiles for the carbonitrided (PC-1) and nitrocarburized torque converter pistons (PN₅₁₀-1, PN₅₆₅-3 and PN₆₀₅-2). 68
- Figure 5.2b Retained austenite profiles for the nitrocarburized torque converter pistons (PN₅₁₀-1, PN₅₆₅-3 and PN₆₀₅-2) from the surface to a depth of 0.25 mm. 69
- Figure 5.3 Residual stress profiles for the carbonitrided and nitrocarburized Navy C-ring specimens, NCR-C10 and NCR-N2, respectively. 73
- Figure 5.4 Residual stress profiles for the carbonitrided and nitrocarburized torque converter pistons from groups PC, PN₅₁₀, PN₅₆₅, and PN₆₀₅. (a) 0 - 2.25 mm 76
- Figure 5.5 Residual stress versus retained austenite for carbonitrided steel; NCR-C10. . 77

Chapter 6

- Figure 6.1 NCR-C10: SAE 1020 steel, carbonitrided 4 h at 845 °C, oil quenched, and tempered for 1 h at 165 °C. (a) Microstructure at the case. Structure is tempered martensite and retained austenite. (b) Microstructure at the core. Structure is upper bainite, fine pearlite, and Widmanstatten ferrite. 2% Nital etch..... 80
- Figure 6.2 NCR-N2: SAE 1020 steel, nitrocarburized 8 h at 565 °C, furnace cooled using nitrogen to 370 °C, and air cooled to room temperature. (a) Microstructure at the case. Structure is a white layer of epsilon (ϵ) iron carbonitride and an underlying diffusion zone containing Fe₄N. (b) Microstructure at the core. Structure is α -ferrite and pearlite. 2% Nital etch..... 80
- Figure 6.3 PC-1: SAE 1010 steel, carbonitrided 90 min at 870 °C, oil quenched, and tempered. Structure is tempered martensite and retained austenite. 2% Nital etch..... 81
- Figure 6.4 Nitrocarburized steel, furnace-cooled using nitrogen to 370 °C, and air cooled to room temperature. a) PN₅₁₀-8: SAE 1010 steel, nitrocarburized 14 h at 510 °C, b) PN₅₄₀-7: SAE 1010 steel, nitrocarburized 10 h at 540 °C, c) PN₅₆₅-7: SAE 1010 steel, nitrocarburized 5 h at 565°C, and d) PN₅₉₅-1: SAE 1010 steel, nitrocarburized 2.5 h at 595°C. Structure is a white layer of epsilon (ϵ) iron carbonitride and an underlying diffusion zone containing Fe₄N. 2% Nital etch. 81
- Figure 6.5 PN₆₀₅-1: SAE 1010 steel, nitrocarburized 2 h at 605 °C, furnace-cooled using nitrogen to 370°C, and air cooled to room temperature. 2% Nital etch..... 82

Figure 6.6 Braunite (SAE 1010 steel, nitrocarburized at 605 °C for 2 h, furnace cooled using nitrogen to 370°C, and air cooled to room temperature). a) SEM micrograph PN₆₀₅₋₁ showing the compound layer, Braunite, and only a small amount of gamma prime (γ') nitride. b) SEM micrograph of the Braunite phase. 2% Nital etch..... 82

Figure 6.7 Optical micrograph of an unmasked section of the nitrocarburized SAE 1010 steel coupon. 2% Nital etch. 83

Figure 6.8 Optical micrograph of the nitrocarburized SAE 1010 steel coupon near the masked section. Both the original surface of the steel and white layer is shown. 2% Nital etch..... 84

LIST OF ABBREVIATIONS

CMM	coordinate measuring machine
EDM	electrical discharge machining
ID	inside diameter
M_f	martensite finish temperature
M_s	martensite start temperature
MIC	maximum inscribed circle
MCC	minimum circumscribed circle
NSERC	Natural Sciences and Engineering Research Council of Canada
OD	outside diameter
OGS	Ontario Graduate Scholarship
R	roundness
SEM	scanning electron microscopy
T	thickness
TMP	Toledo Machining Plant
XRD	x-ray diffraction

I. INTRODUCTION

Carbonitriding is a thermochemical diffusion process which utilizes the diffusion of carbon and nitrogen into the surface of austenized ferrous metals to impart a hard and wear resistant case [1-5]. The process significantly enhances the surface properties of both plain carbon and low alloy steels and is a popular choice amongst manufacturers, particularly in the automotive industry, where highly stressed parts such as gears, shafts, and bearings are often treated using this method [2, 6].

Chrysler LLC currently uses carbonitriding to improve the hardness and wear resistance of vehicle torque converter pistons. Stamped from sheets of cold-worked SAE 1010 steel, the purpose of a torque converter piston is to engage the converter case to lock the impellor and turbine, ensuring complete power transfer [7]. While 1010 steel may be desired for its high formability during stamping, additional processing is required to enhance the surface properties of the steel [8]. Though the desired surface case is currently achieved using a carbonitriding process, there are issues associated with the quenching step to form martensite, particularly the changes to the final size and shape of the part. Given the close fitting nature of the torque converter assembly, dimensional control of the pistons is important. Schobesberger, Streng, and Abbas [8] note that *the accuracy of the inner diameter, flatness, and the taper of the lockup surface of the piston are essential and critical for the torque converter to perform properly*. As such, it is necessary that any part distortion associated with the heat treatment process be corrected.

Currently at the Toldeo Machining Plant (TMP), Toledo, Ohio U.S.A. where the torque converter pistons are manufactured, the size and shape distortions resulting from heat treatment are corrected using finish grinding, a technique in which excess material is removed from the surface of the steel [9]. While this method ensures that dimensional specifications are met, the added manufacturing step contributes to longer production times and higher part costs; it also raises the risk of grind burns. Since the likelihood of these burns is increased by the presence of retained austenite at the surface of the steel

[2], grind burns are a common, reoccurring defect in the carbonitrided pistons. For this reason, gaseous ferritic nitrocarburizing is being investigated as potential replacement. Similarly to carbonitriding, nitrocarburizing is also a thermochemical diffusion process involving the diffusion of carbon and nitrogen into the surface of the steel forming a hard, wear resistant case. However, unlike the carbonitriding process, nitrocarburizing takes place in the absence of a phase transformation [2, 3, 10, 11]. By eliminating the austenite to martensite phase transformation that occurs during quenching, it is believed that ferritic nitrocarburizing will reduce the distortion associated with heat treatment and result in time and cost savings from the elimination of additional machining steps.

The aim of this research project was to compare the carbonitriding and gaseous ferritic nitrocarburizing processes with respect to distortion, retained austenite, and residual stress. The results of this study are then intended to be used as a guide in the selection of a suitable heat treatment schedule for the torque converter pistons allowing the manufacturer to minimize size and shape distortions while continuing to achieve the desired surface characteristics.

The approach to this investigation involved the use of two test specimens, the Navy C-ring and current production torque converter piston. Navy C-ring specimens were used for preliminary comparisons; the distortion, volume of retained austenite, and residual stress profiles were evaluated for each process. Because these initial results indicated the potential benefit of ferritic nitrocarburizing in lowering part distortion, a second, more thorough round of testing followed in which the torque converter pistons were used. In addition to comparing the processes with respects to distortion, retained austenite, and residual stress, the nitrocarburized pistons were divided into five separate heat treatment groups with process temperatures ranging from 510-605 °C. The strategy of comparing the current carbonitriding process to a range of nitrocarburizing temperatures was employed in order to be able to suggest a heat treatment process and temperature range that would allow manufacturers to minimize distortion, reduce manufacturing costs, and continue to achieve desired surface characteristics.

II. LITERATURE REVIEW

The following literature review addresses all major aspects of this thesis topic. Much of this discussion is centered on the torque converter pistons including their function in the torque converter, their fabrication, and their need for additional processing in the form of surface heat treatment. The current carbonitriding process is outlined as well as the issues associated with it and the need for investigation into gaseous ferritic nitrocarburizing. Many of the major effects of these surface heat treatment processes are also discussed, including the changes in size and shape distortion, residual stress, and retained austenite.

2.1 Automotive Torque Converter Pistons

2.1.1 Function

A torque converter piston, Figure 2.1a, is a thin-shelled automotive powertrain component located within the torque converter of an automatic transmission. The purpose of a torque converter is similar to that of a clutch in a manual transmission, *i.e.*, it allows for separation between the engine and transmission and is used for the purpose of torque transfer. A torque converter consists of three main components, namely the pump impeller, the turbine runner, and the stator, Figure 2.2. When the impeller and turbine are rotating at similar speeds, torque is transmitted at a ratio of 1:1. While it is expected that 100% of the torque is transmitted, differences in rotational speed between the impeller and turbine result in unnecessary energy losses of approximately 4-5%. A torque converter piston and lock-up clutch mechanism are used to correct this problem. The piston engages the converter case to lock the impeller and turbine. By engaging the lock-up clutch, not only is 100% of the power transferred, but also vehicle fuel consumption is reduced [7].

2.1.2 Fabrication

Torque converter pistons are manufactured from 3-mm thick sheets of cold-worked SAE 1010 steel. Beginning as circular blanks, the pistons are formed using a successive five-stage stamping operation, Figure 2.3.

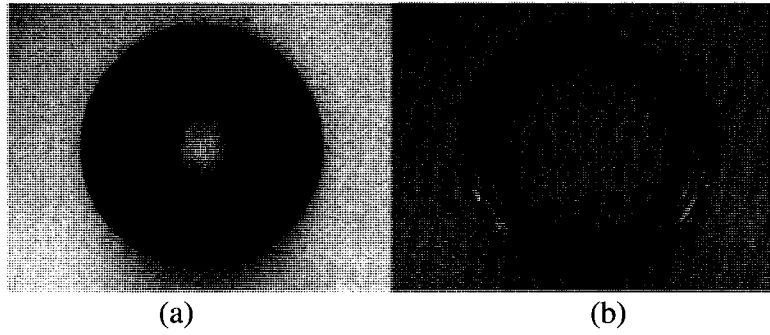


Figure 2.1 Top view of the torque converter piston and spring retainer ring. (a) Torque converter piston; nominal OD of 261.3 mm; (b) spring retainer ring.

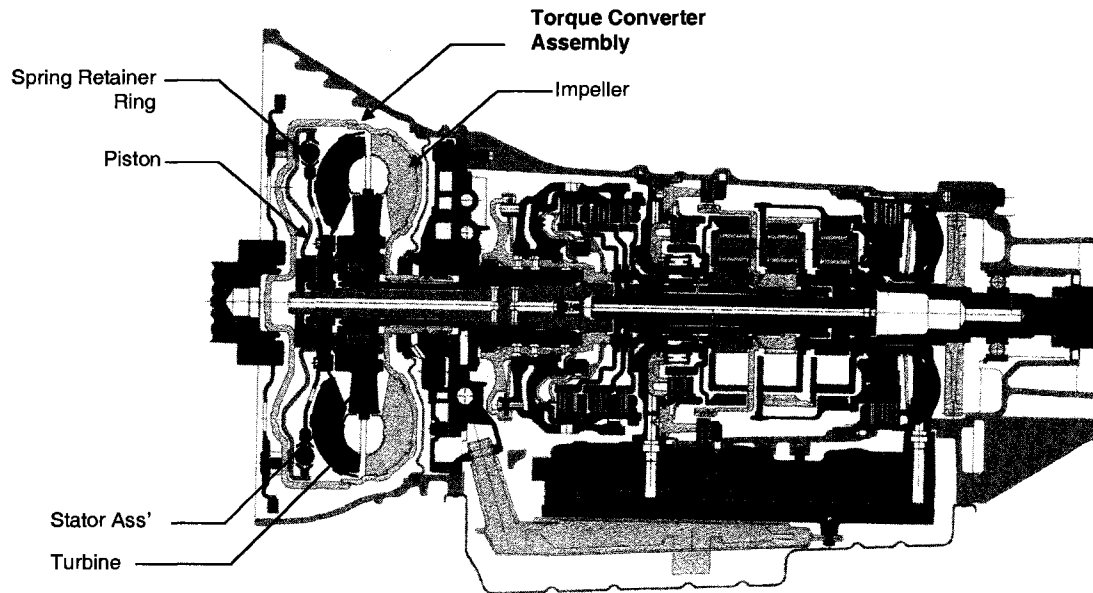


Figure 2.2 Schematic diagram of an automotive transmission highlighting the major components of the torque converter assembly including the stator, impeller, turbine, spring retainer ring, and torque converter piston. *Courtesy of Chrysler LLC, Auburn Hills, Michigan U.S.A.*

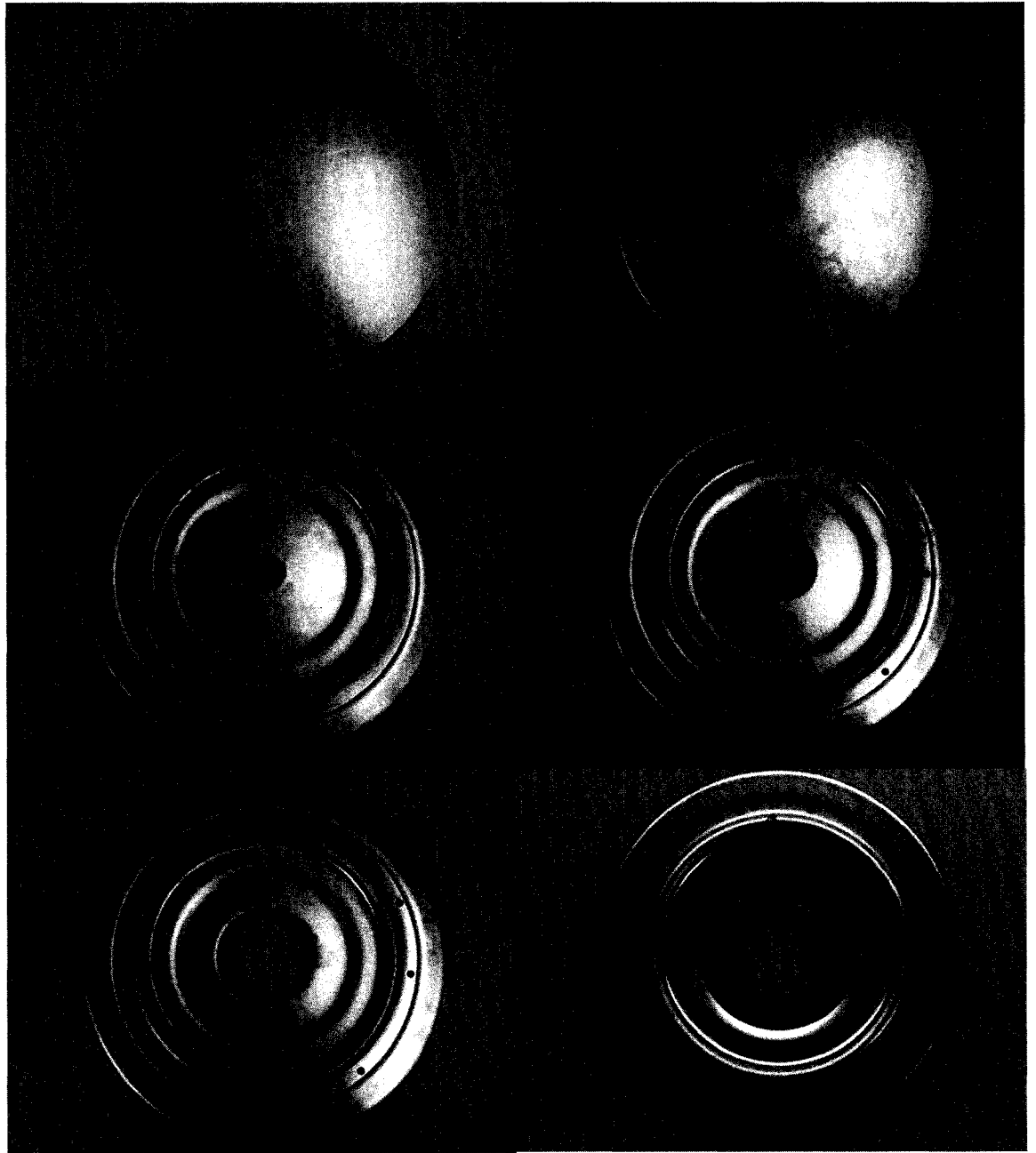


Figure 2.3 Five stage stamping operation of a torque converter piston. (a) Piston blank, (b) piston at stamping stage 1, (c) at stamping stage 2, (d) at stamping stage 3, (e) at stamping stage 4, and (f) at stamping stage 5.

The current heat treatment schedule for the torque converter pistons is a three-step process involving a heat treatment, polymer press quench, and temper. Following a pre-cleaning step to remove surface contaminants, the pistons are fed into an 895 °C (1640 °F) rotary hearth furnace for 55 min. They are then removed from the furnace and immediately press quenched for 25 s in Aqua-Quench 140, a water-based quench medium maintained at a concentration of 9-11% and a temperature of 50 °C (120 °F). The pistons are then drained, washed, and dried prior to tempering at 175 °C (350 °F). After 1 h, the pistons are removed from the furnace and transferred to a cooling station where they are cooled to ambient temperature. To remove the oxide scale formed during heat treatment, the surface of the pistons is cleaned using a sand blasting operation lasting 10-12 min. In the final step prior to assembly, the inside diameter (ID) of pistons is machined, using grinding, to ensure the final dimensions are met.

During assembly, each piston is joined together with a spring retainer ring, Figure 2.1b, and fastened using rivets. Figure 2.4 shows the assembled unit. In the final stages of production, the assembly undergoes two more quality inspections: ID gauging and mass balancing.

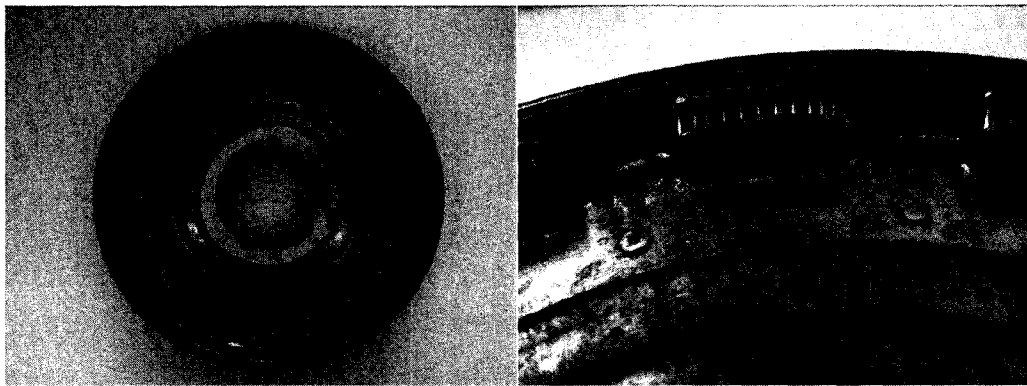


Figure 2.4 Torque converter piston assembly (left) showing the attachment of the piston and spring retainer ring using rivets (right).

2.1.3 Low Carbon Steel and the Importance of Surface Heat Treatment

AISI/SAE 1010 steel is a popular choice amongst manufacturers in high volume stamping operations for its ease of formability [4, 12] and its low tooling and raw-material costs [8]. While such properties make AISI/SAE 1010 steel desirable for stamping, additional processing is required to enhance the surface properties of the steel [8].

2.2 Surface Hardening of Steel

Surface hardening as defined by Krauss [3, 13] is a method of heat treatment *used to extend the versatility of certain steels by producing combinations of properties not readily attainable in other ways*. It is a means of improving hardness and wear resistance at the surface of the steel while continuing to maintain its core properties [14]. There are two distinct approaches to surface hardening - layer additions and substrate treatments. While layering involves the addition of a new layer to the surface of the steel, substrate treatments involve surface and subsurface modifications without any intentional build-up. Substrate treatments encompass both selective hardening and diffusion methods, the later of which will be the focus of this study [14]. Carbonitriding and gaseous ferritic nitrocarburizing are both thermochemical diffusion processes which utilize the diffusion of carbon and nitrogen into the surface of the steel to form a hard, wear resistant case [1-5, 10, 11, 13].

2.2.1 Carbonitriding

Carbonitriding is a widely accepted method of surface heat treatment used by industry in the production of highly stressed parts [6]. The process, which takes place between 705 and 900 °C (1300 and 1650 °F) [3, 13], is a modified form of carburizing [2, 5, 15, 16] that incorporates the addition of ammonia (NH₃) into the standard gas-carburizing atmosphere [2, 5, 16]. Ferrous metals are heated into the austenitic phase field of the steel. It is at this point that the NH₃ and carburizing gases are introduced; the NH₃ dissociates at the surface of the steel and both the carbon and nitrogen diffuse into the workpiece [2, 3, 5, 13, 16, 17].

Upon quenching from the austenitic phase field, a hard, wear resistant martensitic case is formed, Figure 2.5; cases range in thickness from 0.075 mm to a maximum of

0.75 mm [3, 13, 17]. The preferred case depth of carbonitrided steels is generally governed by the core hardness and surface requirements of the component [1]. By controlling processing variables such as time and temperature, manufacturers can consistently achieve desired uniformity and case thickness [1].

While the carbonitriding process is successful in achieving the desired surface properties required by the manufacturer of the torque converter pistons, the process is also associated with part distortion. Though distortion in carbonitrided steels is low in comparison to other higher temperature processes, *e.g.* carburizing [16], the changes in the size and shape of the pistons have resulted in added processing time and manufacturing costs. The cause of this problem is believed to be associated with the quenching step. Because carbonitriding takes place in the austenitic phase field, upon quenching the microstructure of the steel changes to that of martensite, defined by Smith [4] as *a metastable structure consisting of supersaturated solid solution of carbon in a ferrite*. Accompanying this phase change is a volume expansion of the microstructure; face-centered cubic austenite is transformed to the more open, body-centered structures of ferrite and martensite [17].

Because of the problems associated with distortion in carbonitrided steels, alternative processes were investigated; gaseous ferritic nitrocarburizing was selected as a potential replacement. The process utilizes similar hardening species as carbonitriding, and more importantly, it takes place below the A_{c1} temperature thus minimizing distortion [3, 17].

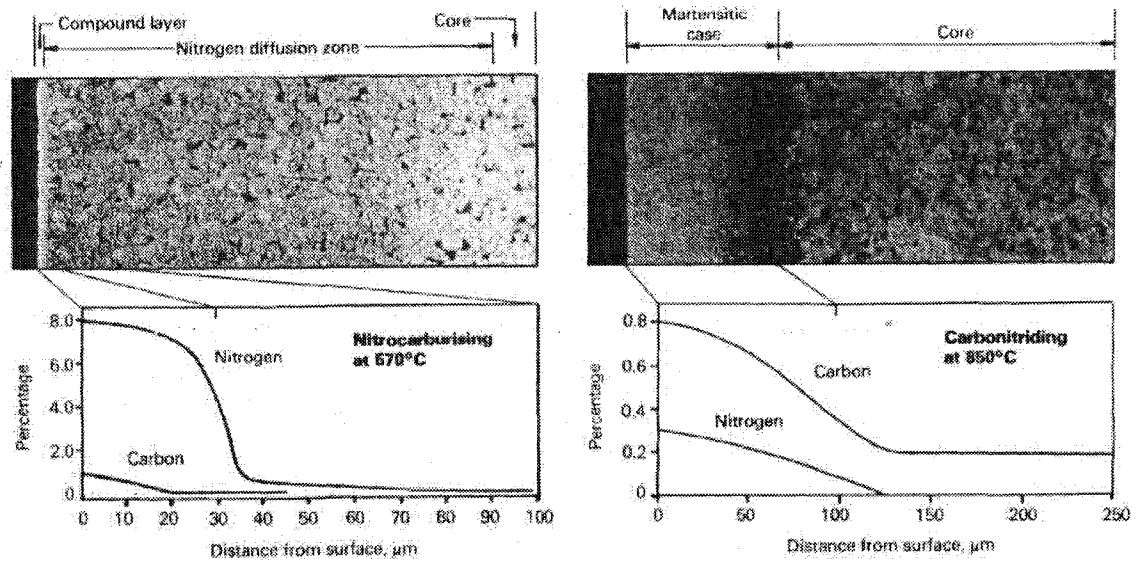


Figure 2.5 Comparison between the carbonitriding and nitrocarburizing processes [18].

2.2.2 Gaseous Ferritic Nitrocarburizing

Gaseous ferritic nitrocarburizing was first established and patented in 1961 by Lucas Ltd. [18, 19] and can be defined as a *thermochemical treatment involving the surface enrichment of a ferrous object with nitrogen and carbon where enrichment by nitrogen is predominant* [18]. The process is a low temperature substrate treatment that takes place in the ferritic phase field of the steel between temperatures of 525 and 650 °C (975 and 1200 °F) [20]. Carbon and nitrogen diffuse into the solid solution of iron and become trapped within the interstitial lattice spaces of the steel [2, 3, 10, 11, 13, 20]. The result is the formation of a compound layer and diffusion zone [2, 10], Figure 2.5. The compound layer, also known as the white layer contains varying amounts of gamma prime phase (γ'), epsilon (ϵ) iron-carbonitride phase, cementite, and various alloy carbides and nitrides [2, 11]. It forms a thin layer between 10 - 40 μm (0.0004 – 0.0016 in.) on the surface of the steel [2] and is associated with such attractive tribological properties as improved hardness, wear, scuffing and corrosion resistance [20]. The underlying diffusion zone consists of iron (and alloy) nitrides and absorbed nitrogen [2] and is associated with improved fatigue properties, particularly in carbon and low alloy steels [2].

Formation of the Compound Layer:

Although the formation of the compound layer begins with the nucleation of cementite [21], the main constituent is ϵ iron-carbonitride ($\text{Fe}_{2-3}(\text{N,C})$), a hexagonal ternary compound of iron, nitrogen, and carbon formed at temperatures between 450 and 590 °C (840 and 1095 °F) [2, 3, 13, 17]. This ϵ -phase easily nucleates on the cementite forming a thin, continuous layer along the surface of the steel [21]. The presence of cementite and γ' phase are also possible. While the cementite developed in the early stages of the nitrocarburizing process is dissolved if the carbon activity is low, high carbon activity will result in the presence of cementite at some distance from the surface [21]. The γ' -nitride will appear in the compound layer adjacent to the diffusion zone, but only after the formation of the ϵ -phase. The initial intake of carbon into the compound layer of the steel is responsible for this delay. Since the maximum solubility of carbon in γ' is low, the formation of the γ' only appears after prolonged heat treatment when the carbon has diffused deeper into the steel [21].

Braunite:

Braunite is a eutectoid compound formed in nitrated and nitrocarburized steels as a result of the slow cooling of austenite from treatment temperatures above 590 °C. During cooling, the austenite transforms to a special microstructure of ferrite and γ' -nitride (Fe_4N) [22] shown in Figure 2.6. Normally at process temperatures below 590 °C, the γ' -nitride is present in the form of needles in a ferrite matrix. However, as process temperatures rise to 500 °C, these needles begin to dissolve and by 590 °C have completely decomposed [23]. The name Braunite was given to this special eutectoid in honour of Braun, who in 1905 established the possibility of iron reacting with ammonia [23, 24].

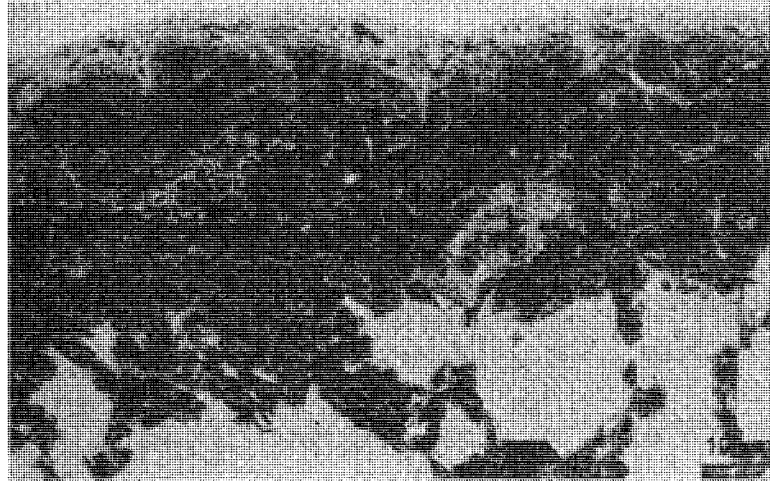


Figure 2.6 Braunitite (St 37, nitrated at 640 °C for 16 h) [22].

Distortion in Nitrocarburized Steel:

Minimal distortion is one of the major advantages of the nitrocarburizing process. The process takes place in the absence of a phase transformation, thus ensuring good control of distortion. Since the nitrogen and carbon are added to the steel at temperatures below the Ac_1 , the phase transformation from austenite to martensite does not occur and part distortion is significantly reduced in comparison to the carbonitriding process. Rockwell International, manufacturers of the seat sliders in the executive Renault R25, chose the Nitrotec process to impart a hard, wear resistant case on the surface of their seat slides and roller tracks [18]. Originally the seat slides, made from low carbon steel, were simply painted, however issues with indentations in the track were caused by the hardened steel ball used to traverse the slide. While the indentation was not a problem for manually adjusted seats, it had a marked influence on those which were adjusted electronically calling for changes in the manufacturing process. Because the profile of the slide and roller track was critical, other heat treatment techniques such as carburizing and carbonitriding were avoided because of the unacceptable levels of distortion. Using nitrocarburizing, the manufacturer was able to obtain resistance to indentation, increased yield strength, as well as improved surface wear and corrosion resistance [18].

2.3 Distortion

Distortion is the unexpected or inconsistent change in size or shape caused by variations in the manufacturing process conditions such as the relief of residual stresses, material movement due to thermal gradients, and the volume changes associated with phase transformations [9]. As it relates to heat treatment, distortion is defined by Pye [25] as *the movement of metal during [the] heat treatment process*, which can take place at any one of the five manufacturing stages listed below [9].

1. Prior to heat treatment
2. During heat-up for heat treatment
3. At treatment temperature (i.e. carbonitriding, nitrocarburizing)
4. During quenching and cooling
5. During postquenching processing

2.3.1 Size Distortion

Size distortion is the change in the volume and linear dimensions of a part, Figure 2.7, that includes such dimensional changes as elongation, shrinkage, thickening, and thinning [20, 25-27, 28]. It occurs due to the thermal expansion or contraction of the microstructure and is the direct result of changing surface chemistry within the steel [17, 25]. Because it is associated with microstructural changes, size distortion is somewhat predictable and can often be accommodated for at the design stage [17, 29].

During the carbonitriding process, volume expansion is expected; changes in part size are associated with the phase transformation of the steel from austenite to martensite upon quenching [17]. The extent of this expansion is a function of carbon content. The size change associated with the microstructural transformation of austenite to martensite can be approximated using the equations for percent volume and dimensional change shown in Table 2.1.

Because the nitrocarburizing process takes place in the absence of a phase transformation, size distortion is believed to be associated with the thermochemical treatment process itself [30]. As the hardening species of nitrogen and carbon enter the steel, a notable volume expansion takes place due to the growth, and a change in size is reported [25].

Table 2.1 Size changes associated with microstructural changes in carbon steels from austenite to martensite [17].

Transformation	Volume Change (%)	Dimensional Change (mm/mm)
Austenite → martensite	$4.64 - 0.53 \times (\%C)$	$0.0155 - 0.0018 \times (\%C)$

2.3.2 Shape Distortion

Shape distortion is the change in the geometrical form of a part, encompassing all twisting, bending, warpage, out of round, and other non-symmetrical changes that affect curvature and angular relation, Figure 2.7 [9, 20, 25-27].

According to Krauss [17], *shape distortion is caused by nonuniform thermal and transformation stresses due to temperature variations throughout parts of complicated shape or parts with large differences in section size.* The larger the variation or nonuniformity within the part, the more prone it will be to the development of residual stresses [17]. Some of the factors influencing the development of residual stresses include: thermal gradients, nonuniform changes in metallurgical structure, nonuniform or high rates of quenching, and nonuniformity in the metal composition [17, 26].

Shape distortion can also be linked to the release of induced stresses developed during previous manufacturing operations [25]. When the workpiece is heated to a temperature where the yield strength of the material is below the residual stress level, these induced stresses are relieved and expressed as changes in the shape of the part [9, 25]. Because of the complexities associated with shape distortion, it is often more difficult to predict than size distortion and poses more of a concern during heat treatment.

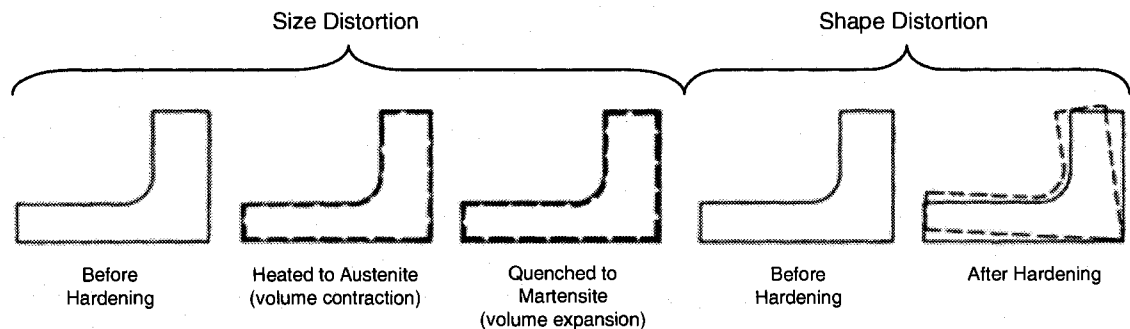


Figure 2.7 Size and shape distortion in hardening [26].

2.3.3 Issues with Distortion in Manufacturing

Distortion in heat treated steel parts is inevitable regardless of the process used [25]. While manufacturers generally expect some distortion as a result of heat treatment, there are instances in which the deformation is so severe that parts are distorted beyond permissible limits rendering them useless for their intended application. Under such circumstances, the manufacturer has the option of scrapping the part entirely or taking the necessary steps to correct the distortion [27]. The issue with each of these options is that they contribute to increased production costs.

2.3.4 Correcting Distortion Through Metal Grinding

Metal grinding is a finishing method used to correct the dimensional changes associated with thermal processing by the removal of excess material from the surface of the steel [9, 31]. Although proper grinding has been shown to improve the residual stresses and fatigue strength of the workpiece [6], there are several drawbacks to using this technique including the risk that effective regions of the case will be removed. Excessive material removal, Figure 2.8, can lead to lack of uniformity in case depth, uneven residual stresses, reduced mechanical strength, and the increased probability of checking, cracking, and grind burns [2, 9]. Because the likelihood of these burns is increased by the presence of retained austenite, which is maximum at the surface of the steel [2], grind burns are a common, reoccurring defect in carbonitrided pistons, Figure 2.9.

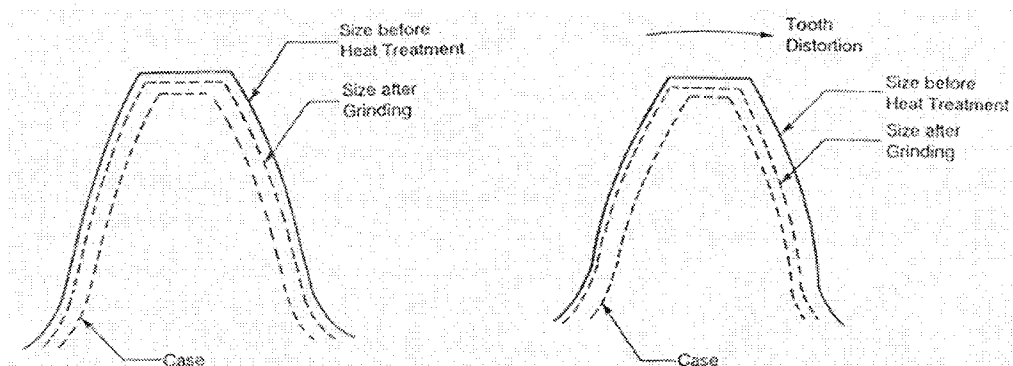


Figure 2.8 Schematic of material ground from a distorted gear tooth after case hardening treatment [9, 32].

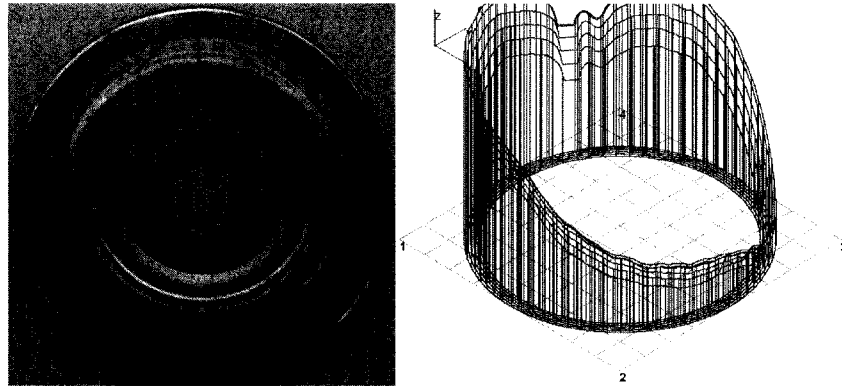


Figure 2.9 Grind burn on the lockup surface of a carbonitrided torque converter piston. Defect can be detected visually (left) and through use of a coordinate measuring machine (CMM) flatness scan of the surface (right).

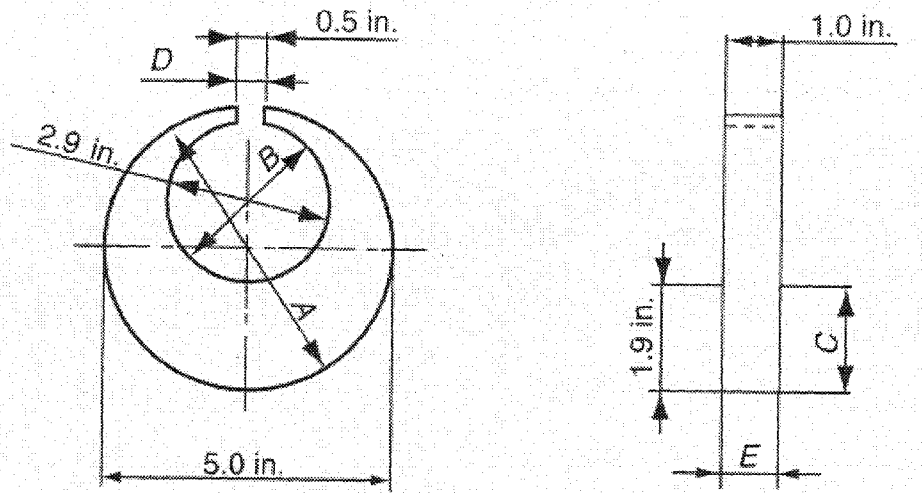
2.3.5 Measurement of Distortion

Numerous test specimens [33] have been developed that allow researchers to study the effects of heat treatment on distortion. They range from simple to complex; they can be as basic as a cylindrical bar or spherical ball, or in some cases involve the use of the production part itself. The Navy C-ring, Figure 2.10, is a common test specimen used to understand distortion. As one of the oldest standards used to evaluate quench distortion [9, 34], the use of Navy C-rings can be traced back to 1921 when they were utilized by the US Navy in the inspection of class 5 tool steels [35].

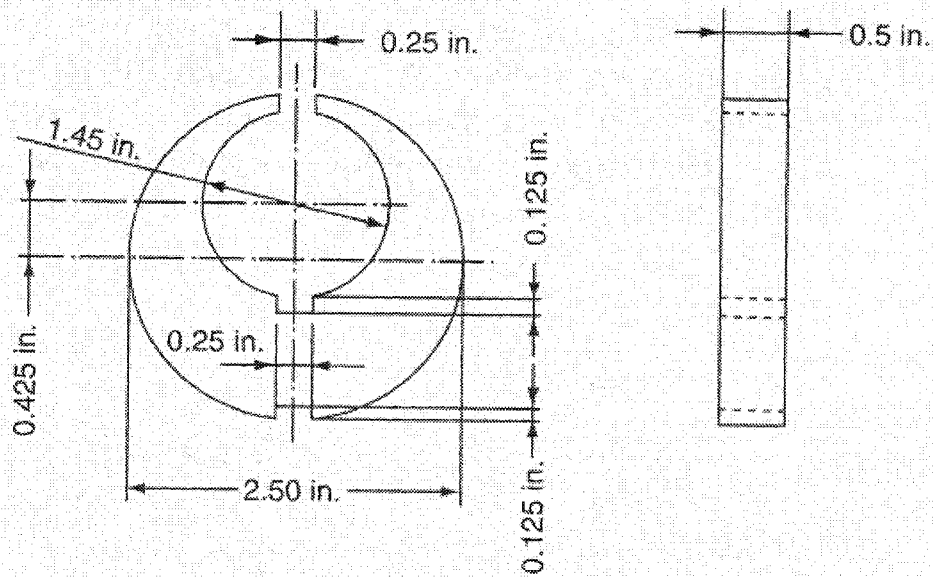
Prior to the development of highly sensitive measurement instruments, distortion in Navy C-rings was measured by the changes in gap width and outside diameter [34, 35]. Today, with the use of highly accurate coordinate measuring machines (CMM), researchers are able to study both size and shape changes at various locations on the C-ring. The system uses an X-Y-Z coordinate system. The test specimen is placed on a worktable, and a small probe is used to locate points of interest along the surface. In advanced systems, the probe can scan the surface taking measurements at specified intervals, a technology which benefited this study because it allowed for the evaluation of more complicated measurements including flatness, roundness, cylindricity, and taper.

Navy C-rings continue to be an important tool in studying distortion [30, 35-39]. There are currently no standard dimensions for the Navy C-ring. Specimens are fabricated from the desired testing material and machined into a variety of sizes [33, 34];

variations in shape such as the modified Navy C-ring [39], shown in Figure 2.10b, also exist.



(a)



(b)

Figure 2.10 Navy C-rings. (a) Example of a Navy C-ring test specimen used in a quench distortion study. (b) Modified Navy C-ring distortion test specimen [9, 39].

2.4 Retained Austenite

Retained austenite as defined by Jatzak [40] is *a face-centered cubic phase which in hardenable steels, is stable at temperatures above the Ac_3 and Ac_m phase boundaries, but is unstable below these temperatures*. Upon cooling, the austenite decomposes into any one of the following phases: ferrite, carbide, pearlite, bainite, or martensite [40, 41]. When dealing with the hardening of steel, the formation of martensite is desirable. By rapidly cooling the steel in a quenching medium, the diffusion of carbon and alloying elements is prevented [40] and a saturated solid solution of martensite is formed instead. The formation of martensite begins at a characteristic start temperature called martensite start (M_s) and continues until essentially 100% transformation is complete, a temperature known as the martensite finish (M_f) [40, 42]. It is very common that a certain amount of untransformed austenite, also known as retained austenite, will be present at the M_f temperature.

The volume of retained austenite measured at room temperature can range from 100% to virtually zero [41]. Factors affecting retained austenite content include the chemical composition, the temperature of the quenchant, and the rate of cooling [40]. The influences of composition and cooling temperature have been quantitatively established by Koisten and Marburger [40, 43], and are given in Equation 2.1.

$$\% R.A. = e^{-1.10 \times 10^{-2} (M_s - T_q)} \quad \text{Equation 2.1}$$

where T_q is the lowest temperature reached in quenching; M_s is the martensite start temperature either measured or calculated using Equation 2.2.

$$M_s (\text{°C}) = 500 - (333 \times \%C) - (34 \times \%Mn) - (35 \times \%V) - (20 \times \%Cr) - (17 \times \%Ni) \\ - (11 \times \%Mo) - (10 \times \%Cu) - (5 \times \%W) + (15 \times \%Co) + (30 \times \%Al) + (0 \times \%Si)$$

Equation 2.2

Of all the alloying elements, carbon promotes the greatest retention of retained austenite [40, 42]. In Fe-C alloys retained austenite has been reported in steels containing as little as 0.3% C [17]. For plain carbon and low alloy steels, a carbon content of at least 0.4% is required [4, 40]. Figure 2.11 shows the effect of dissolved carbon on the retained austenite content in quenched Fe-C alloys at room temperature.

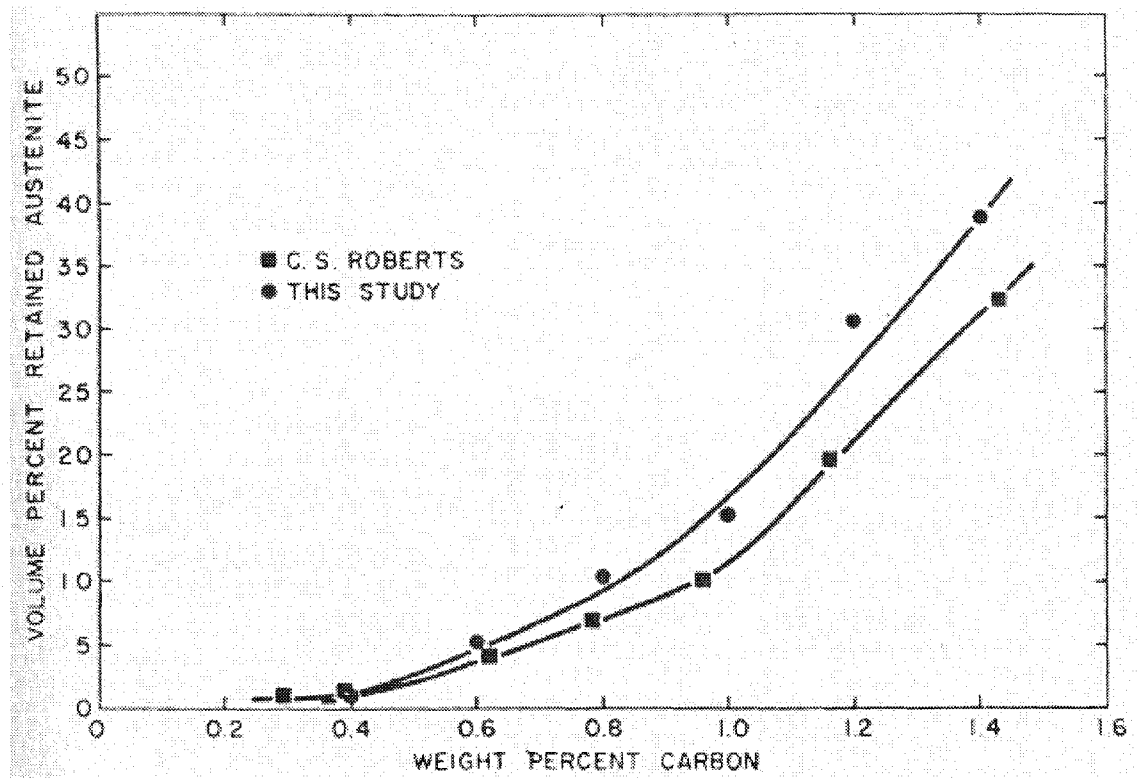


Figure 2.11 Retained austenite in quenched Fe-C alloys at room temperature as function of carbon content [4].

2.4. 1. Effects of Retained Austenite

The presence of retained austenite can have both positive and negative effects on the properties and characteristics of steel.

Positive Attributes of Retained Austenite [40]:

- Improvements in contact, impact, and bending fatigue resistance in high carbon steels
- Enhanced corrosion resistance in martensitic steels
- Increased ductility and fracture toughness at high strength levels in maraging, trip, and high strength steels
- Enhanced corrosion resistance in martensitic steels

Negative Attributes of Retained Austenite [2, 17, 40, 44]:

- Decreased aggregate hardness, resistance to scuffing, and indentation
- Reduced aggregate compressive yield and ultimate strength
- Increased susceptibility to burns and heat checking during grinding
- Undesired dimensional growth

2.4.2 Minimizing Retained Austenite

Cryogenic Treatments:

Because M_f temperatures can be far below room temperature, there generally exists a considerable quantity of retained austenite in steels at ambient temperatures [17, 40, 45]. Such is the case even for low carbon steels. As the carbon content increases, M_f values can drop to temperatures below 0 °C making the complete transformation to martensite under normal quenching conditions near impossible, Figure 2.12. A significant reduction in the amount of retained austenite requires the steel to be quenched to sub-zero temperatures near or below the M_f temperature [1, 46]. Cryogenic treatments have been shown to reduce the retained austenite content in steel to as little as 1 vol%. Reducing the amount of retained austenite is associated with increasing hardness, wear resistance, and dimensional stability of the workpiece and decreasing susceptibility to grind burns [2, 45]

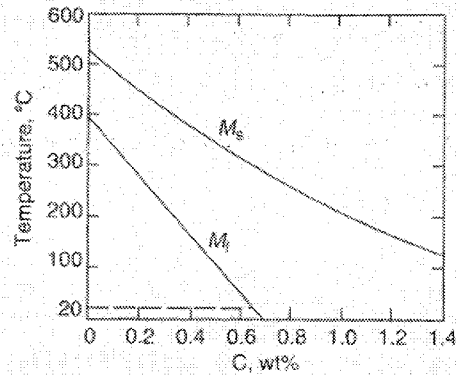


Figure 2.12 Martensitic start (Ms) and martensitic finish (Mf) temperatures versus carbon content in unalloyed steels [45].

Reducing Retained Austenite in Carbonitrided Steels:

The martensitic case formed in carbonitrided steels usually contains some quantity of retained austenite. In most cases, because of the absorption of nitrogen, levels of retained austenite are higher in carbonitrided steels than carburized steels of similar carbon content. While retained austenite at the surface can be removed by grinding or transformed to martensite using cryogenic treatments, its presence can be avoided through modifications to the process itself by lowering the carbon potential, increasing the furnace temperature, or restricting the ammonia content to the minimum amount required to obtain the desired hardenability. It is important that the nitrogen at the surface be controlled. Increasing furnace temperature allows the nitrogen to diffuse farther into the case and away from the surface, while controlling ammonia content helps to decrease the rate of nitrogen penetration [1, 2].

2.4.3 Measurement of Retained Austenite Using X-ray Diffraction

The presence of retained austenite in steels can be measured using metallographic, dilatometric, saturation magnetization intensity, electrical resistivity, and thermal analysis methods [40, 47]. While these methods are able to provide reasonable results under favourable conditions, they are inaccurate in measuring retained austenite levels below 10% [47, 48] and are often unreliable when dealing with highly alloyed steels or those with large quantities of carbide [47].

X-ray diffraction (XRD) is a non-destructive technique that can be used to measure retained austenite quantities to a far greater accuracy than the techniques listed above. Beu, Beard, and Ogilvie have reported that measurements could be made in steels containing as little as 2% retained austenite [40, 47]. Durnin and Ridal reported an accuracy of $\pm 0.5\%$ for measurements between 1.5 - 38.0% retained austenite [47]. Improving the accuracy beyond $\pm 0.5\%$ is a more time consuming process, requiring an increase in the number of individual determinations and the time taken for each measurement [47, 49].

When a crystalline substance is irradiated by x-rays, it produces a characteristic diffraction pattern which is determined by the crystal structure of all phases existing within that substance [40]. From these diffraction patterns, peaks of varying heights are located at discrete 2θ angles and correspond to the diffraction of the x-rays from the various (hkl) planes in the crystal structure of each phase [50]. For as-hardened and tempered steel, x-ray radiation from Cr, monochromated Cu, or Mo is used [40], and intensities diffracted from the austenite and martensite planes are measured and recorded [49]. For Cr radiation, common diffraction lines are (200) and (211) for martensite and (200) and (220) for austenite [40]. Quantitative determination of the relative volume fractions of martensite and austenite can be made from diffraction results because the x-ray intensity diffracted from each of these phases is proportional to the volume fraction of the phase [40]. In randomly orientated specimens, the measurement of integrated intensity of just one line pair of austenite and martensite will accurately establish the volume fraction of each phase [40]. In preferred orientated specimens, such as cold worked steel, the intensities diffracted by austenite and martensite with certain orientations in relation to the surface no longer truly represent the amount of the two

phases [49]. When dealing with preferred orientation, measurements must be made on at least four austenite and four martensite lines to provide accurate results by averaging [40].

For the diffraction peaks, the integrated intensities above the background are determined using a planimeter; I_A represents the austenite line and I_M represents the martensite line. Typically, as-hardened and tempered steels usually have low preferred orientation and can often be determined using only a one line pair comparison [40]. Equation 2.3 is used to determine the volume of retained austenite in steel which exhibits no, low, or preferred orientation [40, 49]:

$$V_A = \frac{\frac{I_A^{hkl}}{R_A^{hkl}}}{\frac{I_A^{hkl}}{R_A^{hkl}} + \frac{I_M^{hkl}}{R_M^{hkl}} + \frac{I_C}{R_C}} \quad \text{Equation 2.3}$$

I^{hkl} is the integrated intensity per unit length of the diffraction line (hkl) for a given phase, R^{hkl} is proportional to the integrated intensity which should be diffracted by a specific (hkl) reflection, when 100% of that phase exists and no preferred orientation is present, and I_C/I_R is the corrected intensity ratio for a carbide line. C, A, and M represent the carbide, austenite, and martensite phases in the steel, respectively.

While the errors associated with XRD are generally very small, there are certain corrective actions laboratories must make to ensure the accuracy of their results. Measuring retained austenite in thin surface layers requires that the penetration of the X-ray beam be adjusted. It is recommended that measuring several pairs of lines can help to confirm the original value, uncover errors in observations and calculations, and determine the presence of preferred orientation [40].

2.5 Residual Stress

As defined by Grum [51], residual stresses are *the stresses present in a material or a workpiece when there is no external force and/or external moment acting upon it*. For heat treated components, a residual stress will arise as a consequence of thermal and transformation stresses. If the sum of these stresses exceeds the yield strength of the material plastic deformation in the form of size and shape distortions will occur [52].

Thermal Stresses:

Thermal stresses develop as a result of temperature gradients in the workpiece, and are especially likely if uniform heating/cooling cannot be ensured. If one part of the workpiece is hotter/cooler than the other, the rate of expansion/contraction will vary, thereby causing thermal stresses to develop [52-54]. In heat treatment, quenching processes usually produce the largest temperature gradients across the section, and hence the greatest residual stresses [45].

Thermal stresses are influenced by the thermal conductivity, modulus of elasticity, and the coefficient of thermal expansion of the material [52]. While copper and aluminum are excellent thermal conductors, metal such as steel have lower thermal conductivity values and therefore are susceptible to developing the high temperature gradients associated with thermal stresses [52]. Equation 2.4 can be used to approximate the thermal stresses developed in a constrained part due to temperature differences upon cooling [52]:

$$\sigma_{thermal} = E \cdot \alpha \cdot \Delta T \quad \text{Equation 2.4}$$

In this equation, $\sigma_{thermal}$ is the thermal stress, E is the modulus of elasticity, α is the coefficient of thermal expansion, and ΔT is the temperature difference.

Transformation Stresses:

If transformation stresses occur, the residual stress pattern becomes even more complicated and less predictable [55]. Transformation stresses are developed as a result of structural changes in the material [52] and are common in high temperature heat treatment processes. Any phase transformation that causes a change in volume will produce or modify the residual stress state in a material [54]. Thermal stresses are dependent on three factors: transformation characteristics, cooling rate, and section size [52]. For steels, the development of stresses is common during quenching. The decomposition of austenite to martensite results in a volume expansion of the microstructure, which in turn causes the development of residual stresses [52, 53, 55].

2.5.1 Residual Stresses in Surface Hardened Steels

Compressive residual stresses in the surface layer are advantageous because they enhance the overall surface quality of the steel by improving fatigue, stress corrosion, hydrogen embrittlement [54], as well as preventing the occurrence of new cracks and possible propagation of old ones [53].

Residual Stresses in Carbonitrided Steels:

For carbonitriding, the favourable compressive stresses developed between the case and the core can be used to enhance surface properties of the steel including wear and fatigue resistance [1]. In carbonitrided steels, compressive residual stresses are developed at the surface because the transformation of the core precedes that of the case. When plain carbon steels are quenched, the core is transformed to a combination of ferrite and pearlite. Because of the high carbon and nitrogen contents at the surface, the transformation of the case to form martensite takes place at much lower temperatures. Because the core has already transformed, the expansion associated with the formation of martensite results in the presence of desired compressive residual stresses at the surface [52].

Residual Stresses in Nitrocarburized Steels:

An understanding of the residual stresses developed in nitrocarburized steels, however, is far more complicated; the stresses in the compound layer, the substrate, and the interface between the two must be considered [56].

Very little data exists on residual stresses in nitrocarburized parts. Technical difficulties, even with XRD methods, make it difficult to determine the residual stresses in the compound layer [56]. While it is generally agreed that tensile stresses are present within the ϵ compound layer [56], the compressive stresses associated with the diffusion layer play a more important role in the residual stress state of the steel [56] because they contribute to an improvement in fatigue strength [27].

The role of residual stresses in the compound layer continues to be debated. While some experimental results indicate that it is of less importance, others have concluded that removal of the compound layer would virtually eliminate the compressive residual stresses [56].

2.5.2 Measurement of Residual Stresses

While residual stresses can be determined by means of ultrasonic, magnetic, mechanical, and XRD methods [54], measurement using XRD has become increasingly popular since it was first used by Aborn at U.S. Steel Co. [57].

XRD is non-destructive method of determining the residual stresses in crystalline materials [33], particularly metals and their alloys. The crystalline sample is irradiated with X-rays and the angle of incidence (θ) of the beam within the sample is measured. Using the diffracted angle (2θ) measured experimentally, and the wavelength of the x-rays, Bragg's Law, Equation 2.5, can be applied to calculate the interplanar spacing (d-spacing) between the crystallographic planes [33, 54, 57 58]. An illustration of Bragg's angle is shown in Figure 2.13.

$$n\lambda = 2d \sin \theta$$

Equation 2.5

In this equation n is an interger equal to the order of reflection. For stress work, the value of n is usually unity.

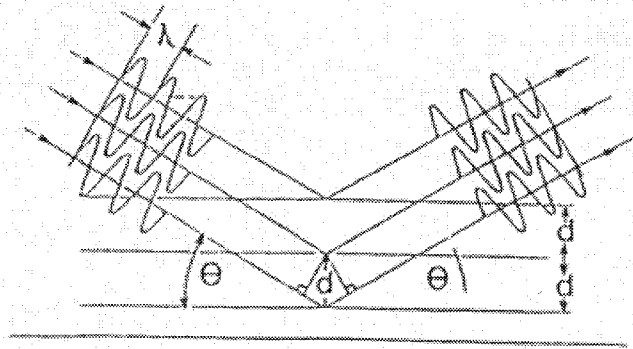


Figure 2.13 Illustration of the Bragg relation [33, 54].

The presence of residual stresses in the material produces a shift in the x-ray diffraction peak measured by the detector and a perturbation of d-spacing; the d-spacing increases when the material is in tension and decreases when it is in compression [57, 58]. Because the spacing between the planes is so small, it is affected by both macro and micro stresses both of which are measured using the x-ray method [57]. Once the d-spacing is measured for the stressed (d) and unstressed conditions (d_o), Equation 2.6 is then used to calculate strain (ϵ) [58].

$$\epsilon = \frac{d - d_o}{d_o} \quad \text{Equation 2.6}$$

There are a number of methods for calculating residual stress from the diffraction data. The most common is the $\sin^2\psi$ method, in which the surface of the crystallographic sample is irradiated and changes in the diffraction angle (ψ) pattern are related to the interplanar spacing (d) and thus to strain (ϵ) [33]. A number of d-spacings are measured and stresses are calculated from an equation derived from Hooke's law for isotropic, homogeneous, fine grain materials [59-60]. The stress-strain relationship is given by Equation 2.7 [58-60]. The definition of the reference axes and the direction of measurement are presented in Figure 2.14.

$$\varepsilon_{\phi\psi} = \frac{1}{2} S_2 (\sigma_{\phi} - \sigma_{33}) \sin^2 \psi + \frac{1}{2} S_2 \sigma_{33} - S_1 (\sigma_{11} + \sigma_{22} + \sigma_{33}) + \frac{1}{2} S_2 \tau_{\phi} \sin 2\psi$$

$$\sigma_{\phi} = \sigma_{11} \cos^2 \phi + \sigma_{12} \sin 2\phi + \sigma_{22} \sin^2 \phi \quad \tau_{\phi} = \sigma_{13} \cos \phi + \sigma_{23} \sin \phi$$

Equation 2.7

In these equations, $\frac{1}{2} S_2$ and S_1 are the x-ray elastic parameters of the material replacing the mechanical parameters $(1+\nu)/E$ and ν/E , respectively; σ_{ϕ} is the stress in the direction of the measurements; ψ is the angle subtended by the bisector of the incident and diffracted beam and the surface normal; and $\varepsilon_{\phi\psi}$ is the strain for a given $\phi\psi$ [59,60].

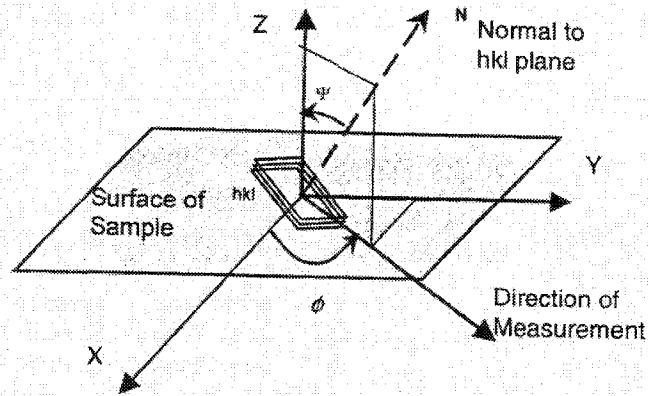


Figure 2.14 Definition of the axis and the direction of measurement [59,60].

Evaluation of the stress tensor components σ_{ij} is generally straightforward and is normally carried out by plotting the measured d-spacing versus $\sin^2 \psi$, with careful selection of the measurement directions ψ and ϕ . A variety of mathematical models and measurement approaches have been proposed to evaluate stress-tensor components of interest [60]. The data can be categorized as follows: linear, elliptical with ψ -splitting, and non-linear with oscillatory behaviour [60]. In general a minimum of five ψ tilts are required for a reasonable assessment of shape of the d-spacing versus $\sin^2 \psi$ curve; however, it is recommended that more than five tilts be used as a general practice [60].

Because there is often variation in the residual stress state at the surface and subsurface of a workpiece, techniques have been developed to allow for the measurement of residual stress profiles. Because of the limited depth of penetration of the x-rays, it is necessary that electropolishing techniques be used to etch back from the surface in controlled increments. Since the removal of the stress layers will cause relaxation due to equilibrium disturbance, measurement results must be corrected for this effect [59]. Other possible sources of X-ray measurement errors include: error in peak position, stress relief by aging, and sample anisotropy [33, 61].

III. EXPERIMENTAL DETAILS

3.1 Overview

Figure 3.1 shows the test methodology used to compare the carbonitriding and gaseous ferritic nitrocarburizing processes. Evaluations were made with respect to size and shape distortions, percent volume of retained austenite, and residual stress profiles. Two different test specimens, the Navy C-ring and torque converter piston, were used.

Navy C-ring specimens were used in the preliminary comparisons between the carbonitriding and nitrocarburizing processes; distortion, retained austenite, and residual stress values were compared. Similar assessments were also made for the torque converter pistons with the added emphasis of studying the effects of treatment temperature on the surface characteristics of nitrocarburized SAE 1010 steel. In addition to the C-rings and pistons, SAE 1010 steel coupons were also used and designed to study the growth direction of the nitrocarburized case.

Results for the C-rings, pistons, and coupons were analyzed and used to recommend a suitable heat treatment schedule (process, temperature, and time), which will yield lower part distortion while meeting the manufacturer's standard for a high quality surface layer.

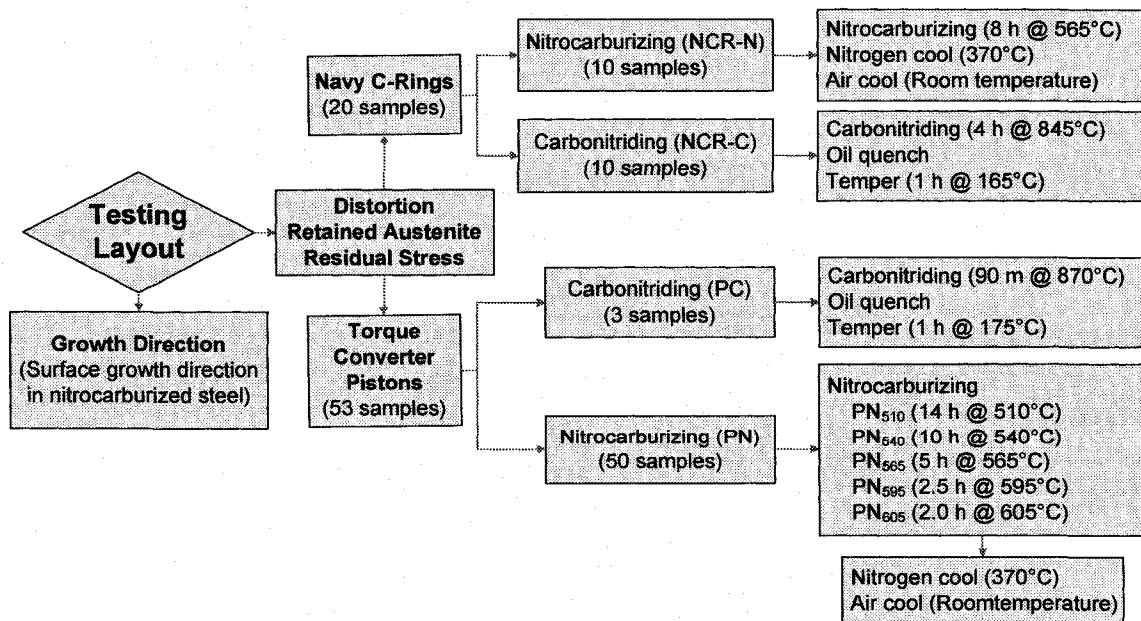


Figure 3.1 Testing methodology.

3.2 Test Specimens

Navy C-rings:

Initial comparisons between the carbonitriding and gaseous ferritic nitrocarburizing processes were made using the Navy C-ring (NCR) specimen shown in Figure 3.2. Twenty C-rings were machined from a bar stock of hot-rolled SAE 1020 steel; the composition of the steel is given in Table 3.1. The specimens were divided into two groups:

- NCR-C → 10 Navy C-ring specimens, carbonitrided
- NCR-N → 10 Navy C-ring specimens, nitrocarburized

Torque Converter Pistons:

The torque converter pistons, shown in Figure 2.1, were manufactured using SAE 1010 steel; the nominal composition of the steel is given in Table 3.2. Pistons were fabricated from 3-mm sheets of cold-worked steel at the Toledo Machining Plant (TMP) by means of a five-stage stamping operation. In total, fifty un-treated pistons were collected and divided into two separate heat treatment groups:

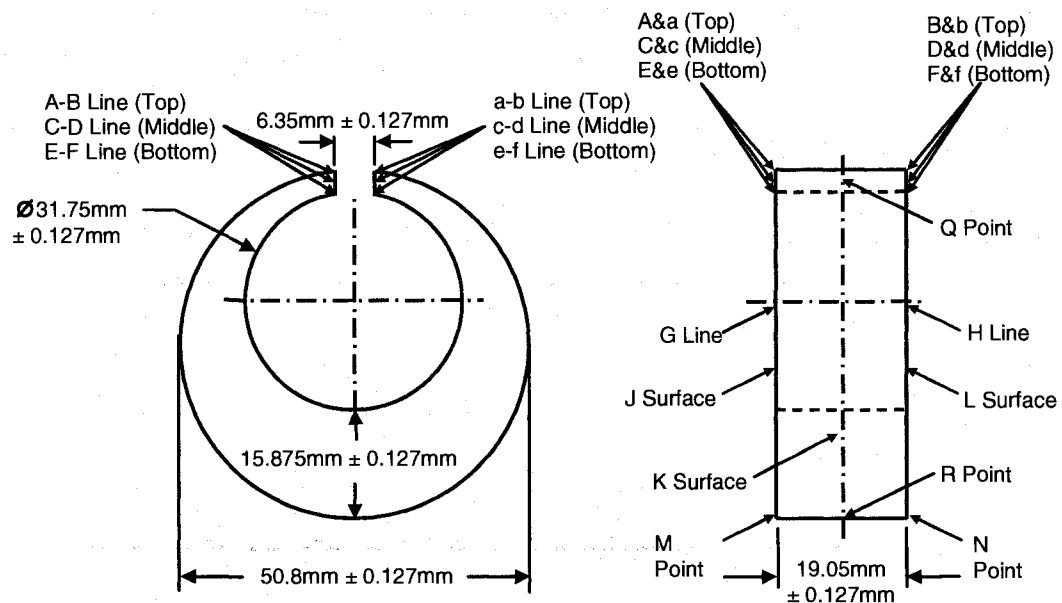
- PC → 3 torque converter pistons, carbonitrided
- PN → 50 torque converter pistons, nitrocarburized

Table 3.1 Chemical composition of AISI 1019/1021 steel.

Type of Steel	Chemical Composition, %							
	C	Si	S	P	Mn	Ni	Cr	Mo
AISI 1019/1021	0.200	0.290	0.027	0.023	0.750	0.080	0.100	0.020

Table 3.2 Nominal chemical composition of AISI 1010 steel [12].

Type of Steel	Chemical Composition, %			
	C	Mn	S	P
AISI 1010	0.08-0.13	0.30-0.60	0.050 max	0.040 max



CMM report shows:

1. Flatness (L surface flatness)
2. OD (Outside Diameter)
3. Cylindricity (Outside Cylindricity)
4. ID-1 (Inside Diameter at J Surface)
5. ID-2 (Inside Diameter at K Surface)
6. ID-3 (Inside Diameter at L Surface)
7. Roundness-1 (Inside Roundness at J Surface)
8. Roundness-2 (Inside Roundness at K Surface)
9. Roundness-3 (Inside Roundness at L Surface)
10. Thickness-1 (Thickness between A Point and B Point)
11. Thickness-2 (Thickness between G Line and H Line)
12. Thickness-3 (Thickness between M Point to N Point)
13. Gap Width-Top (Gap Between A-B Line and a-b Line)
14. Gap Width-Middle (Gap Between C-D Line to c-d Line)
15. Gap Width-Bottom (Gap Between E-F Line to e-f Line)

Figure 3.2 Navy C-ring test specimen; dimensions and measurement positions [37].

3.3 Heat Treatment Details

Navy C-rings:

The carbonitrided C-rings from group NCR-C were treated at the Chrysler Technology Center in Auburn Hills, Michigan U.S.A. in a sealed, 75 kW quench furnace with a carbon potential of 0.8%. Ten C-rings were placed in the furnace and held at 845 °C (1550 °F) for 4 h. The specimens were removed from the furnace after heat treatment, immediately oil quenched to room temperature, and then tempered for 1 h temper at 165 °C (325 °F).

Gaseous ferritic nitrocarburizing was used to treat the ten C-rings from group NCR-N. The heat treatment process was performed at Woodworth Inc., Detroit, Michigan U.S.A. in the large commercial nitrocarburizing furnace shown in Figure 3.3. Specimens were placed in the furnace (gas composition proprietary), held at 565 °C (1050 °F) for 8 h, then furnace-cooled to 370 °C (700 °F) using nitrogen gas. The C-rings were then removed from the furnace and air cooled to room temperature.

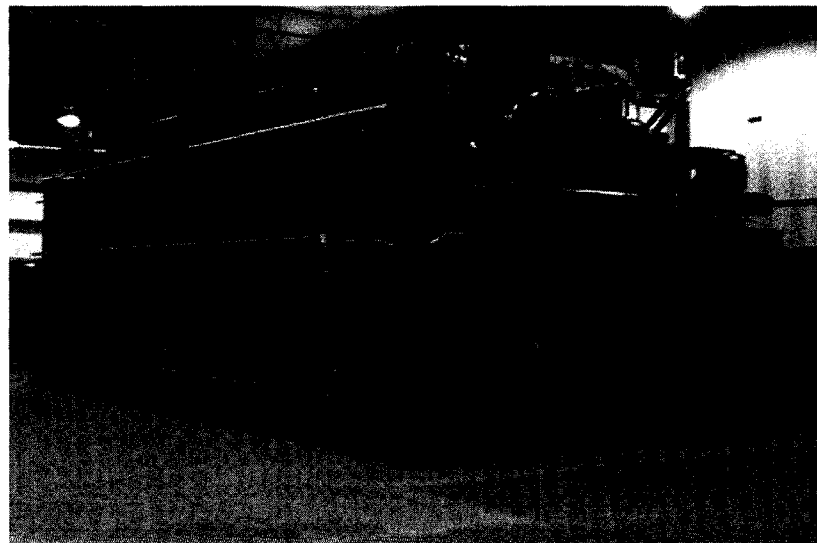


Figure 3.3 Nitriding/nitrocarburizing furnace. This furnace was used in the heat treatment of the nitrocarburized Navy C-rings and torque converter pistons from groups NCR-N and PN, respectively. Furnace dimensions measure 8 ft x 8 ft x 33 ft. Figure courtesy of Woodworth Inc., Detroit, Michigan U.S.A.

Torque Converter Pistons:

The torque converter pistons from group PC were treated in a similar manner to the current manufacturing process [8]. The same laboratory furnace used in the carbonitriding of the C-rings from group NCR-C was also employed in this case. The pistons were placed into the furnace and held at 870 °C (1600 °F) for 90 min, after which they were then removed, oil quenched, and tempered at 175°C (350 °F) for 1 h.

Gaseous ferritic nitrocarburizing was used to treat the fifty torque converter pistons in group PN. To study the effects of temperature on the quality of the nitrocarburized case, the pistons from group PN were further divided into five separate heat treatment sub-groups with furnace temperatures of 510 to 605 °C. Cycle times ranged from 2-14 h and were determined based on the time required to form a compound layer with a thickness of 7.5-20 µm (0.0003-0.0008 in.). Following heat treatment, pistons were held in the furnace and cooled using nitrogen to 370 °C (700 °F) before being removed and air cooled to room temperature. All nitrocarburized pistons were treated in large commercial furnaces at Woodworth Inc.,. Table 3.3 summarizes the specimen identification and the heat treatment details for both the Navy C- rings and torque converter pistons.

Table 3.3 Specimen identification and heat treatment details for the Navy C-rings and torque converter pistons.

Specimen	Heat Treatment	Group	No.of Samples	Temperature °C (°F)	Time (h)
Navy C-ring (NCR)	Carbonitriding (C)	NCR-C	10	845 (1550)	4.0
	Nitrocarburizing (N)	NCR-N	10	565 (1050)	8.0
Torque Converter Piston (P)	Carbonitriding (C)	PC	3	870 (1600)	1.5
	Nitrocarburizing (N)	PN ₅₁₀	10	510 (950)	14.0
		PN ₅₄₀	10	540 (1000)	10.0
		PN ₅₆₅	10	565 (1050)	5.0
		PN ₅₉₅	10	595 (1100)	2.5
PN ₆₀₅	10	605 (1125)	2.0		

3.4 Dimensional Measurements and Calculation of Distortion

To quantify the size and shape distortion associated with each process, a PRISMO (Carl Zeiss IMT Company) coordinate measuring machine (CMM) was used, Figure 3.4. Contact scans of the Navy C-rings and torque converter pistons were conducted prior to and following heat treatment. The dimensional measurements, precise to 0.1 μm , were obtained during the scan and provided a set of points referred to as a “point cloud” in the computational analysis. The analysis of both the C-ring and piston features was completed using Imageware Surface scanning software. Both size and shape distortions were calculated in terms of dimensional change and measured in millimeters (mm) using Equation 3.1.

$$\text{Distortion} = \text{Final Value} - \text{Initial Value} \quad \text{Equation 3.1}$$

The final and initial values in this equation represent the CMM measurements taken before and after heat treatment.

While distortion can also be expressed as a percentage change, this approach was avoided. Shape measurements such as flatness, roundness, and cylindricity reflect the maximum deviation between the points along a particular surface. In the event of zero deviation prior to heat treatment, even the slightest deviation would give rise to an infinite percentage change. Such results would be ineffective in trying to compare the heat treatment processes against one another.

Navy C-rings:

In total, fifteen specified dimensions, Figure 3.2, were used to evaluate size and shape distortion through the thickness of each C-ring. Size parameters were used to measure the changes in part dimension and included outside diameter (OD), inside diameter (ID-1, ID-2, ID-3), gap width (Top, Middle, Bottom), and thickness (T-1, T-2, T-3). Shape parameters were calculated by determining maximum deviation between the points of a given surface; the parameters evaluated included flatness, roundness (R-1, R-2, R-3), and cylindricity.

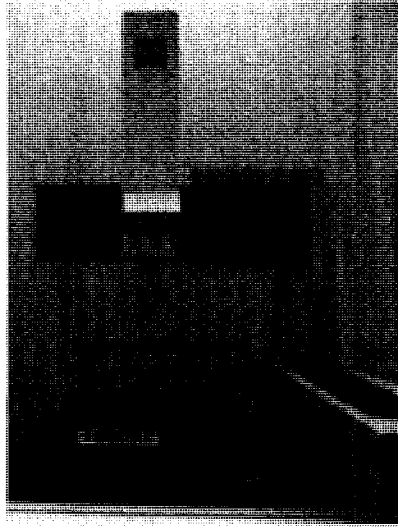


Figure 3.4 PRISMO coordinate measuring machine (CMM).

Flatness, is defined by the National Standard on Dimensioning and Tolerancing [62], as the *condition of a surface having all elements in one plane*. A flatness tolerance specifies a zone defined by parallel planes separated by the specified tolerance within which the surface must lie. The flatness values for this study were determined scanning approximately 2100 points along the perimeter of the C-ring at surface ‘L’ and calculating the difference between the maximum and minimum points of deviation from the reference surface. An example of a flatness form plot is shown in Figure 3.5; the reference surface, designated as “1-2-3-4”, coincides with the minimum point of deviation.

Roundness is expressed by the dimension of out-of-roundness, the deviation of a surface from the ideal form [63]. Roundness measurements were made at three separate locations along the ID of the Navy C-rings (R-1, R-2, R3); approximately 850 points were scanned along each ID circle. Roundness values were then calculated by determining the maximum deviation between the points located closest to and farthest from the central axis of each circular profile. An example of a roundness form plot is shown in Figure 3.6.

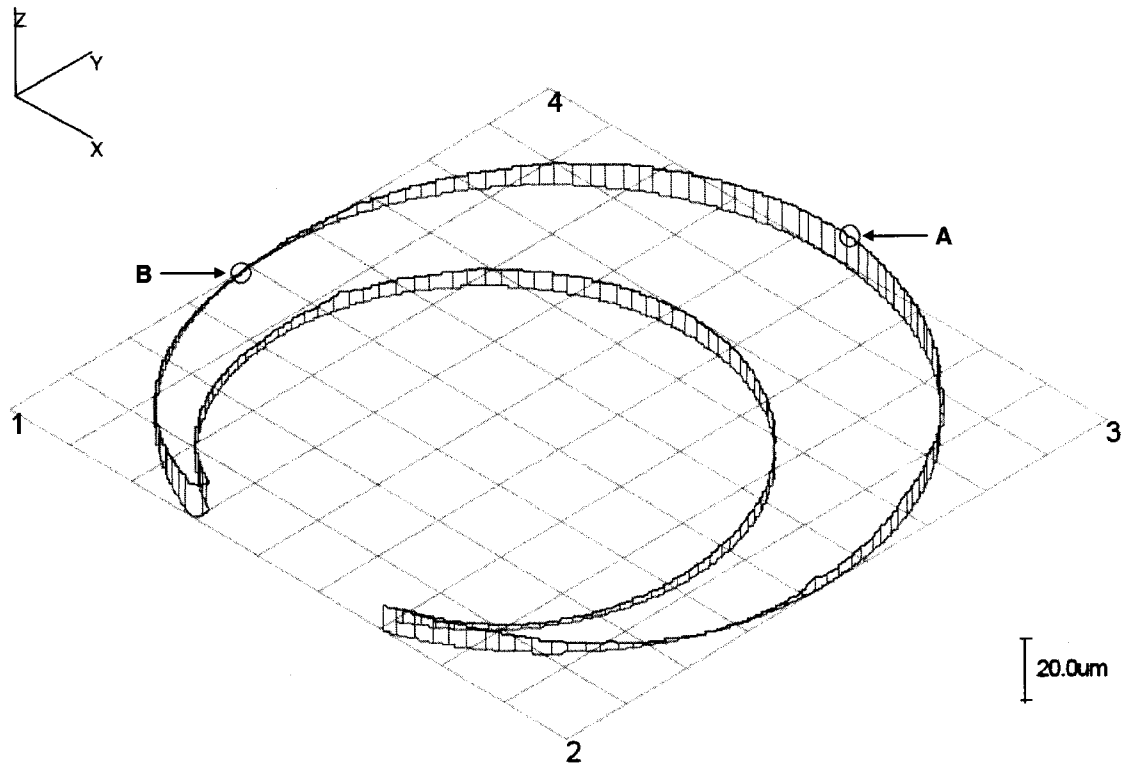


Figure 3.5 Example of a flatness form plot obtained using a CMM; specimen NCR-C6 after heat treatment. Points “A” and “B” are the points of maximum and minimum deviation away from surface “1-2-3-4”, respectively.

Cylindricity is the condition in which all points along the surface of a cylinder are equidistant from the axis [64]. Unlike roundness, it is a value that applies to the entire surface area of the cylinder simultaneously. In this study, cylindricity values were used to evaluate the straightness, circularity, and taper along the OD of each Navy C-ring [65]. A combined total of approximately 4300 points were scanned at three separate locations along the OD of each C-ring. A value for cylindricity was then calculated by determining the deviation between the points located closest to, and farthest from, the central axis. An example of a cylindricity form plot is shown in Figure 3.7.

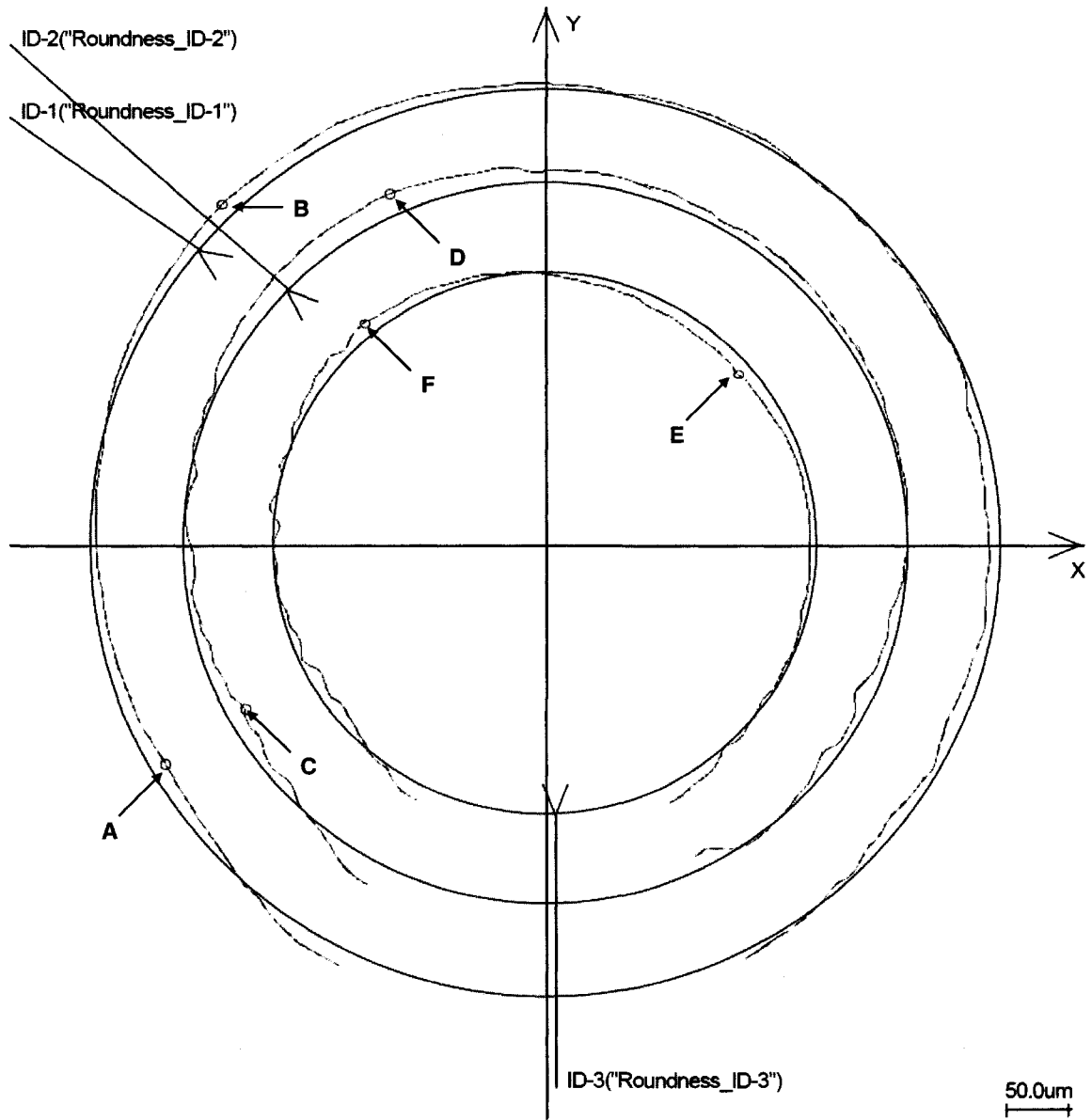


Figure 3.6 Example of a roundness form plot; specimen NCR-C1 after heat treatment. Plots for R-1, R-2, and R-3 are shown. Points "A" and "B" are the points of maximum deviation toward and away from circle ID-1, respectively. Points "C" and "D" are the points of maximum deviation toward and away from circle ID-2, respectively. Points "E" and "F" are the points of maximum deviation toward and away from circle ID-3, respectively. The three circles (ID-1, ID-2, and ID-3) have equal diameters, but have been scaled to avoid overlapping of the measured profiles.

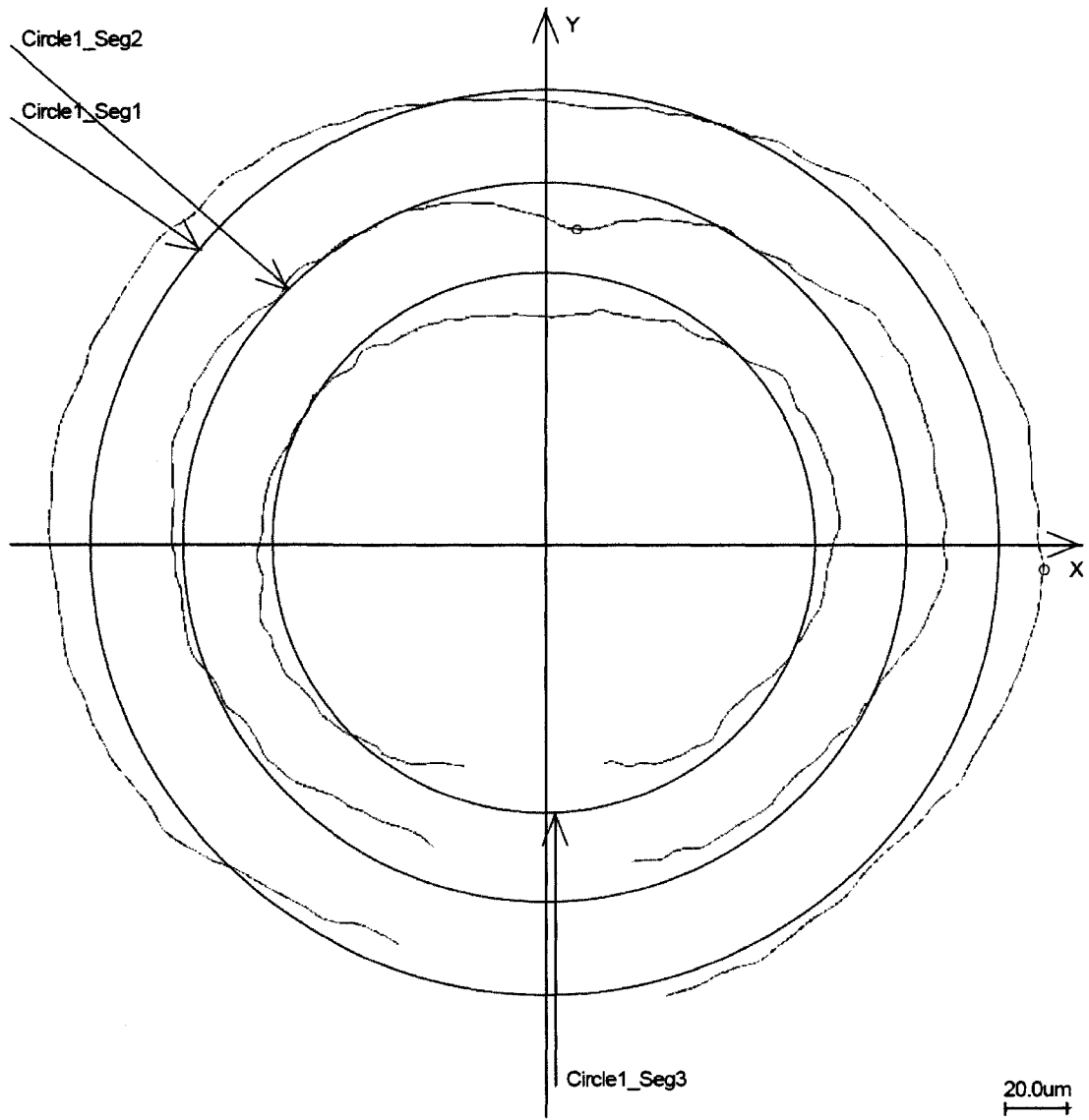


Figure 3.7 Example of a cylindricity form plot; specimen NCR-C1 after heat treatment. Points “A” and “B” are the points of maximum deviation toward and away from the centre of three circles along the OD of the C-ring. The three circles have equal diameters, but have been scaled to avoid overlapping of the measured profiles.

Torque Converter Pistons:

The size and shape distortions of the pistons were evaluated using ID, OD, total flatness, and taper of the lockup surface, Figure 3.8. The accuracy of the ID, the flatness and the taper of the lockup surface are required for the torque converter to function properly [8].

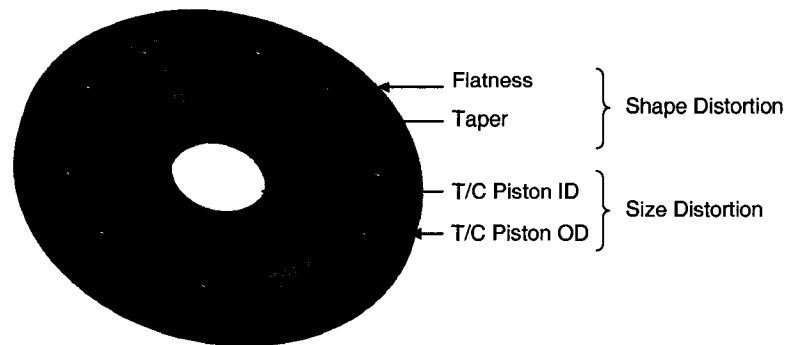


Figure 3.8 Torque converter piston measurement positions.

OD and ID measurements were used to give an indication of the linear and volumetric changes associated with size distortion [17, 26, 27]. Both OD and ID were measured at multiple locations along the height of each piston using the Minimum Circumscribed Circle (MCC) and Maximum Inscribed Circle (MIC), respectively. Measurement positions are given with respect to the lockup surface; OD was evaluated at -7.5 mm and -21.5 mm and ID evaluated at -11 mm and -15 mm.

Flatness and taper of the lockup surface were used to measure changes to the geometrical form of the part associated with shape distortion [17, 26, 27]. Total flatness of the pistons was evaluated at the lockup surface along six separate diameters (225, 230, 235, 240, 245, and 250 mm). Between 6,500 and 7,300 points were scanned at each measurement position, approximately 41,000 points in total. The number of points measured at each location increased with increasing diameter. By taking into consideration each of the six scans and calculating the difference between the overall highest and lowest points of deviation from reference surface, the total flatness was determined. The reference surface, designated as “1-2-3-4” coincides with the minimum

point of deviation. An example of the total flatness form plot of a torque converter piston is provided in Figure 3.9.

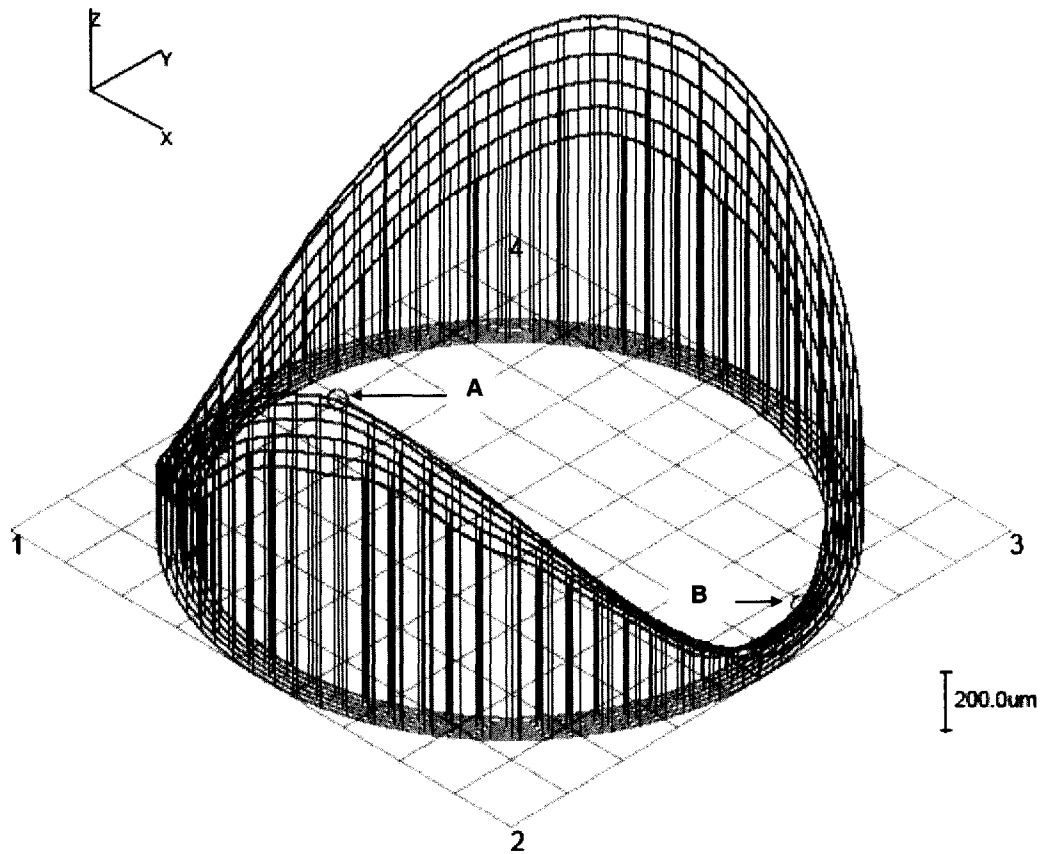


Figure 3.9 Example of a total flatness form plot obtained using a CMM; specimen PC-3 after heat treatment. Total flatness represents the maximum and minimum points of deviation along the lockup surface, measured at six separate diameters. Points “A” and “B” are the points of maximum and minimum deviation away from surface “1-2-3-4”, respectively.

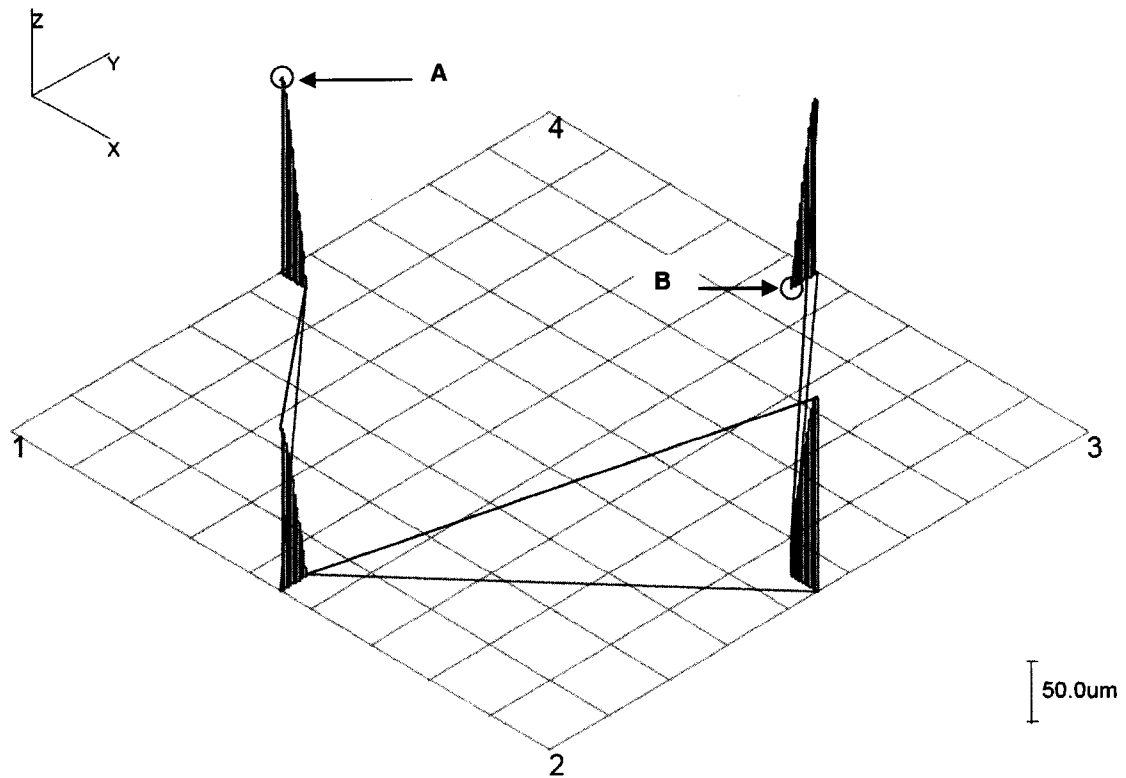


Figure 3.10 Example of a flatness taper form plot obtained using a CMM; specimen PN605-1 after heat treatment. The flatness taper represents the maximum and minimum points of deviation measured along the $\pm Y$ and $\pm X$ directions of the lockup surface. Points “A” and “B” are the points of maximum and minimum deviation away from surface “1-2-3-4”, respectively.

The taper of the lockup surface was calculated using a CMM. In total, approximately 490 points were scanned along the $\pm Y$ and $\pm X$ directions of the lockup surface. Flatness taper values were determined by measuring the difference between the points of maximum and minimum deviation away from surface “1-2-3-4”, respectively. The reference surface, designated as “1-2-3-4” coincides with the minimum point of deviation. An example of a flatness taper form plot of a torque converter piston is provided in Figure 3.10.

3.5 Retained Austenite Measurement

The percent volume of retained austenite was determined by x-ray diffraction (XRD) at the facilities of Proto Manufacturing Ltd., Oldcastle, Ontario. Measurements were made at the surface and near surface of the hardened steels using the *Four-Peak Method*, an XRD technique which compares the intensities of the (200) and (211) diffraction peaks of the α -Fe phase and the (200) and (220) diffraction peaks of the γ -Fe phase. $\text{CrK}\alpha$ X-ray radiation with a wavelength of 0.2291 nm was used with a vanadium filter in the diffracted beam. Generator voltage and current settings were set to 30 kV and 25 mA, respectively.

To create the retained austenite profiles, measurements were taken from the surface of the steel inward through the case. Due to the limited depth penetration of x-rays, determining the amount of retained austenite within the subsurface of the steel required the use of electro-polishing techniques to etch back from the surface in controlled increments.

Navy C-rings:

The volume percent of retained austenite was measured for one C-ring from the carbonitrided and nitrocarburized groups, samples NCR-C10 and NCR-N2 respectively. As shown in Figure 3.11a, measurements were taken at the 'bottom' of each C-ring extending inward from the surface of the steel to a depth of approximately 1.5 mm; six measurements were recorded.

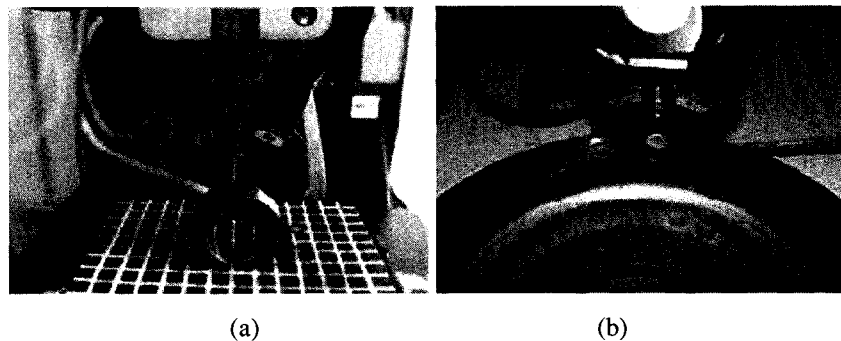


Figure 3.11 Test set-up for the measurement of retained austenite and residual stresses for the (a) Navy C-ring specimens (b) Torque converter pistons.

Torque Converter Pistons:

The volume percent of retained austenite was measured for four torque converter pistons, one from each of the following heat treatment groups - PC, PN₅₁₀, PN₅₆₅, and PN₆₀₅, pistons PC-1, PN₅₁₀-1, PN₅₆₅-3 and PN₆₀₅-2, respectively. Measurements were taken at the lock-up surface of each piston, Figure 3.11b, extending inward from the surface of the steel to a depth of 1.5 mm; six measurements were recorded.

3.6 Residual Stress Measurement

XRD techniques were also used by Proto Manufacturing Ltd. in determining the residual stresses at the surface and near surface of the steel for the Navy C-rings and torque converter pistons. The same specimens used in determining the retained austenite profiles were also chosen for measuring residual stress. These specimens were selected from their heat treatment groups because they most closely represented the average dimensional changes experienced by the specimens within their group.

For both the C-rings and pistons, multiple residual stress measurements were made from the surface of the steel inward through the case. CrK α X-ray radiation with a wavelength of 0.2291 nm was used to measure the lattice deformations on the {211} diffraction planes of the martensite peak. Target power for C-rings and pistons varied; generator voltage and current settings were 30 kV, 25 mA for the C-rings and 20 kV, 4 mA for the pistons.

Navy C-rings:

For the C-rings, residual stress values were determined at the following Ψ angles: 0°, $\pm 5.51^\circ$, $\pm 12.00^\circ$, $\pm 19.41^\circ$, and $\pm 25.00^\circ$. The Bragg angle, 2θ , was set at 156° . Hoop and axial stresses were measured at eleven locations at the 'bottom' of each C-ring specimen from the surface to a depth of approximately 2.5 mm. Hoop stress (tangential stress) was measured in the direction perpendicular to the radius; axial stress was measured in the direction along the radius.

Torque Converter Pistons:

For the pistons, residual stress values were determined at the following Ψ angles: 0° , $\pm 11.80^\circ$, $\pm 16.32^\circ$, $\pm 23.46^\circ$, and $\pm 30.00^\circ$. The Bragg angle, 2θ , was set at 156° . Hoop stress was measured at ten locations extending inward from the lock-up surface, through the case, to a depth of approximately 2 mm.

3.7 Determination of Surface Growth Direction in Nitrocarburized SAE 1010 Steel

Unlike coatings in which a material is deposited on the surface of the steel, thermochemical diffusion processes use both heat and the diffusion of hardening species to modify the surface of the steel and achieve the desired surface characteristics [14].

To further understand the changes in the size and shape of the nitrocarburized C-rings and pistons, additional testing was performed to verify the growth direction of the nitrocarburized case. Coupons were cut from a sheet of 3-mm ($\frac{1}{8}$ -in.) normalized SAE 1010 steel into 28 x 8 x 3-mm sections. The ends were masked using Acheson Nitrostop N4, as shown in Figure 3.12 and the coupons were subjected to a heat treatment schedule identical to that of group NCR-N. When applied to steel prior to heat treatment, Nitrostop forms a protective layer; it inhibits diffusion and maintains the initial properties of the steel. Following the heat treatment of the coupons, optical microscopy was used to compare the surface position of the masked steel against that of the unmasked region.

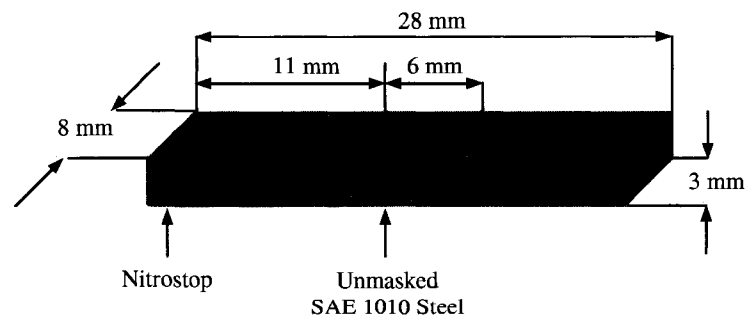


Figure 3.12 Schematic diagram of the SAE 1010 steel coupon. To prevent the formation of the compound layer, a layer of Nitrostop was applied prior to heat treatment.

3.8 Metallographic Procedure

After heat treatment and the completion of all distortion, retained austenite, and residual stress measurements, selected C-rings, torque converter pistons, and coupons were cut, mounted, and examined using optical and scanning electron microscopy. Though cutting methods differed for each type of test specimen, all were mounted, polished, and etched in a similar fashion. Buehler Mineral Filled Diallyl Phthalate powder and a Buehler Simplimet 3 Mounting Press were used to create the mount for each sample. Mounted samples were then rough ground on a Buehler Handimet II Roll Grinder through 240, 320, 400, and 600 grit silicon carbide papers. Rough polishing was accomplished on a Buehler Ecomet 3 Variable Speed Grinder-Polisher with 9 μm diamond compound on a Buehler Metcloth. Fine polishing was done on a Buehler Metaserv Grind-Polisher using a deagglomerated alpha alumina oxide powder (Al_2O_3) suspended in water. This two-step process involved 1- μm powder on Buehler Billiard Cloth, followed by 0.05- μm powder on Buehler Microcloth. Polished samples were etched using a 2% Nital solution (2 ml nitric acid (HNO_3) and 98 ml ethanol). Samples were swabbed for approximately 4 s, immediately rinsed in cold water, and dried.

A ZEISS Axiovert 25 light optical microscope and JEOL 5800 scanning electron microscope, Figure 3.13, were both used to document the microstructures.

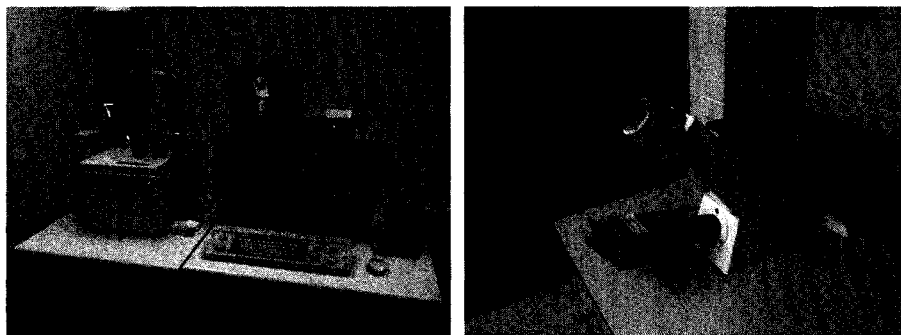


Figure 3.13 Metallographic observation of the microstructures was made using a scanning electron microscope (left) and light optical microscope (right).

Navy C-rings:

Mounting samples from the Navy C-rings were cut from the 'bottom' of each specimen, very close to the area in which the retained austenite and residual stress measurements were made. Sectioning was accomplished with a Buehler Isomet 100 Precision Saw using a diamond blade.

Torque Converter Pistons:

Because of the size of the torque converter pistons, wire electrical discharge machining (EDM) was first used to remove a 19-mm (0.75-in.) section from each of the pistons, cut parallel to the radius. Then the Precision Saw was used to section smaller samples for mounting. The lockup surface and side wall of the pistons were examined.

Coupons:

Entire coupons could be accommodated in the mounting press; no additional sectioning was necessary.

RESULTS AND DISCUSSION

IV. EFFECT OF HEAT TREATMENT ON SIZE AND SHAPE DISTORTIONS

This section discusses the distortion associated with the carbonitriding and gaseous ferritic nitrocarburizing of plain carbon steels. Using a coordinate measuring machine (CMM), distortion values were determined by measuring each of the test specimens before and after heat treatment. The carbonitriding and nitrocarburizing processes were evaluated in terms of both size and shape distortion; the average distortion values were calculated and a comparison of the results is presented. For the size and shape distortion values associated with each test specimen, refer to Appendix A.

4.1 Navy C-rings

Figure 3.2 identifies the fifteen specified dimensions used to evaluate distortion in the carbonitrided and nitrocarburized Navy C-rings, groups NCR-C and NCR-N, respectively. Size distortion was assessed by measuring the dimensional changes in outside diameter (OD), inside diameter (ID), gap width, and thickness. Shape distortion was assessed by measuring the changes in the flatness, roundness, and cylindricity values.

Size Distortion:

The average dimensional changes in diameter, gap width, and thickness for the carbonitrided and nitrocarburized C-rings are listed in Table 4.1 and shown Figures 4.1, 4.2, and 4.3, respectively. In comparing the results, the C-rings from group NCR-N exhibited smaller dimensional changes than those from group NCR-C with respect to OD, ID, and gap width; an increase in the OD and ID and a decrease in the gap width were measured. The largest dimensional change in the nitrocarburized Navy C-rings was with respect to OD; the average dimensional change measured +0.0207 mm.

Changes in the OD, ID, and gap width of the C-rings from group NCR-C were larger than group NCR-N; increases in the OD, ID, and gap widths were measured. For the carbonitrided C-rings, the largest amount of distortion was found at the gap width. The dimensional changes at the top, middle, and bottom of the gap width measured +0.1639 mm, +0.1714 mm, and +0.1676 mm, respectively. Such changes in gap distance

are not uncommon. In a study of the dimensional changes of steel Navy C-rings quenched in water, oil, and hot aqueous solutions, French [35] reported that the *changes in the width of the slot were larger, per unit of measured length, than those in the diameter of the gages*. Similar results were also reported by Webster [38] on a distortion study using oil quenched, high-carbon alloy steel, by Northwood *et al.* [36] on a study of the effects of heat treatment parameters on distortion in carburized SAE 8620 steel, and by Boyle *et al.* [37] in an investigation into the effects of initial microstructure on distortion in carburized SAE 8620 and PS-18 steel.

The increase in gap width of the C-rings from NCR-C and the decrease in gap width of those from NCR-N correspond well with the literature. Based upon previous work by Ohwada *et al.* [66] and Hernández-Morales *et al.* [30], it has been established that for steels which do not transform upon cooling, thermal stresses are responsible for the decrease in gap width. Hernández-Morales *et al.* explained the mechanisms responsible for distortion during quenching by modeling the evolution of the thermal and internal stress fields of a stainless steel Navy C-ring quenched in still water at 40 °C. While the gap width of the C-ring did increase in the early stages of quenching due to the contraction of the tips, over time and as the thicker sections of C-ring contracted, these ends were displaced inward toward the centre of the C-ring resulting in an overall decrease in gap width. For steel undergoing a phase transformation, the opposite effect is noted.

Size distortion was also evaluated by measuring the change in thickness at three locations (T-1, T-2, and T-3) in each of the Navy C-ring specimens. The average change in thickness at each of these locations was calculated for groups NCR-C and NCR-N and the results are listed in Table 4.1. These calculated averages were used to compare the two heat treatment processes. The nitrocarburizing of SAE 1020 steel was noted to give rise to larger overall dimensional changes with respect to the thickness of the Navy C-ring specimens. However, further investigation revealed this statement was not strictly correct because of the large standard deviations calculated, particularly in group NCR-N. The large standard deviations in this group were due, in part, to specimen NCR-N5, which showed a significant increase in thickness at each of the three measurement

positions: 0.1918 mm, 0.1919 mm, and 0.1910 mm at T-1, T-2, and T-3, respectively. When specimen NCR-N5 is excluded from the calculation, the average change in thickness at T-1, T-2, and T-3 decreases substantially becoming smaller than the average thickness distortion values calculated for the C-rings from NCR-C (see Figure 4.3b).

Table 4.1 Average size distortion values (diameter, gap width, and thickness) for the Navy C-ring specimens resulting from the carbonitriding and nitrocarburizing processes. See Appendix A for full results.

Size Distortion	Average Dimensional Change (mm)	
	Nitrocarburizing (NCR-N)	Carbonitriding (NCR-C)
Diameter		
OD	0.0207 (± 0.0007)	0.0683 (± 0.0041)
ID-1	0.0045 (± 0.0010)	0.0615 (± 0.0069)
ID-2	0.0034 (± 0.0004)	0.0481 (± 0.0063)
ID-3	0.0045 (± 0.0006)	0.0583 (± 0.0070)
Gap Width		
Top	-0.0075 (± 0.0017)	0.1639 (± 0.0171)
Middle	-0.0087 (± 0.0033)	0.1714 (± 0.0163)
Bottom	-0.0071 (± 0.0030)	0.1676 (± 0.0142)
Thickness		
T-1	0.0194 (± 0.0608)	-0.0070 (± 0.0076)
T-2	0.0184 (± 0.0611)	-0.0015 (± 0.0091)
T-3	0.0179 (± 0.0610)	-0.0016 (± 0.0068)

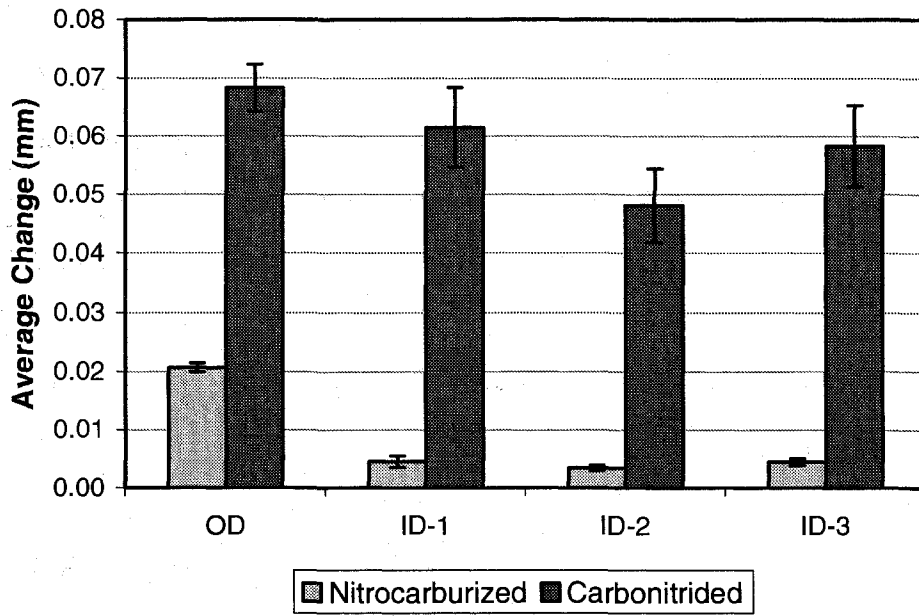


Figure 4.1 Average diameter (OD and ID) distortion for the Navy C-ring specimens induced by carbonitriding and nitrocarburizing.

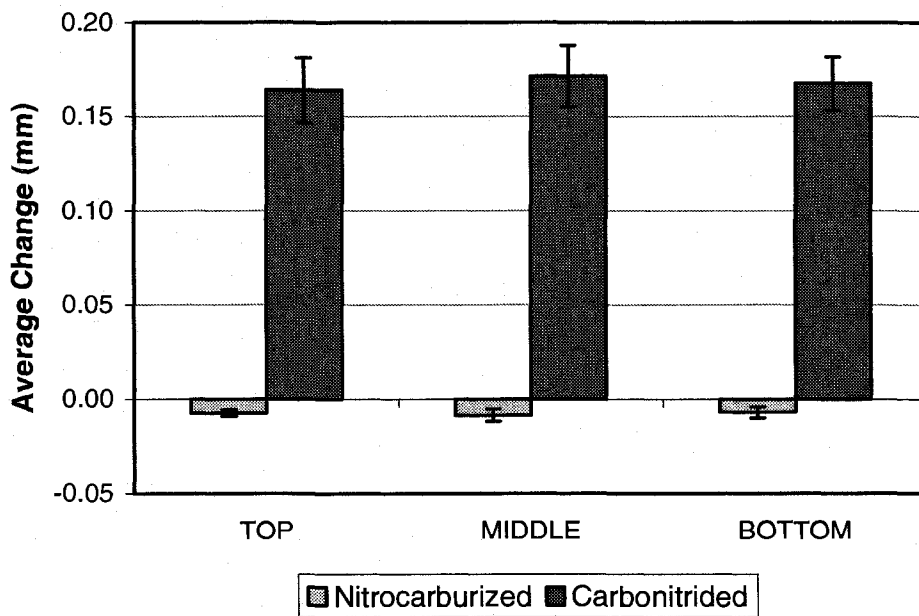
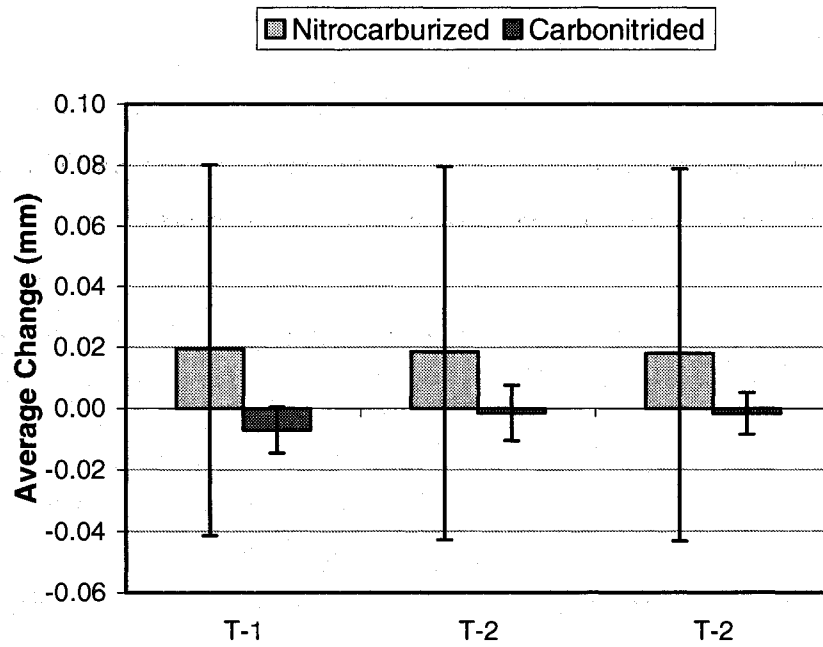
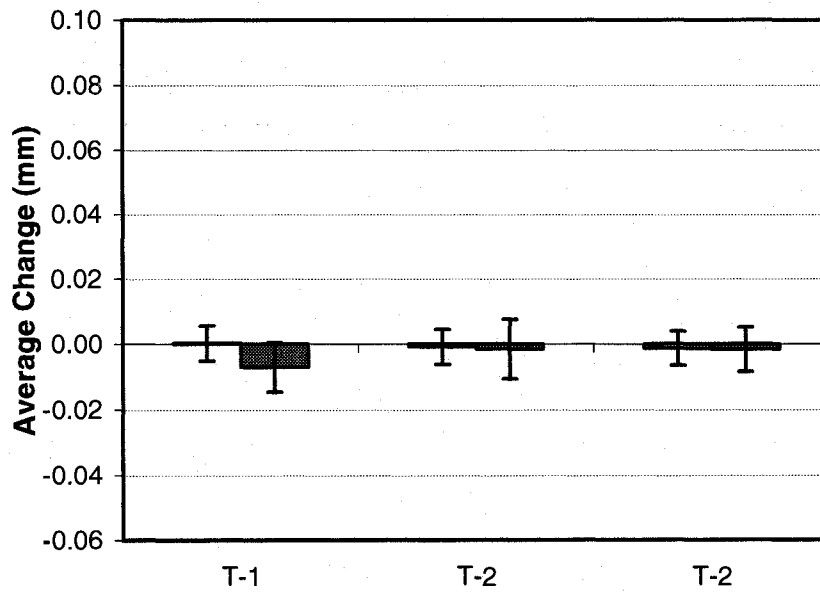


Figure 4.2 Average gap width distortion for the Navy C-ring specimens induced by carbonitriding and nitrocarburizing.



(a)



(b)

Figure 4.3 Average thickness distortion values for the Navy C-ring specimens induced by carbonitriding and nitrocarburizing. (a) Thickness distortion calculated by averaging all NCR-N values. (b) Thickness distortion calculated excluding NCR-N5.

Shape Distortion:

Unlike size distortion, which is a measure of actual dimensional change, shape distortion is evaluated by calculating the difference in the flatness, roundness, and cylindricity values before and after heat treatment. The average shape distortion values for the Navy C-rings from groups NCR-C and NCR-N are reported in Table 4.2. Changes in the flatness, roundness and cylindricity values are shown in Figures 4.4, 4.5, and 4.6, respectively. In comparing the results for both heat treatment processes, the C-rings from group NCR-N exhibited smaller changes in flatness and roundness distortion, but a larger change in cylindricity. For the C-rings from this group, increases in flatness, roundness, and cylindricity values were reported.

For the Navy C-rings from NCR-C, increases in flatness and roundness and a decrease in cylindricity were reported. Of these three values, the change in cylindricity was unexpected. Not only was the magnitude of change smaller than the value reported for the nitrocarburized steel, but also the average cylindricity value decreased, an indication that the C-rings had become more ‘in-shape’ as a result of the carbonitriding process.

Table 4.2 Average shape distortion values (flatness, cylindricity, and roundness) for the Navy C-ring specimens resulting from the carbonitriding and nitrocarburizing processes. See Appendix A for full results.

Shape Distortion	Average Dimensional Change (mm)	
	Nitrocarburizing (NCR-N)	Carbonitriding (NCR-C)
Flatness	0.0004 (± 0.0014)	0.0072 (± 0.0043)
Cylindricity	0.0082 (± 0.004)	-0.0020 (± 0.0031)
Roundness		
R-1	0.0004 (± 0.0028)	0.0060 (± 0.0067)
R-2	0.0011 (± 0.0036)	0.0110 (± 0.0049)
R-3	0.0009 (± 0.0043)	0.0054 (± 0.0065)

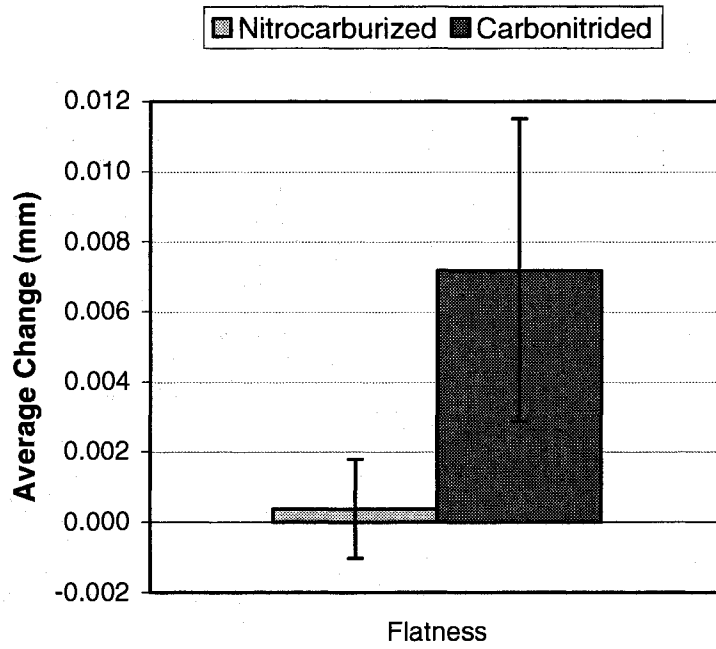


Figure 4.4 Average change in flatness values for the carbonitrided and nitrocarburized Navy C-ring specimens.

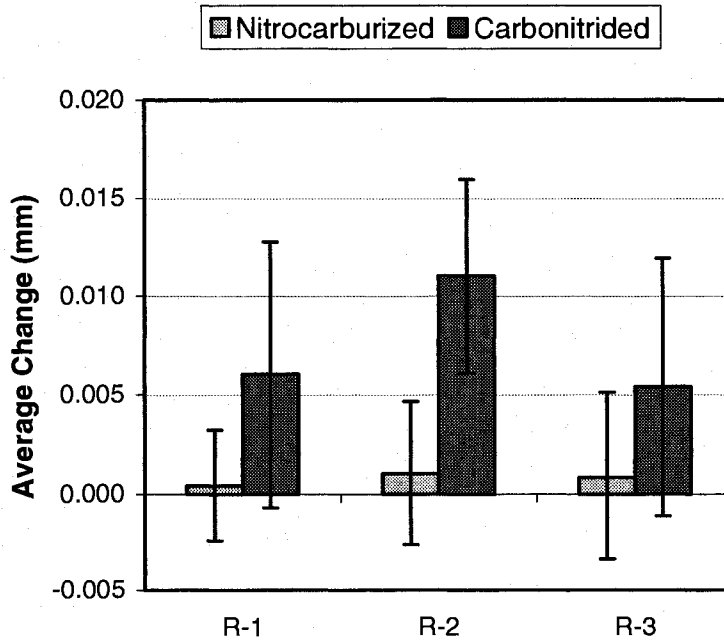


Figure 4.5 Average change in roundness values (R-1, R-2, and R-3) for the carbonitrided and nitrocarburized Navy C-ring specimens.

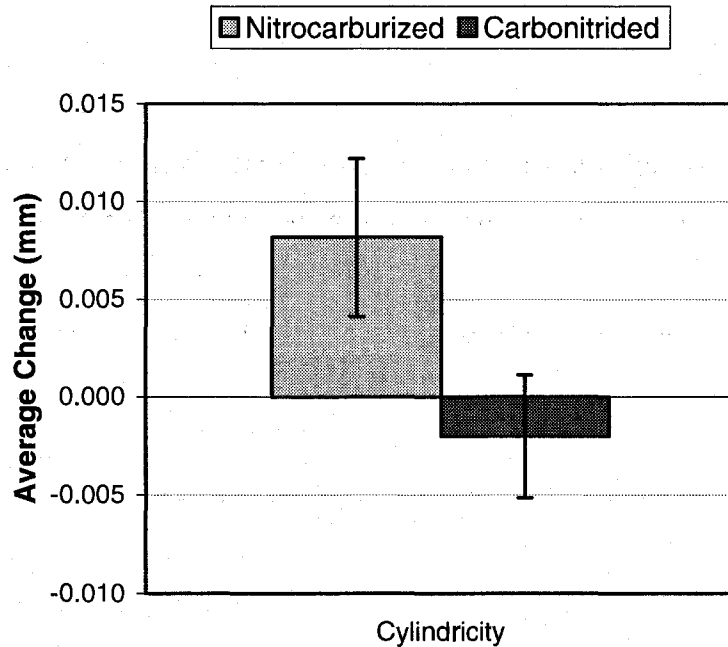


Figure 4.6 Average change in cylindricity values for the carbonitrided and nitrocarburized Navy C-ring specimens.

4.2 Torque Converter Pistons

Distortion in the torque converter pistons was evaluated using OD, ID, flatness, and taper of the lockup surface; their positions are shown in Figure 3.8. Changes in OD and ID were used to calculate size distortion. Changes in the total flatness and taper of the lockup surface were used to calculate shape distortion.

The variability of the distortion measures was difficult to compare between the carbonitrided and nitrocarburized pistons. The experimental design included an unequal number of pistons in the carbonitrided and nitrocarburized groups, three versus ten. In order to provide a more accurate comparison between the mean and standard deviation values, a random sample of three pistons was chosen from each of groups PN₅₁₀, PN₅₄₀, PN₅₆₅, PN₅₉₅, and PN₆₀₅. Consequently, it is expected that the standard deviation values of both treatments should be similar in magnitude; however, evidence of greater variability in results among the carbonitrided pistons is still observed.

Size Distortion:

OD and ID measurements were made at two separate locations along the height of each piston. The coordinates of these positions are given with respect to the lockup surface; -7.5 mm and -21.5 mm for OD and -11 mm and -15 mm for ID. The average dimensional change and standard deviation in the OD and ID of the carbonitrided and nitrocarburized torque converter pistons is reported in Table 4.3a.

The average dimensional changes in OD and ID along the height of the nitrocarburized pistons were similar and the variation was small. For the nitrocarburized pistons, an average increase in OD and ID was reported in all but one of the nitrocarburized heat treatment groups; the ID at -11 mm for the pistons in group PN₆₀₅ decreased by an average of -0.0039 ± 0.0020 mm.

For the carbonitrided pistons, not only was the standard deviation values larger, but the dimensional changes in OD and ID demonstrated both positive and negative variation from the initial values. Decreases in piston OD and ID were measured at those positions closest to the lockup surface at -7.5 mm and -11 mm, respectively. Further from the lockup surface increases in the OD and ID at -21.5 mm and -15 mm, were reported.

To ensure that the comparison between size distortion in the carbonitrided and nitrocarburized steel was indeed accurate, the processes were also compared using similar sample sizes. These results, shown in Table 4.3b and Figure 4.7, are consistent with the findings above.

Table 4.3a Average size distortion values (OD and ID) of the torque converter pistons resulting from the carbonitriding and nitrocarburizing processes. Sample sizes for the carbonitrided and nitrocarburized pistons are three and ten, respectively. See Appendix A for full results.

Size Distortion	No. of Samples	Average Dimensional Change (mm)			
		OD (-7.5 mm)	OD (-21.5 mm)	ID (-11 mm)	ID (-15 mm)
Carbonitriding	3	-0.0980 (± 0.0398)	0.0513 (± 0.0232)	-0.0745 (± 0.0085)	0.0138 (± 0.0083)
Nitrocarburizing					
P-N ₅₁₀	10	0.0934 (± 0.0017)	0.0864 (± 0.0074)	0.0026 (± 0.0019)	0.0147 (± 0.0018)
P-N ₅₄₀	10	0.0815 (± 0.0027)	0.0731 (± 0.0102)	0.0025 (± 0.0008)	0.0149 (± 0.0014)
P-N ₅₆₅	10	0.0764 (± 0.0035)	0.0713 (± 0.0139)	0.0041 (± 0.0010)	0.0165 (± 0.0025)
P-N ₅₉₅	10	0.0744 (± 0.0019)	0.0611 (± 0.0034)	0.0096 (± 0.0007)	0.0264 (± 0.0004)
P-N ₆₀₅	10	0.0696 (± 0.0030)	0.0658 (± 0.0118)	-0.0039 (± 0.0020)	0.0087 (± 0.0037)

Table 4.3b Average size distortion values (OD and ID) of the torque converter pistons resulting from the carbonitriding and nitrocarburizing processes. Sample sizes for the carbonitrided and nitrocarburized pistons are equal.

Size Distortion	No. of Samples	Average Dimensional Change (mm)			
		OD (-7.5 mm)	OD (-21.5 mm)	ID (-11 mm)	ID (-15 mm)
Carbonitriding	3	-0.0980 (± 0.0398)	0.0513 (± 0.0232)	-0.0745 (± 0.0085)	0.0138 (± 0.0083)
Nitrocarburizing					
P-N ₅₁₀	3	0.0940 (± 0.0015)	0.0909 (± 0.0064)	0.0012 (± 0.0007)	0.0131 (± 0.0021)
P-N ₅₄₀	3	0.0807 (± 0.0036)	0.0762 (± 0.0086)	0.0025 (± 0.0012)	0.0154 (± 0.0014)
P-N ₅₆₅	3	0.0745 (± 0.0035)	0.0798 (± 0.0153)	0.0038 (± 0.0012)	0.0177 (± 0.0027)
P-N ₅₉₅	3	0.0747 (± 0.0012)	0.0616 (± 0.0031)	0.0100 (± 0.0010)	0.0262 (± 0.0003)
P-N ₆₀₅	3	0.0698 (± 0.0023)	0.0746 (± 0.0086)	-0.0025 (± 0.0007)	0.0058 (± 0.0008)

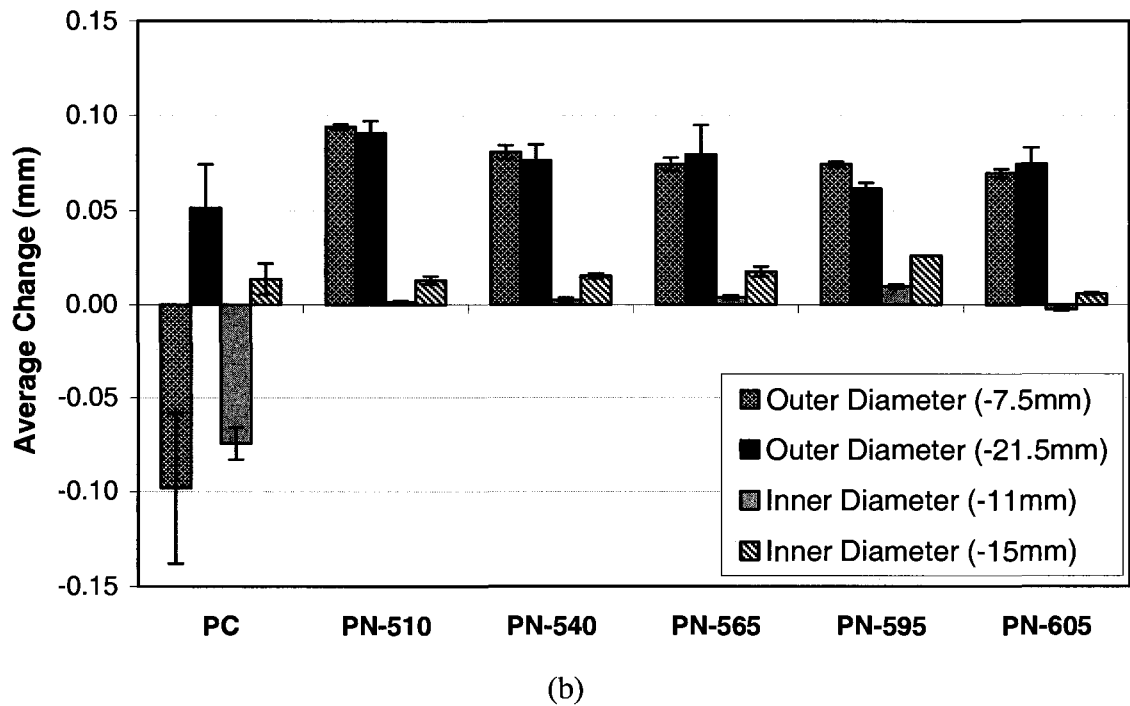
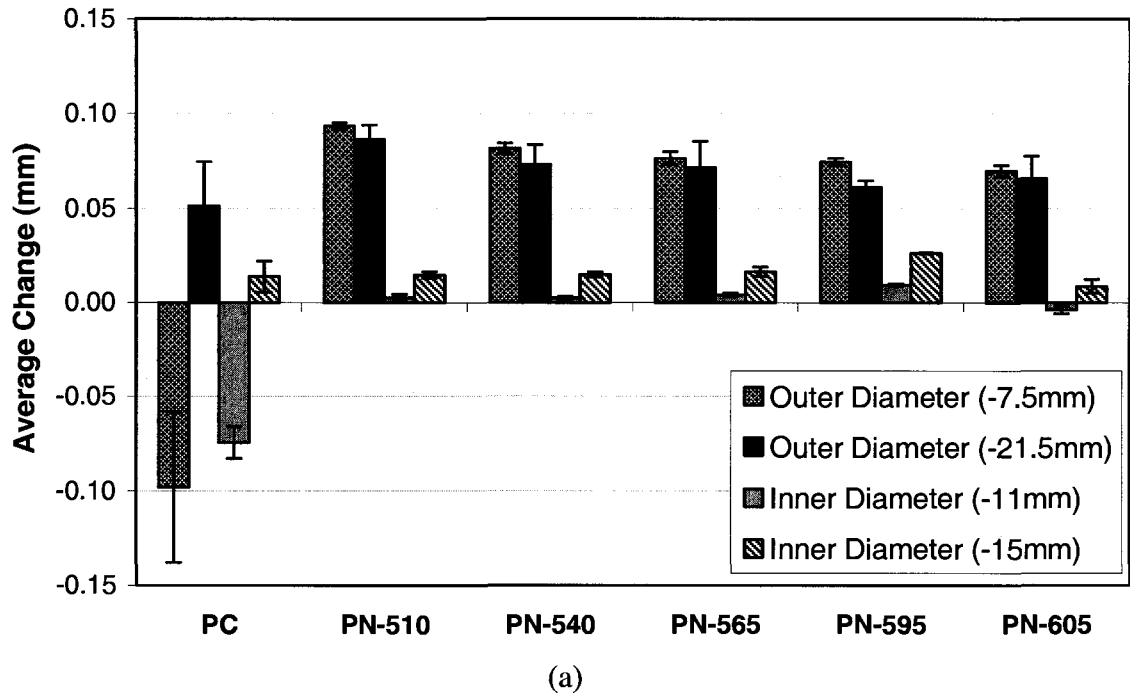


Figure 4.7 Average diameter distortion (OD and ID) for the carbonitrided and nitrocarburized torque converter pistons. (a) Values from Table 4.3a; all nitrocarburized pistons. (b) Values from Table 4.3b; a random sampling of three pistons from each PN group.

Shape Distortion:

Shape distortion for the pistons from groups PC and PN were evaluated by measuring the change in total flatness and flatness taper of the lockup surface. All results are reported in Table 4.4a and shown in Figures 4.8a and 4.9a. An evaluation of the processes using similar sample sizes is provided in Table 4.4b and shown in Figures 4.8b and 4.9b.

Comparing the carbonitriding and nitrocarburizing processes, the pistons from group PC exhibited much larger changes in both flatness and taper values than those in group PN. The standard deviation values calculated for the pistons in group PC were also larger, which provides yet another indication of the difficulty in predicting the distortion associated with the carbonitriding process.

In comparison with ferritic nitrocarburizing, the unpredictability in size and shape distortion of carbonitrided steel makes the process less suited in the production of torque converter pistons. Given the fact that the dimensional changes in nitrocarburized pistons were generally consistent and the variability small, it may be possible to predict and account for the distortion expected during heat treatment [17]. It can be suggested that replacing the carbonitriding process with gaseous ferritic nitrocarburizing and designing tooling to account for the dimensional changes expected during heat treatment will help to improve the production process by decreasing manufacturing time and reducing the costs associated with part scrap and the elimination of the finish grinding step.

Table 4.4a Average shape distortion values (total flatness and taper) of the torque converter pistons induced by carbonitriding and nitrocarburizing. Sample sizes for the carbonitrided and nitrocarburized pistons are three and ten, respectively. See Appendix A for full results.

Average Dimensional Change (mm)			
Shape Distortion	No. of Samples	Total Flatness	Taper of the Lockup Surface
Carbonitriding	3	0.5632 (± 0.3336)	0.3873 (± 0.3349)
Nitrocarburizing			
P-N ₅₁₀	10	0.0310 (± 0.0151)	0.0308 (± 0.0107)
P-N ₅₄₀	10	0.0380 (± 0.0182)	0.0332 (± 0.0195)
P-N ₅₆₅	10	0.0417 (± 0.0110)	0.0399 (± 0.0158)
P-N ₅₉₅	10	0.0334 (± 0.0103)	0.0348 (± 0.0086)
P-N ₆₀₅	10	0.0291 (± 0.0142)	0.0241 (± 0.0138)

Table 4.4b Average shape distortion values (total flatness and taper) of the torque converter pistons induced by carbonitriding and nitrocarburizing. Sample sizes for the carbonitrided and nitrocarburized pistons are equal.

Average Dimensional Change (mm)			
Shape Distortion	No. of Samples	Total Flatness	Taper of the Lockup Surface
Carbonitriding	3	0.5632 (± 0.3336)	0.3873 (± 0.3349)
Nitrocarburizing			
P-N ₅₁₀	3	0.0337 (± 0.0063)	0.0268 (± 0.0085)
P-N ₅₄₀	3	0.0406 (± 0.0143)	0.0405 (± 0.0368)
P-N ₅₆₅	3	0.0449 (± 0.0013)	0.0340 (± 0.0059)
P-N ₅₉₅	3	0.0293 (± 0.0067)	0.0344 (± 0.0008)
P-N ₆₀₅	3	0.0311 (± 0.0128)	0.0297 (± 0.0105)

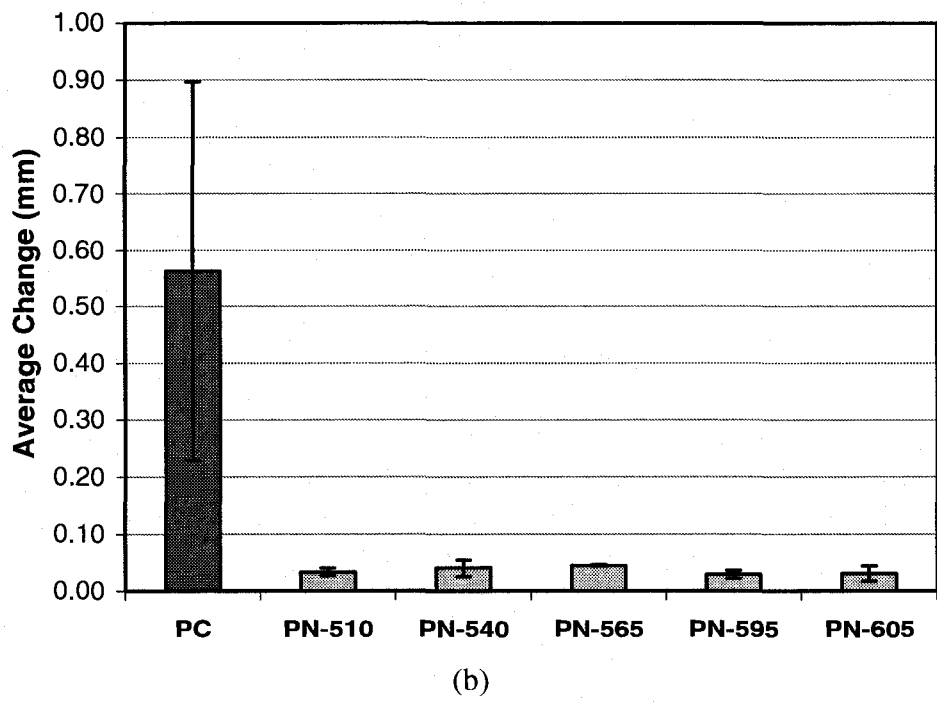
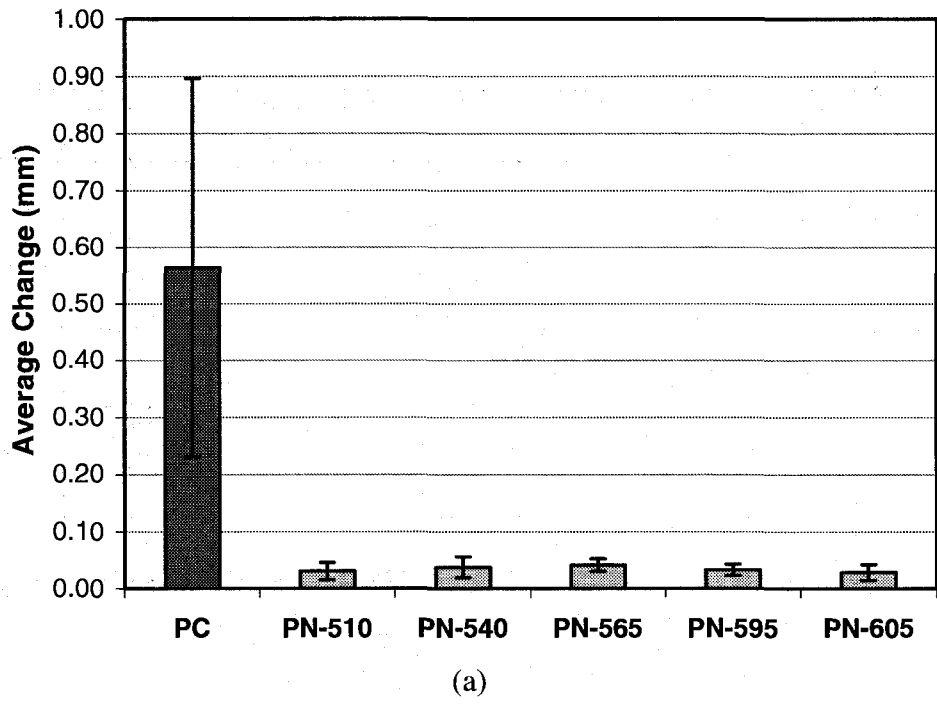
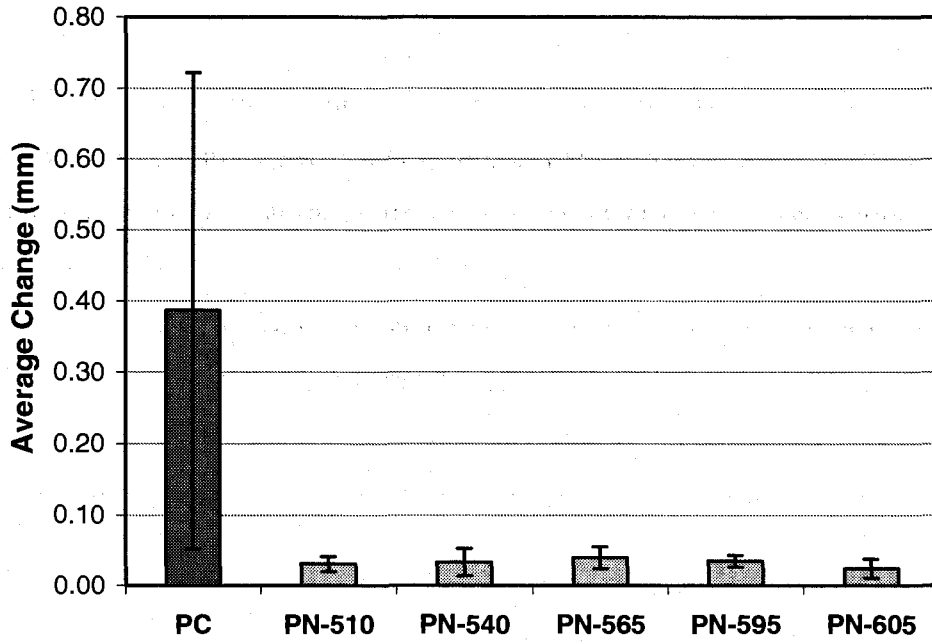
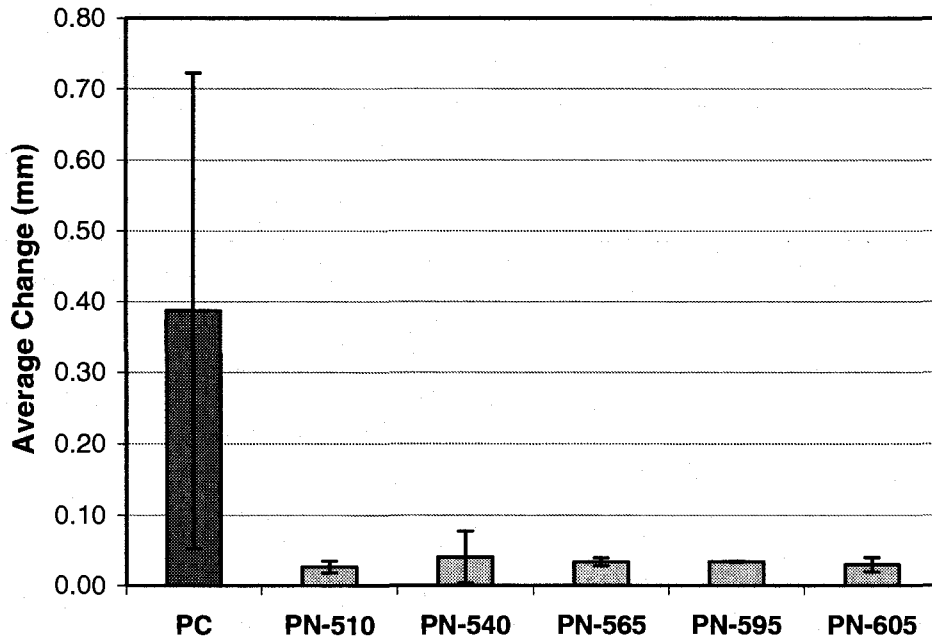


Figure 4.8 Average change in total flatness values for the carbonitrided and nitrocarburized torque converter pistons. (a) Values from Table 4.4a; all nitrocarburized pistons. (b) Values from Table 4.4b; a random sampling of three pistons from each PN group.



(a)



(b)

Figure 4.9 The average change in flatness taper values for the carbonitrided and nitrocarburized torque converter pistons. (a) Values from Table 4.4a; all nitrocarburized pistons. (b) Values from Table 4.4b; a random sampling of three pistons from each PN group.

4.3 Hypothesis Testing of Size and Shape Distortion

The purpose of hypothesis testing is to formulate and test a null hypothesis (H_0). In this study, hypothesis testing attempted to prove that the mean size and shape distortion values for the pistons in groups PN₅₁₀, PN₅₄₀, PN₅₆₅, PN₅₉₅, and PN₆₀₅ were less than the mean size and shape distortions for the pistons in group PC. The system has eleven degrees of freedom ($n_{\text{carbonitriding}} + n_{\text{nitrocarburizing}} - 2$) and an ' α ' value of 0.050 was chosen; the value of t_{α} , from the 'Table of Percentage Points of the t-Distributions' [67] is therefore 1.796. An example of the hypothesis testing performed in this study is provided in Appendix B.

The results from hypothesis testing show a failure to reject the null hypothesis occurred in a majority of the cases with the exception those groups listed below:

- OD (-21.5 mm) - PN₅₁₀, PN₅₄₀, and PN₅₆₅
- OD (-7.5 mm) - PN₅₆₅, PN₅₉₅, and PN₆₀₅
- ID (-15 mm) - PN₅₉₅

Accordingly, in thirty of the tests there were seven instances in which the null hypothesis could be rejected with a confidence interval of 95%. Therefore, it can be stated with a high level of certainty that the mean size distortion and particularly the shape distortion of the nitrocarburized pistons is in fact less than the mean distortion of the carbonitrided pistons.

4.4 Understanding Size and Shape Distortion

Overall, the dimensional changes of the carbonitrided C-Rings are consistent with the test results of Boyle *et al.* [37] for the distortion of carburized Navy C-Rings machined from SAE 8620 and PS-18 steels. The larger dimensional changes in the Navy C-rings and torque converter pistons from groups NCR-C and PC, respectively can be explained by the high temperatures associated with the carbonitriding process, particularly the phase transformation of austenite to martensite that takes place when the steel is quenched. Because this phase transformation is absent in the nitrocarburizing process much of this distortion is avoided. Size distortion in the nitrocarburized steel is thought to be attributed to the diffusion of nitrogen. According to Pye [25], *with the*

diffusion of nitrogen into the steel surface, volume change will occur, which means a size change in the form of growth.

There are a number of factors that give rise to shape distortion. While the stresses developed during the manufacturing process tend to manifest themselves upon heating [25], it is generally thought that the quenching step is a major contributing factor. During carbonitriding, not only is there a risk of non-uniform quenching, but also of an incomplete phase transformation of austenite to martensite. The presence of retained austenite in the surface of the steel is an indication that mixed phases do exist. According to the literature [25], these phases give rise to residual stresses that contribute to dimensional changes in the steel. The percent volume of retained austenite in carbonitrided and nitrocarburized steel is discussed in Section V.

RESULTS AND DISCUSSIONS

V. EFFECT OF HEAT TREATMENT ON RETAINED AUSTENITE AND RESIDUAL STRESS

This section discusses the effect of heat treatment on the retained austenite content and residual stress values at the surface and near surface of plain carbon steels. X-ray diffraction (XRD) techniques were used to make retained austenite and residual stress measurements at multiple locations, extending from the surface of the steel inward through the case. For the Navy C-rings, two specimens were chosen, one from group NCR-C and the other from NCR-N; both retained austenite and residual stress measurements were made at the 'bottom' position of each C-ring along the outside diameter (OD). For the torque converter pistons, retained austenite and residual stress values were measured at the lockup surface for four of the torque converter pistons, one from each of the following groups: P-C, P-N₅₁₀, P-N₅₆₅, and P-N₆₀₅. Retained austenite and residual stress profiles for the Navy C-rings and torque converter pistons were generated, and a comparison of the results is presented.

5.1 Retained Austenite

Retained austenite content was measured using an XRD technique known as the *Four-Peak Method*. Measurement positions extended from the surface of the steel inward through the case to a depth of approximately 1.5 mm. Volume data for retained austenite in the carbonitrided and nitrocarburized Navy C-rings and torque converter pistons are provided in Table 5.1 and 5.2, respectively.

5.1.1 Navy C-rings

Figure 5.1 shows the retained austenite profiles for the carbonitrided and nitrocarburized Navy C-rings, specimens NCR-C10 and NCR-N2, respectively. Overall, the general shape of the profiles is similar. The volume of retained austenite is highest at the surface of the steel and decreases with increasing depth, results that are consistent with the profiles of properly carburized and hardened steels [6]. The depth values indicated in Table 5.1 and Figure 5.1 represent the location of the retained austenite measurements with respect to the surface of the Navy C-ring.

The difference between the carbonitrided and nitrocarburized profiles lies in the retained austenite content. Overall, the volume of retained austenite was higher in the carbonitrided steel, 23.0% at the surface of NCR-C10 in comparison with 6.8% at the surface of NCR-N2. While the retained austenite level in NCR-C10 slowly decreased to 2.4% at a depth of 1.47 mm, the retained austenite level in NCR-N2 dropped immediately; a value of 1.0% was measured at a depth just 13 μm below the surface.

Table 5.1 Retained austenite content in the Navy C-ring specimens. Measurements were made at the 'bottom' position of the C-ring inward through the case to a depth of approximately 1.5 mm. Error in the results: $\pm 2\%$.

Percent Retained Austenite (% RA)			
Nitrocarburizing (NCR-N2)		Carbonitriding (NCR-C10)	
Depth (mm)	% RA	Depth (mm)	% RA
0.0000	6.8	0.0000	23.0
0.0127	1.0	0.0127	19.7
0.0254	0.8	0.0254	18.1
0.1397	1.6	0.1295	15.8
0.5080	1.3	0.5080	4.5
1.4986	1.6	1.4732	2.4

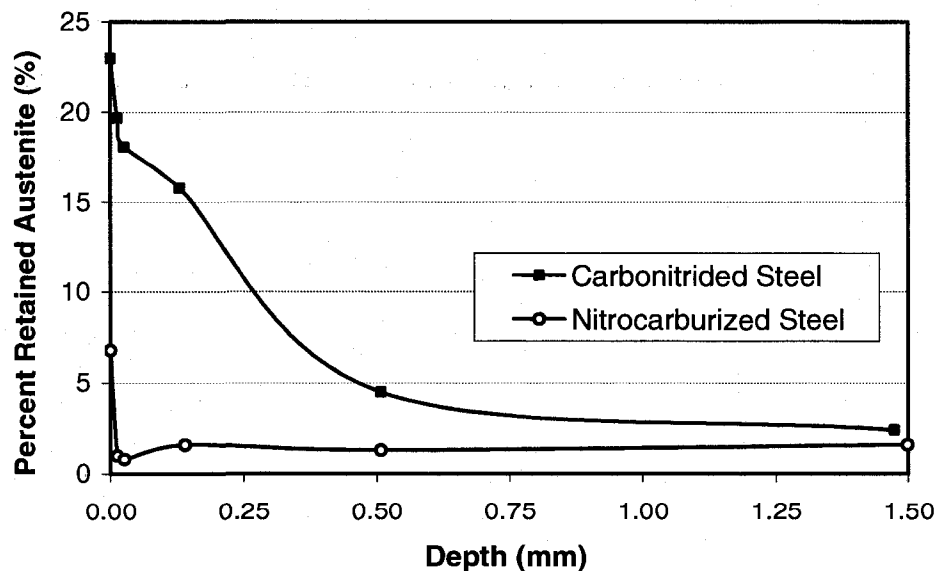


Figure 5.1 Retained austenite profiles of the carbonitrided and nitrocarburized Navy C-ring specimens, NCR-C10 and NCR-N2, respectively.

5.1.2 Torque Converter Pistons

The retained austenite profiles of the carbonitrided and nitrocarburized torque converter pistons are shown in Figure 5.2a. The depth values indicated in Table 5.2 and Figure 5.2a represent the location of the retained austenite measurements with respect to the surface of the torque converter piston. Similar to the results obtained for the Navy C-ring specimens, the largest percent volume of retained austenite was measured in the carbonitrided steel. For PC-1, a maximum value of 12.7% was measured, not at the surface but at a distance of 28 μm below it. Similar results have also been reported by researchers studying retained austenite values in carburized [22, 68, 69] and carbonitrided [68] steels indicating that the maximum value of retained austenite does not necessarily occur at the surface of carburized and carbonitrided steels. In a study performed by Gu *et al.* [68] on the mechanical properties of carburized and carbonitrided Cr-Ni-Mo steels, the retained austenite profiles for both heat treatment processes showed that the maximum percent volume of retained austenite was not measured at the surface, but rather at some distance below it.

For the nitrocarburized pistons, maximum values of retained austenite were measured at the surface of the steel; values of 2.5%, 4.2%, and 5.3% for pistons PN₅₁₀-1, PN₅₆₅-3 and PN₆₀₅-2 were reported. The fact that the retained austenite content was highest in the piston from group PN₆₀₅ was not surprising. At temperatures between 590 and 721°C which correspond to the eutectoid (A₁) on the Fe-N and Fe-C systems, respectively, the process is no longer classified as ferritic nitrocarburizing but is instead referred to as austenitic nitrocarburizing [70, 71]. Because austenitic nitrocarburizing takes place in the austenitic phase field of the steel, some retained austenite is expected in the final component. Upon quenching, austenite is retained and can be seen as an intermediate zone located beneath the compound layer. Upon slow cooling, the retained austenite transforms into a pearlite-like structure referred to as Braunitite [22, 70]. Although all the nitrocarburized pistons were furnace-cooled, it is suspected that some of the austenite did not undergo this transformation thus resulting in the presence of retained austenite at the surface and near surface of the steel.

Table 5.2 Retained austenite content in the torque converter pistons. Measurements were made from the lockup surface inward through the case to a depth of approx. 1.5 mm.

Percent Retained Austenite (% RA)							
PC, Sample 1		PN-510, Sample 1		PN-565, Sample 3		PN-605, Sample 2	
Depth (mm)	% RA	Depth (mm)	% RA	Depth (mm)	% RA	Depth (mm)	% RA
0.0000	11.8	0.0000	2.5	0.0000	4.2	0.0000	5.3
0.0127	12.3	0.0127	1.1	0.0127	1.2	0.0127	5.0
0.0279	12.7	0.0305	0.3	0.0254	0.6	0.0254	0.5
0.1346	8.5	0.1422	0.6	0.1270	0.5	0.1549	1.4
0.5410	0.7	0.5182	0.6	0.5309	0.6	0.4953	0.4
1.5215	5.0	1.6129	0.4	1.5342	0.6	1.5443	0.3

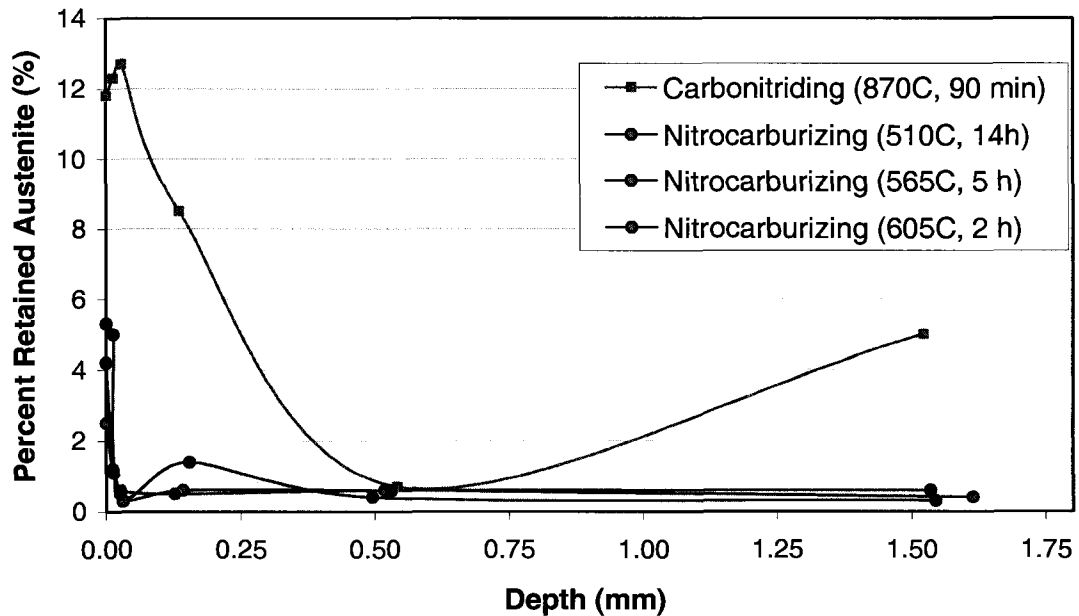


Figure 5.2a Retained austenite profiles for the carbonitrided (PC-1) and nitrocarburized torque converter pistons (PN₅₁₀-1, PN₅₆₅-3 and PN₆₀₅-2).

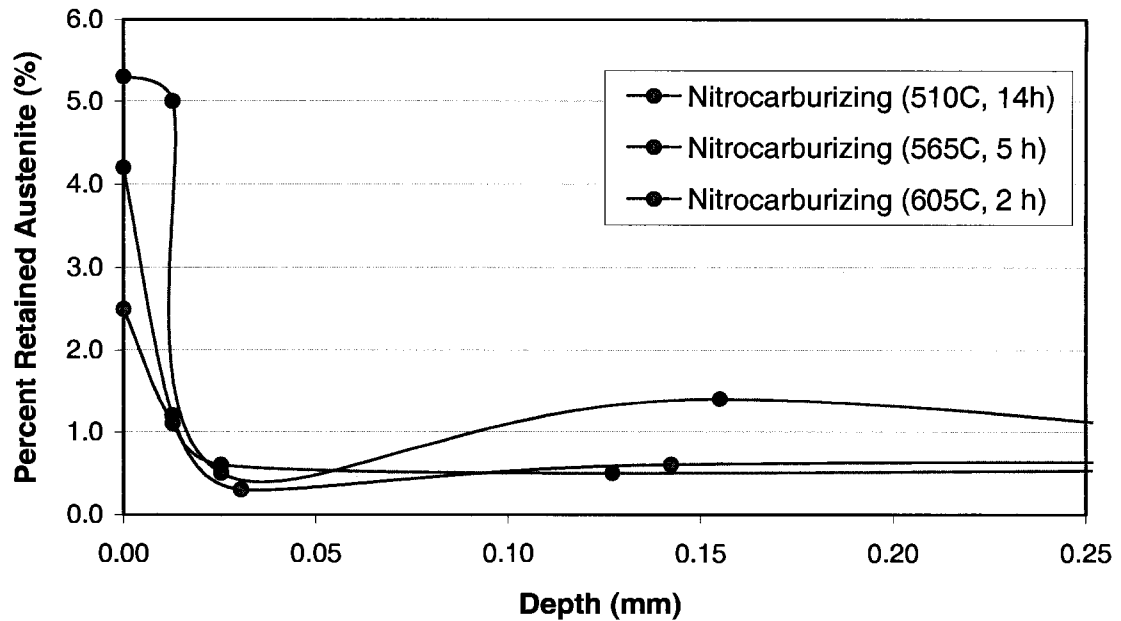


Figure 5.2b Retained austenite profiles for the nitrocarburized torque converter pistons (PN₅₁₀-1, PN₅₆₅-3 and PN₆₀₅-2) from the surface to a depth of 0.25 mm.

5.1.3 Understanding the Presence of Retained Austenite in Surface Treated Steels

Since the carbonitriding process takes place in the austenitic phase field of the steel, the higher percentages of retained austenite in NCR-C10 and PC-1 were not unexpected. According to the literature [31, 40], the presence of retained austenite can be attributed to the following principal factors - chemical composition, austenitizing temperature, the lowest temperature to which the hardened specimen is cooled, and the cooling rate from the austenite phase field. As mentioned earlier, the diffusion of carbon and nitrogen into the surface of the steel are also contributing factors; both are known to depress the M_s temperature and cause the austenite to be retained within the steel [71]. Of all the alloying elements, carbon promotes the greatest retention of austenite during quenching and is especially unfavourable in carbon and low alloy steels [31, 42].

Eliminating the presence of retained austenite in the steel requires cooling the workpiece below the M_f temperature. Because this temperature generally falls below room temperature in many hardenable steels [40], cryogenic cooling is often required.

Because neither the carbonitrided C-rings nor the pistons were cooled to such extremely low temperatures, the presence of retained austenite at the surface is expected.

The effect of processing temperature on retained austenite content is apparent not only between the carbonitriding and nitrocarburizing processes, but also when comparing the volume of retained austenite between the nitrocarburized pistons. The higher the process temperature, the more retained austenite present in the final component. In comparing the carbonitriding and nitrocarburizing processes, the lower retained austenite content in the nitrocarburized samples is attributed to the lower processing temperatures, and consequently the lack of phase transformation to and from austenite. The effect of process temperature was even evident in the absence of a phase transformation. A closer look at the retained austenite profiles of the nitrocarburized pistons from groups PN₅₁₀, PN₅₆₅, and PN₆₀₅ is presented in Figure 5.2b. Results here show that even small variations in process temperature (40-55 °C) appear to affect the volume of retained austenite; the higher the process temperature, the higher the retained austenite content measured. It is considered that this increase is the result of increased diffusion rates of carbon and nitrogen into the surface of steel [18]. As discussed earlier, carbon influences the amount of retained austenite in steel; nitrogen acts as an austenite stabilizer by reducing both the transformation temperature and transformation rate of the austenite and by preventing the formation of the more stable martensitic structure.

5.2 Residual Stress

Residual stress values were also determined by means of XRD using CrK α X-ray radiation to measure the lattice deformations on the {211} diffraction planes of the martensite peak. Stresses in both the Navy C-rings and torque converter pistons were measured at multiple locations, extending from the surface of the steel inward through the case. The residual stress values for the carbonitrided and nitrocarburized Navy C-rings and torque converter pistons are provided in Tables 5.3, 5.4, 5.5, and 5.6. The depth values, mm, represent the location of the residual stress measurements with respect to the surface of the Navy C-rings and torque converter pistons.

5.2.1 Navy C-rings

Surface Residual Stresses:

Surface residual stresses, Table 5.3, were measured during the preliminary phase of the study and used in the initial comparison between the carbonitriding and nitrocarburing processes. Values of -262 MPa and -97 MPa were measured at the surface of NCR-N2 and NCR-C10, respectively. While these preliminary findings led to the initial assumption that compressive residual stresses were higher in nitrocarbured steels, the residual stress profiles of the Navy C-rings revealed otherwise.

Residual Stress Profiles:

The residual stress profiles for the nitrocarbured and carbonitrided Navy C-rings are shown in Figure 5.3. Hoop and axial stresses were measured at eleven locations, extending inward from the surface to a depth of approximately 2.5 mm. For NCR-N2, the maximum compressive residual stresses were measured at the surface; values of -241 MPa and -290 MPa for hoop and axial stresses were reported. For NCR-C10, maximum compressive stresses were not measured at the surface of steel but rather at a depth of 0.5080 mm. Hoop and axial stresses measured -352 MPa and -427 MPa, respectively.

Table 5.3 Surface residual stress values for the Navy C-rings and torque converter pistons.

	Surface Residual Stress (MPa)	
	Nitrocarburing	Carbonitriding
Navy C-ring	-262	-97
Torque Converter Piston	117	-207

Table 5.4 Residual stresses measurements for the Navy C-ring specimens. Measurements were made from the 'bottom' position of the C-ring inward through the case to a depth of approximately 2.5 mm. (a) NCR-C10 (b) NCR-N2.

Carbonitriding (NCR-C10)		
Depth (mm)	Residual Stress (MPa)	
	Hoop Stress	Axial Stress
0.0000	-110.32 ± 14	-151.68 ± 21
0.0127	-144.79 ± 34	-117.21 ± 21
0.0254	-220.63 ± 21	-193.05 ± 14
0.0737	-220.63 ± 21	-193.05 ± 21
0.1295	-248.21 ± 41	-268.90 ± 21
0.2718	-337.84 ± 28	-399.90 ± 21
0.5080	-351.63 ± 7	-427.47 ± 14
1.0160	-172.37 ± 7	-268.90 ± 14
1.4732	-89.63 ± 14	-234.42 ± 14
2.0320	-27.58 ± 7	-137.90 ± 14
2.6416	34.47 ± 7	-41.37 ± 14

(a)

Nitrocarburizing (NCR-N2)		
Depth (mm)	Residual Stress (MPa)	
	Hoop Stress	Axial Stress
0.0000	-241.32 ± 21	-289.58 ± 7
0.0127	-158.58 ± 21	-179.26 ± 21
0.0254	-151.68 ± 14	-158.58 ± 28
0.0737	-158.58 ± 21	-158.58 ± 14
0.1397	-241.32 ± 21	-234.42 ± 21
0.2413	-158.58 ± 14	-144.79 ± 21
0.5080	-55.16 ± 7	-55.16 ± 14
1.0160	-20.68 ± 14	-41.37 ± 14
1.4986	-6.89 ± 14	20.68 ± 14
1.9812	0.00 ± 21	-6.89 ± 14
2.4892	-20.68 ± 21	-20.68 ± 14

(b)

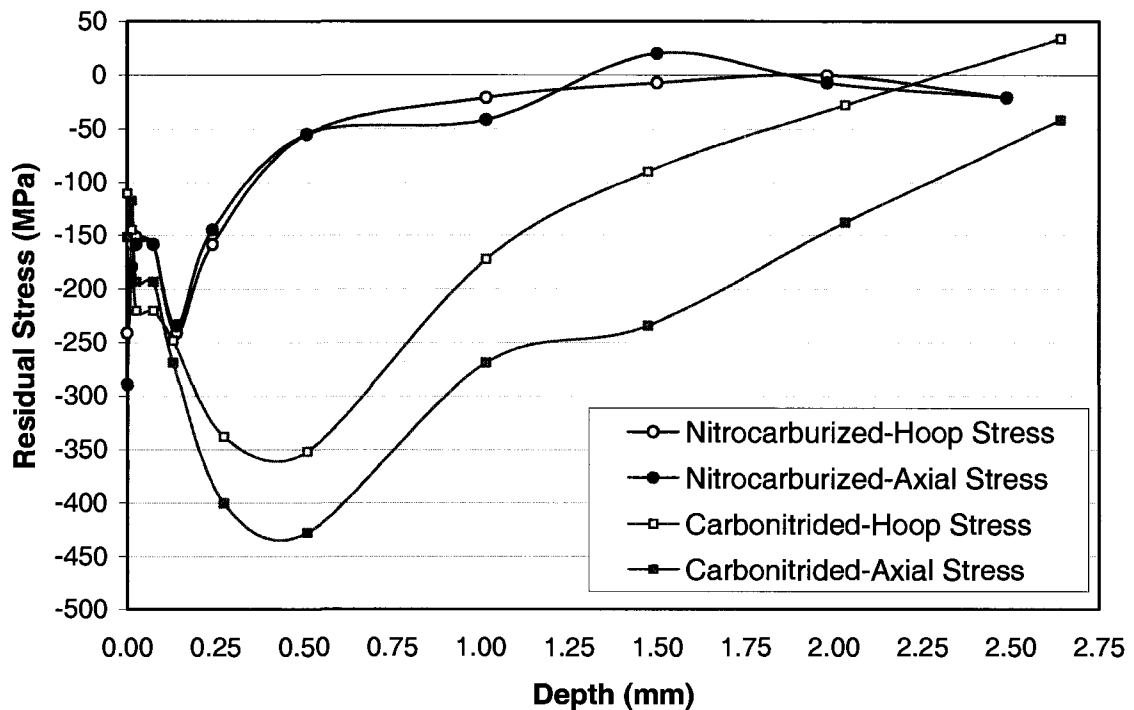


Figure 5.3 Residual stress profiles for the carbonitrided and nitrocarburized Navy C-ring specimens, NCR-C10 and NCR-N2, respectively.

5.2.2 Torque Converter Pistons

Surface Residual Stresses:

Surface residual stresses were also used in the preliminary comparison between the carbonitriding and nitrocarburizing processes. Stresses were measured in two pistons, one from group PC and the other from PN₅₆₅; values of -207 MPa and +117 MPa were reported for PC-1 and PN₅₆₅-2, respectively. To confirm the presence of tensile stresses at the surface of the nitrocarburized steel, an additional residual stress measurement was made on the surface of PN₅₆₅-3 and a value of +103 MPa was reported. According to Kolozsváry [56], *data in the literature show a wide range of values for residual stresses, [in nitrided and nitrocarburized steels, however,] it is generally agreed that tensile stresses appear in the ϵ compound layer* but are sometimes not detected due to technical difficulties with XRD. Because the compound layer is so thin, the x-rays often penetrate beyond the surface, returning values of compressive residual stress from deeper within the case.

To isolate the residual stresses in the compound layer of the nitrocarburized pistons, further testing was performed, this time using the {302} reflection from the iron nitride (Fe_3N) phase. The x-ray diffractometer was operated at 22 kV and 5 mA with $\text{CrK}\alpha$ radiation. Surface residual stresses were measured on the lockup surface of eight of the ten torque converter pistons from group PN_{510} . These surface residual stress values, all tensile, are shown in Table 5.5. In their paper entitled ‘Measurement and Analysis of Residual Stress in ϵ -Phase Iron Nitride Layers as a Function of Depth’, T.R. Watkins *et al.* [72] found, using both ψ tilt and grazing incidence x-ray diffraction methods, that the residual stresses in ϵ -phase layer of the nitrided steel were tensile and varied within the first 2 μm of the 10 μm layer. Using standardized hole drilling techniques (ASTM E 837), V. Leskovšek *et al.* [73] found tensile residual stresses at the surface of H11 tool steel nitrocarburized for 8 h at 580°C.

Table 5.5 Surface residual stress values for the torque converter pistons from group PN_{510} .

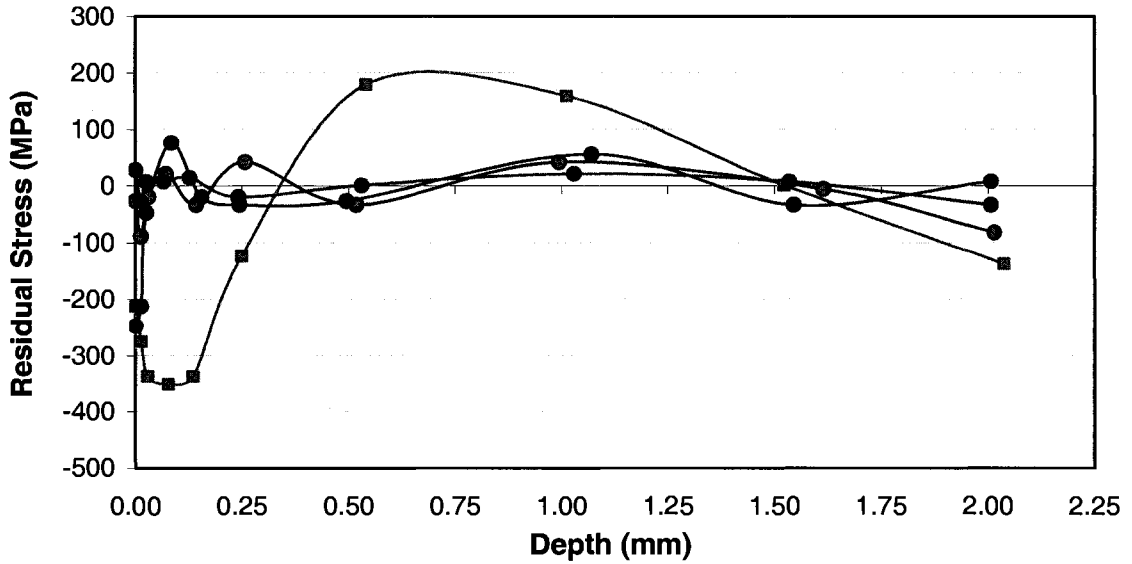
Surface Residual Stress (MPa)	
Group PN_{510}	
Sample No.	Residual Stress (MPa)
2	138 \pm 55
3	179 \pm 41
4	117 \pm 41
5	214 \pm 41
6	110 \pm 48
7	152 \pm 34
9	76 \pm 41
10	103 \pm 55

Residual Stress Profiles:

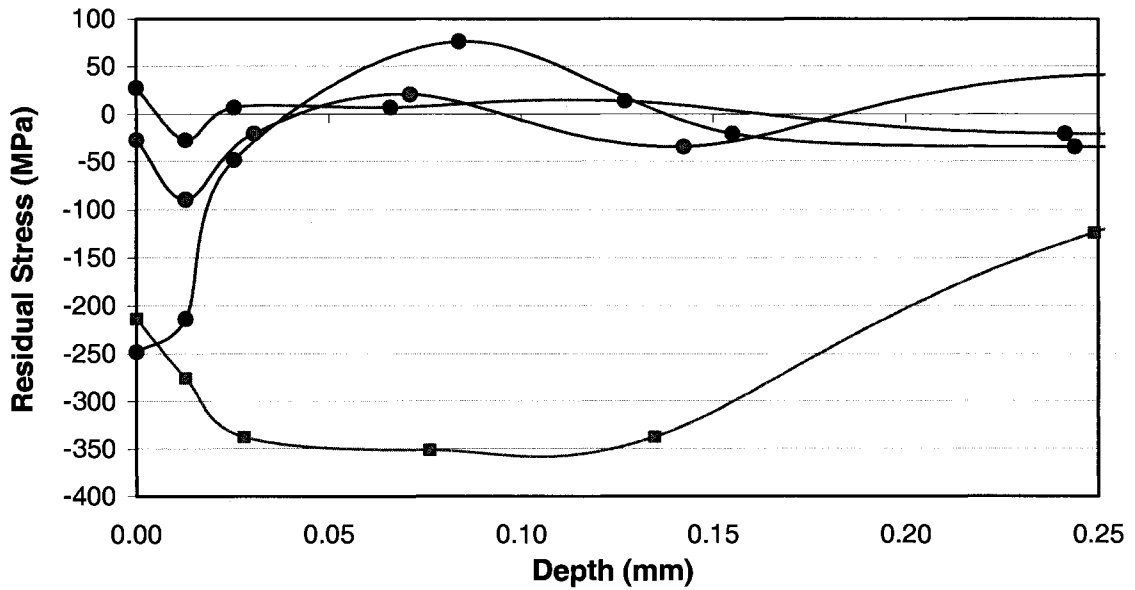
The residual stress profiles of the carbonitrided and nitrocarburized pistons are shown in Figure 5.4. Hoop stresses were measured at ten locations extending from the lockup surface to a depth of approximately 2 mm. Overall, maximum compressive residual stresses were measured in the carbonitrided steel. For PC-1, a value of -352 MPa was measured at a depth of 0.0762 mm from the surface. The nitrocarburized pistons, PN₅₁₀-1, PN₅₆₅-3, and PN₆₀₅-2, were noted to give rise to overall lower compressive stress values than those found in PC-1; their maximum compressive residual stress values were measured closer to the surface of the steel. It should also be noted that because the residual stresses were measured using the {211} diffraction planes of the martensite peak instead of the {302} reflection from the iron nitride (Fe₃N) phase, it is not known for certain whether or not the surface stresses measured in the nitrocarburized pistons are an accurate representation of the actual stresses at the surface of the steel.

Table 5.6 Residual stress values for the torque converter pistons. Measurements were made from the lockup surface inward through the case to a depth of approximately 2 mm.

Residual Stress Content (MPa)							
PC, Sample 1		PN-510, Sample 1		PN-565, Sample 3		PN-605, Sample 2	
Depth (mm)	RS (MPa)	Depth (mm)	RS (MPa)	Depth (mm)	RS (MPa)	Depth (mm)	RS (MPa)
0.0000	-214 ± 14	0.0000	-28 ± 14	0.0000	28 ± 21	0.0000	-248 ± 69
0.0127	-276 ± 21	0.0127	-90 ± 28	0.0127	-28 ± 21	0.0127	-214 ± 21
0.0279	-338 ± 21	0.0305	-21 ± 28	0.0254	7 ± 14	0.0254	-48 ± 21
0.0762	-352 ± 21	0.0711	21 ± 28	0.0660	7 ± 21	0.0838	76 ± 21
0.1346	-338 ± 21	0.1422	-34 ± 21	0.1270	14 ± 28	0.1549	-21 ± 14
0.2489	-124 ± 7	0.2565	41 ± 21	0.2413	-21 ± 21	0.2438	-34 ± 21
0.5410	179 ± 21	0.5182	-34 ± 28	0.5309	0 ± 14	0.4953	-28 ± 21
1.0109	159 ± 41	0.9931	41 ± 28	1.0287	21 ± 28	1.0693	55 ± 28
1.5215	0 ± 28	1.6129	-7 ± 28	1.5342	7 ± 28	1.5443	-34 ± 28
2.0371	-138 ± 28	2.0142	-83 ± 28	2.0066	-34 ± 21	2.0066	7 ± 34



(a)



(b)

Figure 5.4 Residual stress profiles for the carbonitrided and nitrocarburized torque converter pistons from groups PC, PN₅₁₀, PN₅₆₅, and PN₆₀₅. (a) 0 - 2.25 mm (b) 0 - 0.25 mm.

5.2.3 Relationship Between Retained Austenite Content and Residual Stress Values

The shape of the residual stress profiles for NCR-C10 and PC-1 were consistent with findings in literature for correctly carburized and hardened steel [6]. The maximum residual stress value was not measured at the surface of the steel, but rather at some distance below it. It is the high levels of retained austenite at the surface of the steel that are believed to be a contributing factor. Retained austenite lowers the compressive yield strength of martensitic/austenitic structures [6], giving rise to lower residual stresses than those developed during a complete martensitic transformation [6]. Figure 5.5 plots the residual stress and retained austenite profiles for NCR-C10. This plot provides a clear example of the relationship between compressive residual stress and retained austenite. The maximum compressive residual stress is not measured at the surface of the steel, where the retained austenite content is high, but rather at a distance below the surface, corresponding to a lower retained austenite content. Similar results have also been reported for in-service carburized 8720 steel bearings run at an overload condition of 1×10^6 and 2×10^6 cycles [40]. In comparing the percentage of retained austenite for the as hardened and tempered condition against the results for the bearings tested in overload conditions, it was reported that as the time in overload increased, the percentage of retained austenite decreased. The newly formed martensite resulted in higher compressive residual stresses measured in the steel.

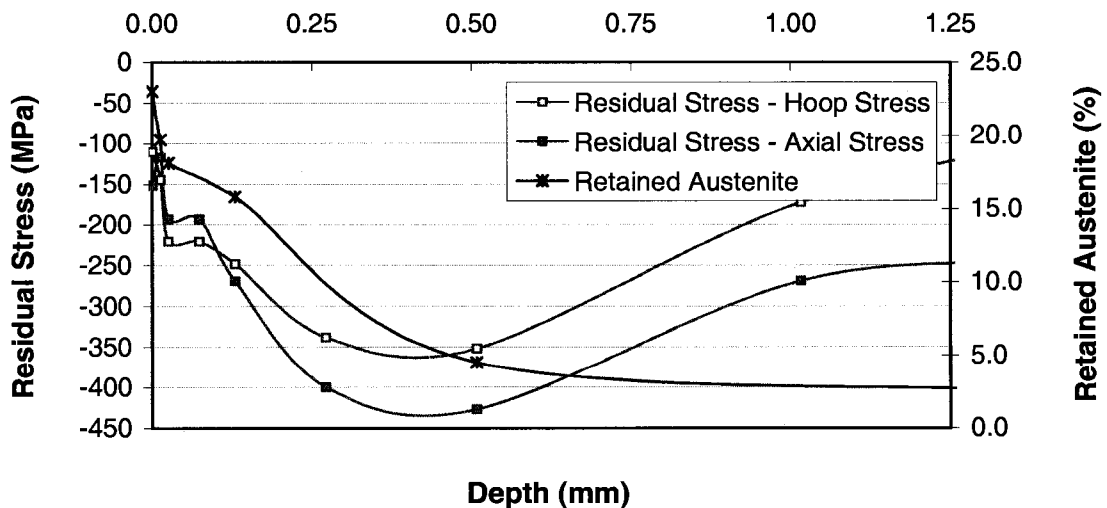


Figure 5.5 Residual stress versus retained austenite in carbonitrided steel; NCR-C10.

RESULTS AND DISCUSSION

VI. EFFECT OF HEAT TREATMENT ON THE CASE AND CORE MICROSTRUCTURES OF PLAIN CARBON STEEL

This section presents optical micrographs of the case and core microstructures for carbonitrided and nitrocarburized plain carbon steels. Selected Navy C-rings and torque converter pistons from each heat treatment group were cut, mounted, polished, and examined using optical and scanning electron microscopy (SEM) to determine the structure of the case formed.

6.1 Case and Core Micrographs

Figures 6.1 – 6.5 show the case and core microstructures for the Navy C-rings and torque converter pistons. The Navy C-rings were machined from hot-rolled bars of SAE 1020 steel and are presented in Figure 6.1 and 6.2. The torque converter pistons were stamped from cold-worked sheets of SAE 1010 steel and are presented in Figure 6.3 , 6.4, and 6.5.

Carbonitriding:

Figure 6.1 and 6.3 show the optical micrographs of carbonitrided SAE 1020 and SAE 1010 steel, respectively. Despite their difference in chemical composition, process time, and temperature, the structure of the SAE 1020 and SAE 1010 carbonitrided cases appear similar; both consist of tempered martensite and retained austenite. The tempered martensite is identified as the dark areas in the microstructure and the retained austenite as the bright, white regions. The core of carbonitrided SAE 1020 steel consists mainly of upper bainite, fine pearlite, and Widmanstatten ferrite.

Together with the retained austenite profiles in Section V, the micrographs in Figure 6.1 and 6.3 also show evidence of the effect of carbon on the retained austenite content in plain carbon steels. As discussed in Section V, carbon, more than any other alloying element, has the greatest effect on retained austenite content. For this reason, it was not surprising that the SAE 1020 steel was associated with a larger amount of retained austenite at the surface and subsurface steel.

Nitrocarburizing:

Optical micrographs of the case and core microstructures of the nitrocarburized SAE 1020 and 1010 steel are shown in Figure 6.2, 6.4, and 6.5. In comparing the compound layer and diffusion zone for each of the microstructures, similarities were noted in the SAE 1020 and SAE 1010 steels treated at process temperatures below 590 °C. For these specimens, the structure of the case is consistent with what is expected for nitrocarburized plain carbon steel [74] - a compound layer at the surface believed to contain epsilon (ϵ) iron carbonitride and an underlying diffusion zone consisting of gamma prime (γ') needles (Fe_4N) in a ferrite matrix. The main difference between the steels was with respect to the structure of the ferrite matrix; for the SAE 1020 steel, in addition to γ' needles, pearlite was also present.

At process temperatures above 590 °C, Figure 6.5, there are differences in the microstructure with respect to both the compound layer and diffusion zone. At this temperature the overall quality of the compound layer of piston is poor. Not only is porosity visible, but it also appears as though the compound layer has detached from the surface of the piston. Differences in the diffusion zone are also evident. The abundance of gamma prime needles seen in the microstructures of Figure 6.2 and 6.4 are absent; instead, in their place, a darker phase suspected to be Braunitite; an SEM micrograph is shown in Figure 6.6. The presence of the Braunitite phase beneath the compound layer is in agreement with previously reported results for nitrocarburized steels heat treated between the eutectoid (A_1) of the Fe-N phase diagram and the corresponding point in the Fe-C system [70]. According to Fry [23], at temperatures above 500 °C, gamma prime needles begin to dissolve and by 590 °C are completely dissociated within the matrix. The slow cooling of nitrocarburized steels above 590 °C results in the eutectoid transformation of austenite to this ferrite and γ' nitride phase [22, 70].

The microstructures of the torque converter pistons from each of the five heat treatment groups were compared. Because the pistons processed at temperatures above 590 °C were associated with development of porosity and detachment of the compound layer, the use of processing temperatures greater than this is not recommended.

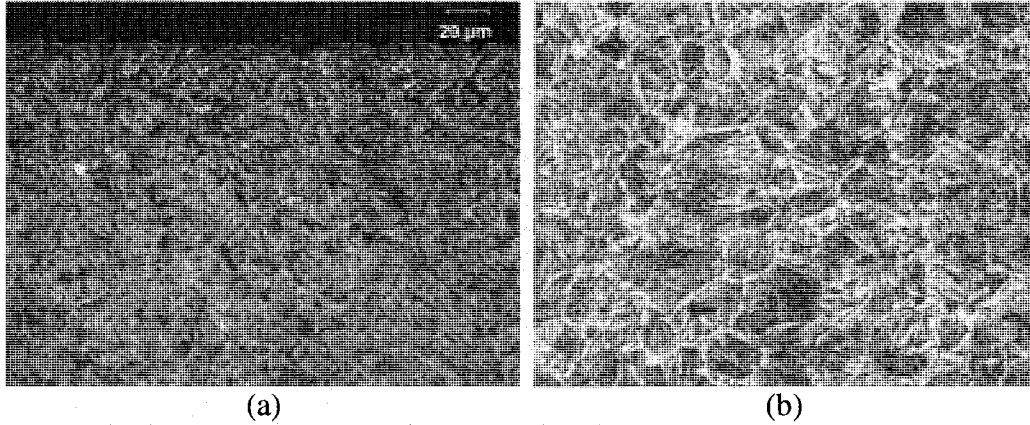


Figure 6.1 NCR-C10: SAE 1020 steel, carbonitrided 4 h at 845 °C, oil quenched, and tempered for 1 h at 165 °C. (a) Microstructure at the case. Structure is tempered martensite and retained austenite. (b) Microstructure at the core. Structure is upper bainite, fine pearlite, and Widmanstatten ferrite. 2% Nital etch.

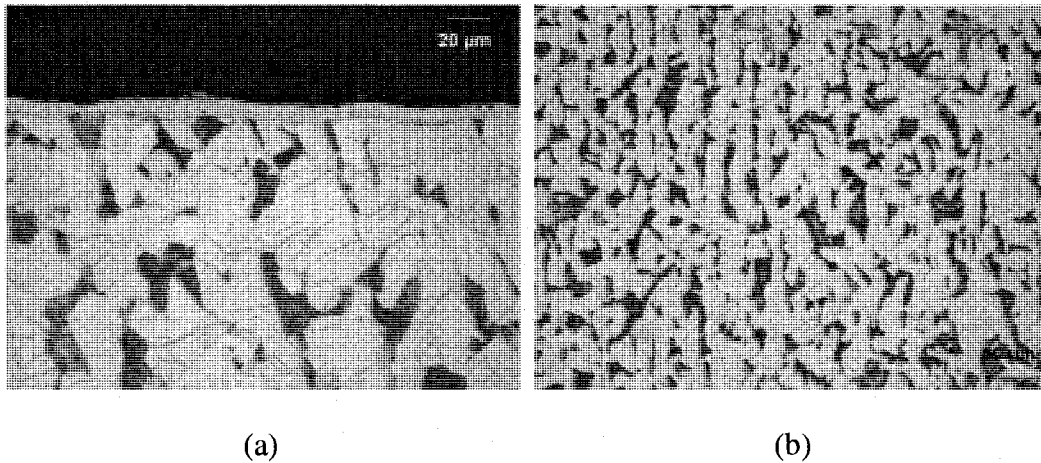


Figure 6.2 NCR-N2: SAE 1020 steel, nitrocarburized 8 h at 565 °C, furnace cooled using nitrogen to 370 °C, and air cooled to room temperature. (a) Microstructure at the case. Structure is a white layer of epsilon (ϵ) iron carbonitride and an underlying diffusion zone containing Fe_4N . (b) Microstructure at the core. Structure is α -ferrite and pearlite. 2% Nital etch.

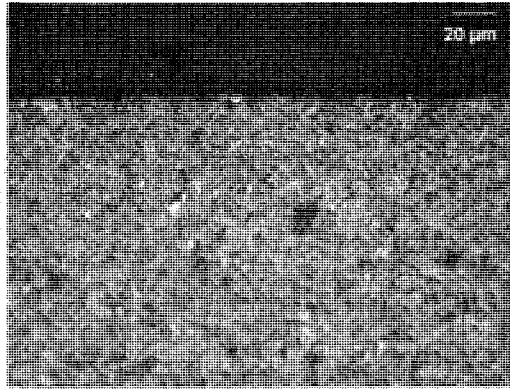


Figure 6.3 PC-1: SAE 1010 steel, carbonitrided 90 min at 870 °C, oil quenched, and tempered. Structure is tempered martensite and retained austenite. 2% Nital etch.

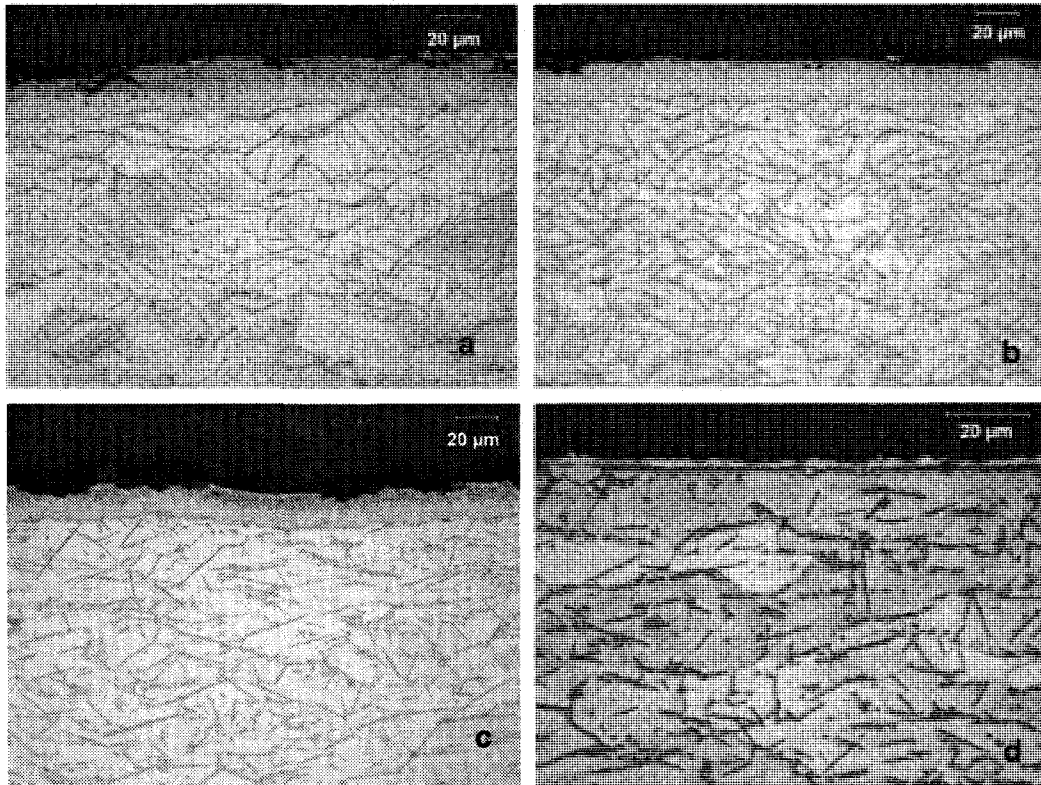


Figure 6.4 Nitrocarburized steel, furnace-cooled using nitrogen to 370 °C, and air cooled to room temperature. a) PN₅₁₀-8: SAE 1010 steel, nitrocarburized 14 h at 510 °C, b) PN₅₄₀-7: SAE 1010 steel, nitrocarburized 10 h at 540 °C, c) PN₅₆₅-7: SAE 1010 steel, nitrocarburized 5 h at 565°C, and d) PN₅₉₅-1: SAE 1010 steel, nitrocarburized 2.5 h at 595°C. Structure is a white layer of epsilon (ϵ) iron carbonitride and an underlying diffusion zone containing Fe₄N. 2% Nital etch.

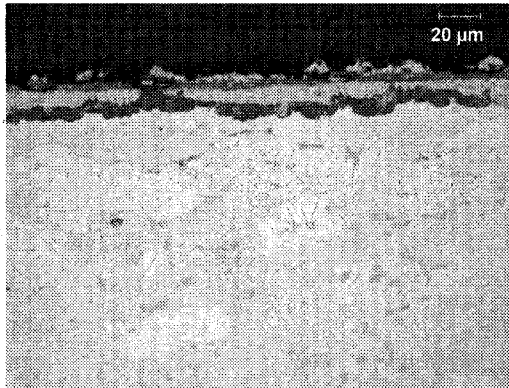


Figure 6.5 PN₆₀₅-1: SAE 1010 steel, nitrocarburized 2 h at 605 °C, furnace-cooled using nitrogen to 370°C, and air cooled to room temperature. 2% Nital etch.

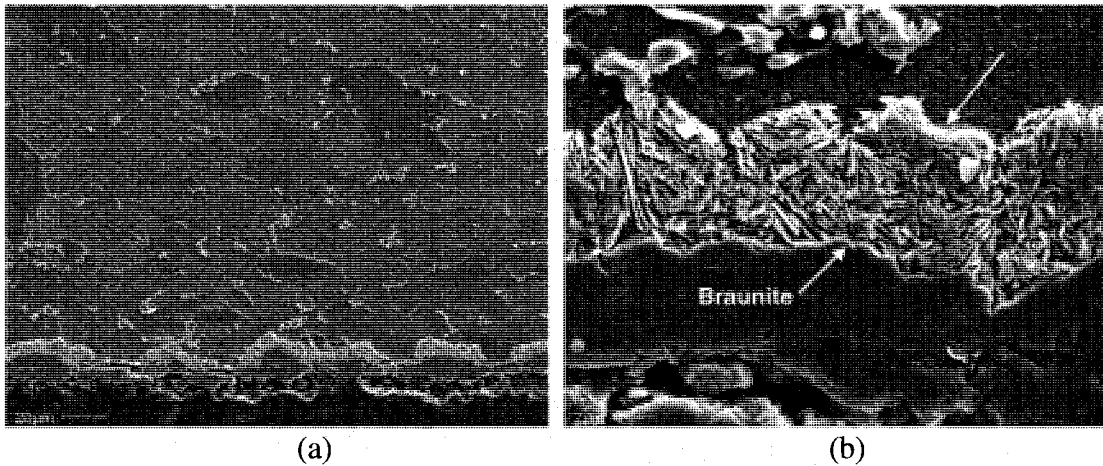


Figure 6.6 Braunite (SAE 1010 steel, nitrocarburized at 605 °C for 2 h, furnace cooled using nitrogen to 370°C, and air cooled to room temperature). a) SEM micrograph PN₆₀₅-1 showing the compound layer, Braunite, and only a small amount of gamma prime (γ') nitride. b) SEM micrograph of the Braunite phase. 2% Nital etch.

6.2 Growth Direction in Nitrocarburized Steel

To confirm the surface growth in gaseous ferritic nitrocarburized steel, coupons were cut from a sheet of normalized SAE 1010 steel and masked on both ends using Acheson Nitrostop N4. Following heat treatment, the coupons were mounted, polished, and examined using optical microscopy.

The optical micrograph in Figure 6.7 shows the formation of the compound layer on an unmasked section of the coupon. In Figure 6.8, the micrograph showing both the masked and unmasked sections of the coupon confirms that compound layer is not 'plated' onto the surface of the steel, but instead appears to grow inward from the surface. Both the original surface and compound layer are visible in this micrograph; the case depth of the white layer extends from the original surface down into the coupon to a depth of approximately 10 μm . This analysis confirms that the white layer does not form on the surface of the steel, but rather at the surface and just below it as a result of the diffusion of carbon and nitrogen.

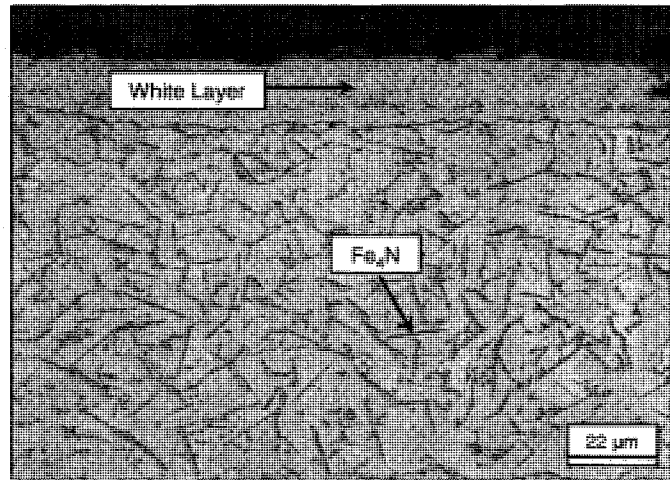


Figure 6.7 Optical micrograph of an unmasked section of the nitrocarburized SAE 1010 steel coupon. 2% Nital etch.

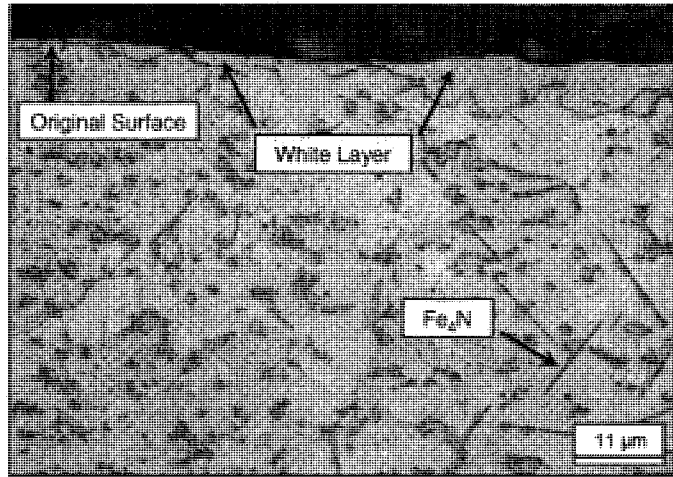


Figure 6.8 Optical micrograph of the nitrocarburized SAE 1010 steel coupon near the masked section. Both the original surface of the steel and white layer is shown. 2% Nital etch.

VII. CONCLUSIONS AND RECOMMENDATIONS FOR FUTURE WORK

The primary focus of this study was to investigate the potential of gaseous ferritic nitrocarburizing as a replacement for the carbonitriding process. The Chrysler Toledo Machining Plant currently uses carbonitriding to impart a hard, wear resistance case on the surface of automotive torque converter pistons. Because ferritic nitrocarburizing takes place in the absence of a phase transformation, it is associated with minimal distortion compared to the carbonitriding process; and as a result, it has the potential to improve manufacturing through the elimination of unnecessary production time and cost.

The carbonitriding and nitrocarburizing processes were compared quantitatively in terms of size and shape distortions, retained austenite content, and residual stress values, and qualitatively in terms of the structure and quality of the cases formed. Because minimizing distortion was one of the key objectives, it was important that the aforementioned factors be studied in order to determine whether or not further investigation into gaseous ferritic nitrocarburizing was necessary.

7.1 Conclusions

The following conclusions were drawn based upon the experimental results gathered during this study.

1. While both processes were associated with size and shape distortions, carbonitriding was noted to give rise to larger overall distortion values in the Navy C-rings. In comparing the distortion of the C-rings from groups NCR-C and NCR-N, those from the former exhibited larger changes in both size (OD, ID, gap width, and thickness) and shape (flatness and roundness). The distortion associated with the carbonitriding process can be attributed to the phase changes as well as the thermal and transformation stresses developed upon quenching. For the nitrocarburized C-rings, because of the lack of phase transformation and its associated transformation stresses, size and shape distortion values, with the exception of cylindricity, were smaller.

2. In general, the average values for both size and shape distortion were smaller in the nitrocarburized pistons. The magnitude of the distortion of the OD and ID was similar between the two processes, yet the carbonitrided steel exhibited larger variability in the results. After carbonitriding, the OD and ID showed both positive and negative deviation from the initial measurements taken prior to heat treatment; that is, while dimensional changes in the OD (-7.5 mm) and ID (-11 mm) taken closest to the lockup surface decreased, dimensional changes in OD (-21.5 mm) and ID (-15 mm) further from the lockup surface increased.

The severity of the shape distortion was larger, particularly in the carbonitrided pistons. In comparing the total flatness and taper values of the processes, the carbonitrided pistons exhibited larger changes than those treated using nitrocarburizing.

3. Results from this study were successful in showing the influence of processing temperature on the presence of retained austenite at the surface of the carbonitrided and nitrocarburized steel. Levels of retained austenite were highest in the carbonitrided steels; 23.0% and 11.8%, were measured in the Navy C-ring (NCR-C10) and torque converter piston (PC-1), respectively.

A relationship between process temperature and retained austenite was evident within the sample of nitrocarburized pistons. Comparing the torque converter pistons from groups PN₅₁₀, PN₅₆₅, and PN₆₀₅, the largest retained austenite content was measured in those pistons treated at higher processing temperatures.

4. In a comparison of the residual stresses in carbonitrided and nitrocarburized steel, overall higher compressive residual stresses were measured in former. Maximum values measured -352 and -427 MPa for hoop and axial stresses in NCR-C10 and -352 MPa for the hoop stress in PC-1. In both cases, maximum residual stress

values were not measured at the surface of the steel, but instead at some distance inward, 0.5080 mm and 0.0762 mm for the NCR-C10 and PC-1, respectively.

5. The location of the maximum residual stress in the carbonitrided steel appears to show dependency upon retained austenite content. Maximum compressive stresses in the steel were not measured at the surface, where retained austenite content was highest, but instead were measured at distances below the surface associated with a lower retained austenite content. While this relationship is clearly demonstrated in Figure 5.5, the nitrocarburized steels failed to demonstrate a similar result due in part to the inaccuracy of the method used to obtain the residual stress profiles, particularly within the compound layer.
6. Based upon the surface residual stress measurements of the pistons from group PN₅₁₀, it is believed that the nitrocarburizing process is associated with the development of tensile stresses at the surface and within the compound layer. The effect of tensile stresses on the wear properties of low carbon steel is not yet known. Additional testing is required to study this effect on the wear of the torque converter pistons and determine whether or not the surface properties of nitrocarburized steel meet the expectations of the manufacturer.
7. The direction of growth of the nitrocarburized layer into the surface of the steel was confirmed. These results, together with those from literature [30, 66], which discuss the effect of thermal stresses on size distortion, can be used to explain the distortion associated with the nitrocarburized Navy C-rings. These results help confirm that the dimensional changes in nitrocarburized steel relate more to changes in thermal stresses than case formation.
8. The variability in the size and shape distortion values was larger in the carbonitrided Navy C-rings and torque converter pistons. Such results suggest that the use of the nitrocarburizing process may be beneficial in allowing

manufacturers to achieve a more consistent product. With less variability in part dimensions after heat treatment, it is possible that designers and engineers can predict and account for part distortion during the design stage of the manufacturing process.

7.2 Summary of Conclusions

The conclusions of this research support the potential of gaseous ferritic nitrocarburizing to replace the current carbonitriding process. Ferritic nitrocarburizing is associated with smaller size and shape distortions after heat treatment; the lower retained austenite content at the surface helps to reduce the likelihood of additional distortion linked to the transformation to martensite. Although the findings support the use of the ferritic nitrocarburizing process as a means of reducing part distortion, the effect of surface tensile stresses on the wear properties is not yet known. As a result, full support of this process cannot be granted until actual wear tests are performed to determine whether the surface of nitrocarburized steel is capable of withstanding the light loads experienced by the pistons while in service.

7.3 Recommendations for Future Work

Recommendations to help improve the accuracy of the results have been outlined below. Also included are suggestions for further testing which can be performed to help determine the potential of ferritic nitrocarburizing as a replacement to the current carbonitriding process.

Recommendations to Improve the Accuracy:

1. When comparing the heat treatment processes, it is important that the sample sizes of the groups are equal to one another. For this study increasing the sample size of group PC from three to ten is necessary. Increasing sample size would increase the precision of the mean and standard deviation helping to more accurately compare the two processes.
2. Increase the number of controlled variables (*i.e.* maintain the same heat treatment time for both the carbonitrided and nitrocarburized Navy C-rings). More control

over the variables will help to determine which factors most influence the behaviour of the steel during heat treatment.

3. Re-determine the residual stress profiles such that the values for the surface stress are more accurately reflected in the nitrocarburized steels. It is suggested that the {302} iron nitride peak be used to calculate the residual stresses in the compound layer and the {211} martensite peak be used for the diffusion zone and substrate. A more accurate representation of the residual stress profile in nitrocarburized steel can then be used to determine whether or not a relationship between retained austenite content and residual stress exists.

Recommendations for Future Work:

1. Perform wear tests to simulate the movement of the retainer ring springs against the lockup surface of a torque converter piston. These tests would allow for a comparison of wear at the surface of the carbonitrided and nitrocarburized pistons in a light loading application.
2. Analyze the cost implications associated with the replacement of the current carbonitriding process with gaseous ferritic nitrocarburizing. In particular, do the savings associated with minimizing part distortion justify the capital, operational, and residual costs of implementing the new process?
3. Determine the carbon and nitrogen profiles to improve understanding the distortion, residual stress, and retained austenite values.
4. Investigate austenitic nitrocarburizing and the formation of Braunite to further understand the distortion resulting from the nitrocarburizing process.

APPENDIX A

Navy C-ring Size Distortion (OD, ID, Gap Width and Thickness)

		Outer Diameter			
		As Received	Heat Treatment	Change in Diameter (mm)	% Change
Nitrocarburized	1	50.8089	50.8302	0.0213	0.0419
	2	50.7724	50.7928	0.0204	0.0402
	3	50.7940	50.8147	0.0207	0.0408
	4	50.7836	50.8034	0.0198	0.0390
	5	50.7928	50.8130	0.0202	0.0398
	6	50.7749	50.7954	0.0205	0.0404
	7	50.7839	50.8055	0.0216	0.0425
	8	50.7778	50.7977	0.0199	0.0392
	9	50.8228	50.8449	0.0221	0.0435
	10	50.7701	50.7905	0.0204	0.0402
		Average Change:		0.0207	0.0407
		Standard Deviation:		0.0007	0.0015
Carbonitrided	1	50.7824	50.8511	0.0687	0.1353
	2	50.7909	50.8618	0.0709	0.1396
	3	50.7502	50.8199	0.0697	0.1373
	4	50.7780	50.8488	0.0708	0.1394
	5	50.8111	50.8720	0.0609	0.1199
	6	50.7949	50.8662	0.0713	0.1404
	7	50.8168	50.8875	0.0707	0.1391
	8	50.7916	50.8531	0.0615	0.1211
	9	50.8043	50.8763	0.0720	0.1417
	10	50.7761	50.8424	0.0663	0.1306
		Average Change:		0.0683	0.1344
		Standard Deviation:		0.0041	0.0080

		Inner Diameter (Diameter ID-1)			
		As Received	Heat Treatment	Change in Diameter (mm)	% Change
Nitrocarburized	1	31.7488	31.7536	0.0048	0.0151
	2	31.7735	31.7776	0.0041	0.0129
	3	31.7714	31.7751	0.0037	0.0116
	4	31.7504	31.7538	0.0034	0.0107
	5	31.7548	31.7598	0.0050	0.0157
	6	31.7607	31.7660	0.0053	0.0167
	7	31.7570	31.7636	0.0066	0.0208
	8	31.7694	31.7729	0.0035	0.0110
	9	31.7461	31.7508	0.0047	0.0148
	10	31.7684	31.7723	0.0039	0.0123
		Average Change:		0.0045	0.0142
		Standard Deviation:		0.0010	0.0031
Carbonitrided	1	31.7713	31.8344	0.0631	0.1986
	2	31.7784	31.8412	0.0628	0.1976
	3	31.7687	31.8291	0.0604	0.1901
	4	31.7481	31.8122	0.0641	0.2019
	5	31.7558	31.8085	0.0527	0.1660
	6	31.7639	31.8326	0.0687	0.2163
	7	31.7581	31.8214	0.0633	0.1993
	8	31.7727	31.8208	0.0481	0.1514
	9	31.7458	31.8171	0.0713	0.2246
	10	31.7674	31.8274	0.0600	0.1889
		Average Change:		0.0615	0.1935
		Standard Deviation:		0.0069	0.0216

		Inner Diameter (Diameter_ID-2)			
		As Received	Heat Treatment	Change in Diameter (mm)	% Change
Nitrocarburized	1	31.7503	31.7541	0.0038	0.0120
	2	31.7663	31.7693	0.0030	0.0094
	3	31.7676	31.7709	0.0033	0.0104
	4	31.7454	31.7484	0.0030	0.0095
	5	31.7528	31.7562	0.0034	0.0107
	6	31.7499	31.7534	0.0035	0.0110
	7	31.7626	31.7669	0.0043	0.0135
	8	31.7628	31.7659	0.0031	0.0098
	9	31.7443	31.7481	0.0038	0.0120
	10	31.7616	31.7647	0.0031	0.0098
		Average Change:		0.0034	0.0108
		Standard Deviation:		0.0004	0.0013
Carbonitrided	1	31.7615	31.8123	0.0508	0.1599
	2	31.7726	31.8242	0.0516	0.1624
	3	31.7633	31.8123	0.0490	0.1543
	4	31.7459	31.7967	0.0508	0.1600
	5	31.7485	31.7853	0.0368	0.1159
	6	31.7640	31.8180	0.0540	0.1700
	7	31.7480	31.7986	0.0506	0.1594
	8	31.7630	31.8007	0.0377	0.1187
	9	31.7388	31.7933	0.0545	0.1717
	10	31.7641	31.8095	0.0454	0.1429
		Average Change:		0.0481	0.1515
		Standard Deviation:		0.0063	0.0197

		Inner Diameter (Diameter_ID-3)			
		As Received	Heat Treatment	Change in Diameter (mm)	% Change
Nitrocarburized	1	31.7523	31.7572	0.0049	0.0154
	2	31.7718	31.7758	0.0040	0.0126
	3	31.7695	31.7741	0.0046	0.0145
	4	31.7538	31.7580	0.0042	0.0132
	5	31.7528	31.7564	0.0036	0.0113
	6	31.7462	31.7502	0.0040	0.0126
	7	31.7659	31.7709	0.0050	0.0157
	8	31.7663	31.7706	0.0043	0.0135
	9	31.7519	31.7576	0.0057	0.0180
	10	31.7655	31.7697	0.0042	0.0132
		Average Change:		0.0045	0.0140
		Standard Deviation:		0.0006	0.0019
Carbonitrided	1	31.7630	31.8263	0.0633	0.1993
	2	31.7721	31.8362	0.0641	0.2017
	3	31.7618	31.8246	0.0628	0.1977
	4	31.7528	31.8145	0.0617	0.1943
	5	31.7477	31.7908	0.0431	0.1358
	6	31.7597	31.8235	0.0638	0.2009
	7	31.7469	31.8055	0.0586	0.1846
	8	31.7677	31.8186	0.0509	0.1602
	9	31.7422	31.8039	0.0617	0.1944
	10	31.7676	31.8207	0.0531	0.1672
		Average Change:		0.0583	0.1836
		Standard Deviation:		0.0070	0.0221

Gap Distance					
Gap Distance-Top					
	As Received	Heat Treatment	Change in Gap Distance (mm)	% Change	
Nitrocarburized	1	6.3628	6.3527	-0.0101	-0.1587
	2	6.3949	6.3867	-0.0082	-0.1282
	3	6.3984	6.3930	-0.0054	-0.0844
	4	6.3701	6.3604	-0.0097	-0.1523
	5	6.3927	6.3854	-0.0073	-0.1142
	6	6.3831	6.3777	-0.0054	-0.0846
	7	6.3777	6.3723	-0.0054	-0.0847
	8	6.3738	6.3662	-0.0076	-0.1192
	9	6.3660	6.3586	-0.0074	-0.1162
	10	6.3795	6.3707	-0.0088	-0.1379
Average Change:			-0.0075	-0.1181	
Standard Deviation:			0.0017	0.0273	
Carbonitrided	1	6.3654	6.5320	0.1666	2.6173
	2	6.3758	6.5490	0.1732	2.7165
	3	6.3743	6.5464	0.1721	2.6999
	4	6.3753	6.5369	0.1616	2.5348
	5	6.3816	6.5093	0.1277	2.0011
	6	6.3805	6.5572	0.1767	2.7694
	7	6.3536	6.5104	0.1568	2.4679
	8	6.3937	6.5396	0.1459	2.2819
	9	6.3535	6.5417	0.1882	2.9621
	10	6.3613	6.5313	0.1700	2.6724
Average Change:			0.1639	2.5723	
Standard Deviation:			0.0171	0.2714	

Gap Distance					
Gap Distance-Middle					
	As Received	Heat Treatment	Change in Gap Distance (mm)	% Change	
Nitrocarburized	1	6.3698	6.3630	-0.0068	-0.1068
	2	6.3928	6.3846	-0.0082	-0.1283
	3	6.3944	6.3861	-0.0083	-0.1298
	4	6.3314	6.3152	-0.0162	-0.2559
	5	6.3763	6.3652	-0.0111	-0.1741
	6	6.3770	6.3682	-0.0088	-0.1380
	7	6.4045	6.3993	-0.0052	-0.0812
	8	6.3761	6.3684	-0.0077	-0.1208
	9	6.3932	6.3889	-0.0043	-0.0673
	10	6.3772	6.3673	-0.0099	-0.1552
Average Change:			-0.0087	-0.1357	
Standard Deviation:			0.0033	0.0528	
Carbonitrided	1	6.3742	6.5555	0.1813	2.8443
	2	6.3818	6.5609	0.1791	2.8064
	3	6.3670	6.5482	0.1812	2.8459
	4	6.4101	6.5910	0.1809	2.8221
	5	6.3935	6.5261	0.1326	2.0740
	6	6.3880	6.5680	0.1800	2.8178
	7	6.3858	6.5591	0.1733	2.7138
	8	6.3729	6.5263	0.1534	2.4071
	9	6.3675	6.5502	0.1827	2.8693
	10	6.3962	6.5657	0.1695	2.6500
Average Change:			0.1714	2.6851	
Standard Deviation:			0.0163	0.2558	

Gap Distance					
Gap Distance-Bottom					
	As Received	Heat Treatment	Change in Gap Distance (mm)	% Change	
Nitrocarburized	1	6.3820	6.3767	-0.0053	-0.0830
	2	6.3824	6.3761	-0.0063	-0.0987
	3	6.3826	6.3771	-0.0055	-0.0862
	4	6.3539	6.3492	-0.0047	-0.0740
	5	6.3729	6.3589	-0.0140	-0.2197
	6	6.3664	6.3601	-0.0063	-0.0990
	7	6.3850	6.3800	-0.0050	-0.0783
	8	6.3809	6.3753	-0.0056	-0.0878
	9	6.3874	6.3796	-0.0078	-0.1221
	10	6.3883	6.3779	-0.0104	-0.1628
Average Change:			-0.0071	-0.1112	
Standard Deviation:			0.0030	0.0463	
Carbonitrided	1	6.3729	6.5475	0.1746	2.7397
	2	6.3815	6.5546	0.1731	2.7125
	3	6.3586	6.5325	0.1739	2.7349
	4	6.3972	6.5696	0.1724	2.6949
	5	6.3592	6.4902	0.1310	2.0600
	6	6.3916	6.5656	0.1740	2.7223
	7	6.3771	6.5522	0.1751	2.7458
	8	6.3760	6.5328	0.1568	2.4592
	9	6.3777	6.5560	0.1783	2.7957
	10	6.3797	6.5461	0.1664	2.6083
Average Change:			0.1676	2.6273	
Standard Deviation:			0.0142	0.2206	

Thickness					
Thickness-1					
	As Received	Heat Treatment	Change in Gap Distance (mm)	% Change	
Nitrocarburized	1	18.5498	18.5521	0.0023	0.0124
	2	19.0627	19.0628	0.0001	0.0005
	3	19.1364	19.1480	0.0116	0.0606
	4	18.6082	18.6081	-0.0001	-0.0005
	5	18.6470	18.8388	0.1918	1.0286
	6	18.6456	18.6461	0.0005	0.0027
	7	18.6672	18.6589	-0.0083	-0.0445
	8	19.0237	19.0241	0.0004	0.0021
	9	18.5765	18.5719	-0.0046	-0.0248
	10	18.9760	18.9767	0.0007	0.0037
Average Change:			0.0194	0.1041	
Standard Deviation:			0.0608	0.3259	
Carbonitrided	1	19.0689	19.0588	-0.0101	-0.0530
	2	19.1625	19.1507	-0.0118	-0.0616
	3	19.0625	19.0547	-0.0078	-0.0409
	4	18.6218	18.6224	0.0006	0.0032
	5	18.6782	18.6652	-0.0130	-0.0696
	6	19.0450	19.0304	-0.0146	-0.0767
	7	18.6544	18.6533	-0.0011	-0.0059
	8	19.0858	19.0758	-0.0100	-0.0524
	9	18.4866	18.4958	0.0092	0.0498
	10	19.0044	18.9925	-0.0119	-0.0626
Average Change:			-0.0070	-0.0370	
Standard Deviation:			0.0076	0.0402	

Thickness					
Thickness-2					
	As Received	Heat Treatment	Change in Gap Distance (mm)	% Change	
Nitrocarburized	1	19.0688	19.0716	0.0028	0.0147
	2	19.0366	19.0344	-0.0022	-0.0116
	3	19.0331	19.0424	0.0093	0.0489
	4	19.0648	19.0631	-0.0017	-0.0089
	5	19.1011	19.2930	0.1919	1.0047
	6	19.0845	19.0853	0.0008	0.0042
	7	19.1016	19.0919	-0.0097	-0.0508
	8	19.0436	19.0442	0.0006	0.0032
	9	19.1079	19.1023	-0.0056	-0.0293
	10	19.0442	19.0425	-0.0017	-0.0089
Average Change:			0.0184	0.0966	
Standard Deviation:			0.0611	0.3201	
Carbonitrided	1	19.0230	19.0251	0.0021	0.0110
	2	19.0393	19.0259	-0.0134	-0.0704
	3	19.0433	19.0380	-0.0053	-0.0278
	4	19.0986	19.1020	0.0034	0.0178
	5	19.0792	19.0701	-0.0091	-0.0477
	6	19.0691	19.0616	-0.0075	-0.0393
	7	19.0638	19.0776	0.0138	0.0724
	8	19.0460	19.0390	-0.0070	-0.0368
	9	19.0904	19.1026	0.0122	0.0639
	10	19.0844	19.0802	-0.0042	-0.0220
Average Change:			-0.0015	-0.0079	
Standard Deviation:			0.0091	0.0478	

Thickness					
Thickness-3					
	As Received	Heat Treatment	Change in Gap Distance (mm)	% Change	
Nitrocarburized	1	19.5293	19.5320	0.0027	0.0138
	2	19.1098	19.1072	-0.0026	-0.0136
	3	19.0383	19.0474	0.0091	0.0478
	4	19.4952	19.4928	-0.0024	-0.0123
	5	19.4382	19.6292	0.1910	0.9826
	6	19.4035	19.4027	-0.0008	-0.0041
	7	19.3850	19.3752	-0.0098	-0.0506
	8	19.1469	19.1456	-0.0013	-0.0068
	9	19.4539	19.4490	-0.0049	-0.0252
	10	19.1787	19.1768	-0.0019	-0.0099
Average Change:			0.0179	0.0922	
Standard Deviation:			0.0610	0.3139	
Carbonitrided	1	19.0919	19.0876	-0.0043	-0.0225
	2	19.0375	19.0319	-0.0056	-0.0294
	3	19.1178	19.1166	-0.0012	-0.0063
	4	19.4228	19.4281	0.0053	0.0273
	5	19.4614	19.4573	-0.0041	-0.0211
	6	18.9899	18.9807	-0.0092	-0.0484
	7	19.4665	19.4729	0.0064	0.0329
	8	19.0987	19.0919	-0.0068	-0.0356
	9	19.5519	19.5627	0.0108	0.0552
	10	19.0448	19.0372	-0.0076	-0.0399
Average Change:			-0.0016	-0.0088	
Standard Deviation:			0.0068	0.0352	

Navy C-ring Shape Distortion (Flatness, Cylindricity, and Roundness)

		Flatness			
		As Received	Heat Treatment	Change in Diameter (mm)	% Change
Nitrocarburized	1	0.0016	0.0025	0.0009	56.2500
	2	0.0038	0.0044	0.0006	15.7895
	3	0.0033	0.0027	-0.0006	-18.1818
	4	0.0033	0.0020	-0.0013	-39.3939
	5	0.0045	0.0044	-0.0001	-2.2222
	6	0.0023	0.0060	0.0037	160.8696
	7	0.0027	0.0031	0.0004	14.8148
	8	0.0027	0.0028	0.0001	3.7037
	9	0.0033	0.0023	-0.0010	-30.3030
	10	0.0034	0.0044	0.0010	29.4118
		Average Change:		0.0004	19.0738
		Standard Deviation:		0.0014	57.3083
Carbonitrided	1	0.0023	0.0082	0.0059	256.5217
	2	0.0024	0.0062	0.0038	158.3333
	3	0.0058	0.0067	0.0009	15.5172
	4	0.0028	0.0075	0.0047	167.8571
	5	0.0037	0.0132	0.0095	256.7568
	6	0.0020	0.0103	0.0083	415.0000
	7	0.0014	0.0165	0.0151	1078.5714
	8	0.0047	0.0076	0.0029	61.7021
	9	0.0043	0.0151	0.0108	251.1628
	10	0.0039	0.0138	0.0099	253.8462
		Average Change:		0.0072	291.5269
		Standard Deviation:		0.0043	298.5527

		Cylindricity_OD			
		As Received	Heat Treatment	Change in Diameter (mm)	% Change
Nitrocarburized	1	0.0433	0.0534	0.0101	23.3256
	2	0.0284	0.0398	0.0114	40.1408
	3	0.0628	0.0722	0.0094	14.9682
	4	0.0396	0.0479	0.0083	20.9596
	5	0.0346	0.0452	0.0106	30.6358
	6	0.0280	0.0257	-0.0023	-8.2143
	7	0.0347	0.0448	0.0101	29.1066
	8	0.0236	0.0336	0.0100	42.3729
	9	0.0362	0.0449	0.0087	24.0331
	10	0.0312	0.0365	0.0053	16.9872
		Average Change:		0.0082	23.4316
		Standard Deviation:		0.0040	14.3108
Carbonitrided	1	0.0331	0.0302	-0.0029	-8.7613
	2	0.0488	0.0396	-0.0092	-18.8525
	3	0.0326	0.0334	0.0008	2.4540
	4	0.0304	0.0269	-0.0035	-11.5132
	5	0.0404	0.0397	-0.0007	-1.7327
	6	0.0475	0.0456	-0.0019	-4.0000
	7	0.0402	0.0380	-0.0022	-5.4726
	8	0.0426	0.0396	-0.0030	-7.0423
	9	0.0554	0.0555	0.0001	0.1805
	10	0.0209	0.0233	0.0024	11.4833
		Average Change:		-0.0020	-4.3257
		Standard Deviation:		0.0031	8.2602

Roundness					
Roundness-1					
	As Received	Heat Treatment	Change in Gap Distance (mm)	% Change	
Nitrocarburized	1	0.0102	0.0087	-0.0015	-14.7059
	2	0.0183	0.0151	-0.0032	-17.4863
	3	0.0147	0.0153	0.0006	4.0816
	4	0.0104	0.0104	0.0000	0.0000
	5	0.0154	0.0144	-0.0010	-6.4935
	6	0.0108	0.0110	0.0002	1.8519
	7	0.0107	0.0174	0.0067	62.6168
	8	0.0146	0.0130	-0.0016	-10.9589
	9	0.0097	0.0107	0.0010	10.3093
	10	0.0122	0.0153	0.0031	25.4098
Average Change:			0.0004	5.4625	
Standard Deviation:			0.0028	23.7553	
Carbonitrided	1	0.0212	0.0265	0.0053	25.0000
	2	0.0184	0.0218	0.0034	18.4783
	3	0.0199	0.0194	-0.0005	-2.5126
	4	0.0230	0.0178	-0.0052	-22.6087
	5	0.0068	0.0249	0.0181	266.1765
	6	0.0152	0.0185	0.0033	21.7105
	7	0.0074	0.0151	0.0077	104.0541
	8	0.0136	0.0202	0.0066	48.5294
	9	0.0095	0.0166	0.0071	74.7368
	10	0.0118	0.0263	0.0145	122.8814
Average Change:			0.0060	65.6446	
Standard Deviation:			0.0067	84.0508	

Roundness					
Roundness-2					
	As Received	Heat Treatment	Change in Gap Distance (mm)	% Change	
Nitrocarburized	1	0.0150	0.0142	-0.0008	-5.3333
	2	0.0133	0.0122	-0.0011	-8.2707
	3	0.0099	0.0132	0.0033	33.3333
	4	0.0174	0.0135	-0.0039	-22.4138
	5	0.0129	0.0134	0.0005	3.8760
	6	0.0062	0.0100	0.0038	61.2903
	7	0.0085	0.0176	0.0091	107.0588
	8	0.0123	0.0115	-0.0008	-6.5041
	9	0.0096	0.0089	-0.0007	-7.2917
	10	0.0121	0.0132	0.0011	9.0909
Average Change:			0.0011	16.4836	
Standard Deviation:			0.0036	40.0062	
Carbonitrided	1	0.0282	0.0358	0.0076	26.9504
	2	0.0206	0.0238	0.0032	15.5340
	3	0.0212	0.0305	0.0093	43.8679
	4	0.0146	0.0259	0.0113	77.3973
	5	0.0118	0.0341	0.0223	188.9831
	6	0.0111	0.0196	0.0085	76.5766
	7	0.0067	0.0180	0.0113	168.6567
	8	0.0100	0.0212	0.0112	112.0000
	9	0.0122	0.0262	0.0140	114.7541
	10	0.0156	0.0272	0.0116	74.3590
Average Change:			0.0110	89.9079	
Standard Deviation:			0.0049	57.0706	

Roundness					
Roundness-3					
	As Received	Heat Treatment	Change in Gap Distance (mm)	% Change	
Nitrocarburized	1	0.0109	0.0092	-0.0017	-15.5963
	2	0.0131	0.0156	0.0025	19.0840
	3	0.0121	0.0107	-0.0014	-11.5702
	4	0.0172	0.0119	-0.0053	-30.8140
	5	0.0164	0.0129	-0.0035	-21.3415
	6	0.0103	0.0106	0.0003	2.9126
	7	0.0149	0.0222	0.0073	48.9933
	8	0.0090	0.0132	0.0042	46.6667
	9	0.0109	0.0101	-0.0008	-7.3394
	10	0.0082	0.0151	0.0069	84.1463
Average Change:			0.0009	11.5141	
Standard Deviation:			0.0043	37.3298	
Carbonitrided	1	0.0224	0.0245	0.0021	9.3750
	2	0.0151	0.0139	-0.0012	-7.9470
	3	0.0163	0.0191	0.0028	17.1779
	4	0.0117	0.0174	0.0057	48.7179
	5	0.0100	0.0301	0.0201	201.0000
	6	0.0276	0.0255	-0.0021	-7.6087
	7	0.0110	0.0149	0.0039	35.4545
	8	0.0141	0.0175	0.0034	24.1135
	9	0.0111	0.0193	0.0082	73.8739
	10	0.0181	0.0293	0.0112	61.8785
Average Change:			0.0054	45.6035	
Standard Deviation:			0.0065	61.1068	

Torque Converter Piston Size Distortion (OD, ID)

Piston Diameter Outer Diameter (-7.5mm)					
Process	Part	As Received	After Heat Treatment	Change (mm)	Average Change (mm)
Carbonitriding	1	261.1980	261.1346	-0.0634	-0.0980
	2	261.2245	261.1353	-0.0892	
	3	261.1937	261.0522	-0.1415	
Nitrocarburizing (Temp: 950°C)	1	261.1727	261.2641	0.0914	0.0934
	2	261.2211	261.3150	0.0939	
	3	261.2225	261.3171	0.0946	
	4	261.2119	261.3074	0.0955	
	5	261.1835	261.2747	0.0912	
	6	261.1881	261.2811	0.0930	
	7	261.2083	261.3022	0.0939	
	8	261.1727	261.2684	0.0957	
	9	261.2173	261.3106	0.0933	
	10	261.1977	261.2889	0.0912	
Nitrocarburizing (Temp: 1000°C)	1	261.1834	261.2691	0.0857	0.0815
	2	261.1653	261.2449	0.0796	
	3	261.2202	261.3039	0.0837	
	4	261.1906	261.2694	0.0788	
	5	261.1970	261.2797	0.0827	
	6	261.2159	261.2997	0.0838	
	7	261.1871	261.2694	0.0823	
	8	261.1939	261.2756	0.0817	
	9	261.2032	261.2828	0.0796	
	10	261.1953	261.2721	0.0768	
Nitrocarburizing (Temp: 1050°C)	1	261.1837	261.2627	0.0790	0.0764
	2	261.1669	261.2496	0.0827	
	3	261.2022	261.2736	0.0714	
	4	261.1839	261.2602	0.0763	
	5	261.1848	261.2568	0.0720	
	6	261.2193	261.2981	0.0788	
	7	261.1994	261.2779	0.0785	
	8	261.2118	261.2870	0.0752	
	9	261.1838	261.2605	0.0767	
	10	261.1847	261.2578	0.0731	
Nitrocarburizing (Temp: 1100°C)	1	261.2265	261.3000	0.0735	0.0744
	2	261.2052	261.2779	0.0727	
	3	261.2023	261.2769	0.0746	
	4	261.1931	261.2642	0.0711	
	5	261.2278	261.3024	0.0746	
	6	261.1981	261.2740	0.0759	
	7	261.2146	261.2896	0.0750	
	8	261.1999	261.2735	0.0736	
	9	261.2083	261.2833	0.0750	
	10	261.2157	261.2939	0.0782	
Nitrocarburizing (Temp: 1125°C)	1	261.1996	261.2700	0.0704	0.0696
	2	261.1732	261.2424	0.0692	
	3	261.1958	261.2722	0.0764	
	4	261.1996	261.2714	0.0718	
	5	261.2231	261.2898	0.0667	
	6	261.1734	261.2398	0.0664	
	7	261.1742	261.2439	0.0697	
	8	261.1877	261.2581	0.0704	
	9	261.1848	261.2528	0.0680	
	10	261.2123	261.2796	0.0673	

Piston Diameter Outer Diameter (-21.5mm)					
Process	Part	As Received	After Heat Treatment	Change (mm)	Average Change (mm)
Carbonitriding	1	262.1033	262.1812	0.0779	0.0513
	2	262.1100	262.1449	0.0349	
	3	262.0829	262.1241	0.0412	
Nitrocarburizing (Temp: 950°C)	1	262.0718	262.1700	0.0982	0.0864
	2	262.1082	262.1948	0.0866	
	3	262.1019	262.1864	0.0845	
	4	262.1015	262.1874	0.0859	
	5	262.1314	262.2054	0.0740	
	6	262.0973	262.1810	0.0837	
	7	262.1002	262.1889	0.0887	
	8	262.0934	262.1919	0.0985	
	9	262.1125	262.1957	0.0832	
	10	262.1066	262.1875	0.0809	
Nitrocarburizing (Temp: 1000°C)	1	262.0749	262.1714	0.0965	0.0731
	2	262.0651	262.1511	0.0860	
	3	262.1095	262.1821	0.0726	
	4	262.0949	262.1607	0.0658	
	5	262.1063	262.1759	0.0696	
	6	262.1105	262.1806	0.0701	
	7	262.0959	262.1666	0.0707	
	8	262.0979	262.1654	0.0675	
	9	262.1057	262.1732	0.0675	
	10	262.0970	262.1615	0.0645	
Nitrocarburizing (Temp: 1050°C)	1	262.0765	262.1609	0.0844	0.0713
	2	262.0615	262.1543	0.0928	
	3	262.0832	262.1568	0.0736	
	4	262.0719	262.1555	0.0836	
	5	262.0945	262.1481	0.0536	
	6	262.1062	262.1691	0.0629	
	7	262.1029	262.1657	0.0628	
	8	262.1074	262.1691	0.0617	
	9	262.0771	262.1601	0.0830	
	10	262.0972	262.1519	0.0547	
Nitrocarburizing (Temp: 1100°C)	1	262.1143	262.1747	0.0604	0.0611
	2	262.1080	262.1654	0.0574	
	3	262.1040	262.1668	0.0628	
	4	262.0986	262.1541	0.0555	
	5	262.1147	262.1782	0.0635	
	6	262.0989	262.1622	0.0633	
	7	262.1020	262.1662	0.0642	
	8	262.1050	262.1630	0.0580	
	9	262.0996	262.1594	0.0598	
	10	262.1036	262.1693	0.0657	
Nitrocarburizing (Temp: 1125°C)	1	262.1026	262.1700	0.0674	0.0658
	2	262.0923	262.1590	0.0667	
	3	262.0789	262.1630	0.0841	
	4	262.1044	262.1643	0.0599	
	5	262.1109	262.1611	0.0502	
	6	262.0708	262.1432	0.0724	
	7	262.0649	262.1421	0.0772	
	8	262.0783	262.1538	0.0755	
	9	262.0903	262.1446	0.0543	
	10	262.1007	262.1511	0.0504	

Piston Diameter Center Bore (-11mm)					
Process	Part	As Received	After Heat Treatment	Change (mm)	Average Change (mm)
Carbonitriding	1	62.1173	62.0495	-0.0678	-0.0745
	2	62.1147	62.0430	-0.0717	
	3	62.1204	62.0363	-0.0841	
Nitrocarburizing (Temp: 950°C)	1	62.1217	62.1202	-0.0015	0.0026
	2	62.1133	62.1173	0.0040	
	3	62.1123	62.1178	0.0055	
	4	62.1141	62.1159	0.0018	
	5	62.1165	62.1189	0.0024	
	6	62.1177	62.1205	0.0028	
	7	62.1153	62.1175	0.0022	
	8	62.1210	62.1222	0.0012	
	9	62.1130	62.1168	0.0038	
	10	62.1151	62.1187	0.0036	
Nitrocarburizing (Temp: 1000°C)	1	62.1178	62.1208	0.0030	0.0025
	2	62.1207	62.1240	0.0033	
	3	62.1127	62.1164	0.0037	
	4	62.1166	62.1194	0.0028	
	5	62.1162	62.1183	0.0021	
	6	62.1136	62.1157	0.0021	
	7	62.1165	62.1178	0.0013	
	8	62.1147	62.1171	0.0024	
	9	62.1147	62.1162	0.0015	
	10	62.1171	62.1194	0.0023	
Nitrocarburizing (Temp: 1050°C)	1	62.1182	62.1208	0.0026	0.0041
	2	62.1190	62.1231	0.0041	
	3	62.1178	62.1217	0.0039	
	4	62.1187	62.1213	0.0026	
	5	62.1170	62.1219	0.0049	
	6	62.1128	62.1185	0.0057	
	7	62.1145	62.1186	0.0041	
	8	62.1139	62.1187	0.0048	
	9	62.1184	62.1217	0.0033	
	10	62.1159	62.1208	0.0049	
Nitrocarburizing (Temp: 1100°C)	1	62.1127	62.1219	0.0092	0.0096
	2	62.1154	62.1253	0.0099	
	3	62.1154	62.1254	0.0100	
	4	62.1180	62.1268	0.0088	
	5	62.1120	62.1214	0.0094	
	6	62.1159	62.1257	0.0098	
	7	62.1127	62.1219	0.0092	
	8	62.1158	62.1244	0.0086	
	9	62.1145	62.1240	0.0095	
	10	62.1125	62.1236	0.0111	
Nitrocarburizing (Temp: 1125°C)	1	62.1173	62.1126	-0.0047	-0.0039
	2	62.1197	62.1145	-0.0052	
	3	62.1173	62.1141	-0.0032	
	4	62.1151	62.1133	-0.0018	
	5	62.1128	62.1108	-0.0020	
	6	62.1216	62.1141	-0.0075	
	7	62.1195	62.1145	-0.0050	
	8	62.1187	62.1128	-0.0059	
	9	62.1165	62.1139	-0.0026	
	10	62.1142	62.1129	-0.0013	

Piston Diameter Center Bore (-15mm)					
Process	Part	As Received	After Heat Treatment	Change (mm)	Average Change (mm)
Carbonitriding	1	62.1044	62.1218	0.0174	0.0138
	2	62.1022	62.1219	0.0197	
	3	62.1051	62.1094	0.0043	
Nitrocarburizing (Temp: 950°C)	1	62.1065	62.1173	0.0108	0.0147
	2	62.0996	62.1154	0.0158	
	3	62.1000	62.1170	0.0170	
	4	62.1011	62.1147	0.0136	
	5	62.1049	62.1198	0.0149	
	6	62.1055	62.1206	0.0151	
	7	62.1021	62.1166	0.0145	
	8	62.1070	62.1201	0.0131	
	9	62.1006	62.1167	0.0161	
	10	62.1027	62.1185	0.0158	
Nitrocarburizing (Temp: 1000°C)	1	62.1026	62.1155	0.0129	0.0149
	2	62.1059	62.1199	0.0140	
	3	62.0977	62.1146	0.0169	
	4	62.1043	62.1209	0.0166	
	5	62.1037	62.1202	0.0165	
	6	62.1008	62.1149	0.0141	
	7	62.1047	62.1185	0.0138	
	8	62.1029	62.1183	0.0154	
	9	62.1019	62.1172	0.0153	
	10	62.1056	62.1192	0.0136	
Nitrocarburizing (Temp: 1050°C)	1	62.1028	62.1174	0.0146	0.0165
	2	62.1052	62.1193	0.0141	
	3	62.1035	62.1181	0.0146	
	4	62.1045	62.1181	0.0136	
	5	62.1059	62.1255	0.0196	
	6	62.1004	62.1194	0.0190	
	7	62.1031	62.1218	0.0187	
	8	62.1012	62.1192	0.0180	
	9	62.1035	62.1174	0.0139	
	10	62.1053	62.1243	0.0190	
Nitrocarburizing (Temp: 1100°C)	1	62.0992	62.1252	0.0260	0.0264
	2	62.1033	62.1294	0.0261	
	3	62.1030	62.1296	0.0266	
	4	62.1048	62.1314	0.0266	
	5	62.0993	62.1253	0.0260	
	6	62.1022	62.1291	0.0269	
	7	62.0998	62.1258	0.0260	
	8	62.1027	62.1287	0.0260	
	9	62.1026	62.1296	0.0270	
	10	62.1001	62.1268	0.0267	
Nitrocarburizing (Temp: 1125°C)	1	62.1035	62.1100	0.0065	0.0087
	2	62.1055	62.1115	0.0060	
	3	62.1020	62.1093	0.0073	
	4	62.1036	62.1165	0.0129	
	5	62.1003	62.1131	0.0128	
	6	62.1075	62.1115	0.0040	
	7	62.1059	62.1126	0.0067	
	8	62.1040	62.1090	0.0050	
	9	62.1044	62.1169	0.0125	
	10	62.1016	62.1149	0.0133	

Torque Converter Piston Shape Distortion (Total Flatness, Flatness Taper)

Total Flatness						
Process	Part	As Received	After Heat Treatment	Change (mm)	Average Change (mm)	Standard Deviation
Carbonitriding	V1	0.1777	0.5381	0.3604	0.5632	0.3336
	V2	0.2105	0.5915	0.3810		
	V3	0.1620	1.1102	0.9482		
Nitrocarburizing (Temp: 950°C)	V8	0.1526	0.1702	0.0176	0.0310	0.0151
	V9	0.1819	0.1943	0.0124		
	V10	0.1847	0.2237	0.0390		
	V11	0.1413	0.1681	0.0268		
	V12	0.1708	0.2013	0.0305		
	V13	0.1442	0.1792	0.0350		
	V14	0.1478	0.2131	0.0653		
	V15	0.1677	0.1855	0.0178		
	V16	0.1602	0.1868	0.0266		
Nitrocarburizing (Temp: 1000°C)	V17	0.1674	0.2066	0.0392	0.0380	0.0182
	V18	0.1748	0.1908	0.0160		
	V19	0.1511	0.1727	0.0216		
	V20	0.1740	0.2296	0.0556		
	V21	0.1824	0.1974	0.0150		
	V22	0.1471	0.1863	0.0392		
	V23	0.1781	0.2052	0.0271		
	V24	0.1494	0.2208	0.0714		
	V25	0.1758	0.2208	0.0450		
Nitrocarburizing (Temp: 1050°C)	V26	0.1496	0.1953	0.0457	0.0417	0.0110
	V27	0.1979	0.2414	0.0435		
	V28	0.1500	0.1935	0.0435		
	V29	0.1564	0.2025	0.0461		
	V30	0.1677	0.1842	0.0165		
	V31	0.1743	0.2131	0.0388		
	V32	0.1678	0.2155	0.0477		
	V33	0.1398	0.1991	0.0593		
Nitrocarburizing (Temp: 1100°C)	V34	0.1502	0.1953	0.0451	0.0334	0.0103
	V35	0.1566	0.2017	0.0451		
	V36	0.1644	0.2043	0.0399		
	V37	0.1538	0.1884	0.0346		
	V38	0.1920	0.2020	0.0100		
	V39	0.1430	0.1846	0.0416		
	V40	0.1826	0.2068	0.0242		
	V41	0.1569	0.1966	0.0397		
Nitrocarburizing (Temp: 1125°C)	V42	0.1583	0.1943	0.0360	0.0291	0.0142
	V43	0.1795	0.2062	0.0267		
	V44	0.1795	0.2191	0.0396		
	V45	0.1540	0.1909	0.0369		
	V46	0.1595	0.2029	0.0434		
	V47	0.1486	0.1847	0.0361		
	V48	0.1600	0.1824	0.0224		
	V49	0.1598	0.2145	0.0547		
Nitrocarburizing (Temp: 1125°C)	V50	0.1818	0.2053	0.0235	0.0291	0.0142
	V51	0.1913	0.1942	0.0029		
	V52	0.1461	0.1819	0.0358		
	V53	0.1529	0.1815	0.0286		
	V54	0.1803	0.2125	0.0322		
	V55	0.1782	0.2215	0.0433		
	V56	0.1627	0.1805	0.0178		
	V57	0.1547	0.1845	0.0298		

Flatness Taper						
Process	Part	As Received	After Heat Treatment	Change (mm)	Average Change (mm)	Standard Deviation
Carbonitriding	V1	0.1687	0.2834	0.1147	0.3873	0.3349
	V2	0.1348	0.4208	0.2860		
	V3	0.1437	0.9048	0.7611		
Nitrocarburizing (Temp: 950°C)	V8	0.1322	0.1521	0.0199	0.0308	0.0107
	V9	0.1374	0.1544	0.0170		
	V10	0.1704	0.2044	0.0340		
	V11	0.1272	0.1541	0.0269		
	V12	0.1565	0.1892	0.0327		
	V13	0.1260	0.1566	0.0306		
	V14	0.1277	0.1643	0.0366		
	V15	0.1318	0.1537	0.0219		
	V16	0.1425	0.1757	0.0332		
Nitrocarburizing (Temp: 1000°C)	V17	0.1263	0.1812	0.0549	0.0332	0.0195
	V18	0.1456	0.1625	0.0169		
	V19	0.1348	0.1547	0.0199		
	V20	0.1261	0.2050	0.0789		
	V21	0.1701	0.1756	0.0055		
	V22	0.1291	0.1664	0.0373		
	V23	0.1648	0.1924	0.0276		
	V24	0.1314	0.1711	0.0397		
	V25	0.1683	0.2054	0.0371		
Nitrocarburizing (Temp: 1050°C)	V26	0.1275	0.1585	0.0310	0.0399	0.0158
	V27	0.1258	0.1637	0.0379		
	V28	0.1313	0.1806	0.0493		
	V29	0.1378	0.1859	0.0481		
	V30	0.1556	0.1566	0.0010		
	V31	0.1357	0.1838	0.0481		
	V32	0.1523	0.1987	0.0464		
	V33	0.1230	0.1822	0.0592		
	V34	0.1293	0.1599	0.0306		
Nitrocarburizing (Temp: 1100°C)	V35	0.1414	0.1823	0.0409	0.0348	0.0086
	V36	0.1551	0.1939	0.0388		
	V37	0.1353	0.1722	0.0369		
	V38	0.1639	0.1786	0.0147		
	V39	0.1270	0.1672	0.0402		
	V40	0.1263	0.1717	0.0454		
	V41	0.1457	0.1857	0.0400		
	V42	0.1445	0.1814	0.0369		
	V43	0.1321	0.1594	0.0273		
Nitrocarburizing (Temp: 1125°C)	V44	0.1702	0.2041	0.0339	0.0241	0.0138
	V45	0.1359	0.1699	0.0340		
	V46	0.1427	0.1833	0.0406		
	V47	0.1285	0.1638	0.0353		
	V48	0.1531	0.1601	0.0070		
	V49	0.1394	0.1470	0.0076		
	V50	0.1723	0.1937	0.0214		
	V51	0.1240	0.1747	0.0507		
	V52	0.1271	0.1534	0.0263		
	V53	0.1359	0.1655	0.0296		
	V54	0.1721	0.1944	0.0223		
	V55	0.1707	0.2122	0.0415		
	V56	0.1381	0.1582	0.0201		
	V57	0.1359	0.1508	0.0149		

APPENDIX B

Sample Hypothesis Test

Flatness Distortion (PC versus PN₅₁₀)

H₀ The mean flatness distortion of the pistons from group PN₅₁₀ is less than the mean flatness distortion of the pistons from group PC.
(Distortion_N < Distortion_C)

H₁ The mean flatness distortion of the pistons from group PN₅₁₀ is less than or equal to the mean flatness distortion of the pistons from group PC.
(Distortion_N ≥ Distortion_C)

α 5 %

Degrees of Freedom = n_{carbonitriding} + n_{nitrocarburizing} - 2
= 3 + 10 - 2
= 11

t_{0.5, 11} = 1.796 (from Ref 67)

ybar_n = 0.03102

ybar_c = 0.5632

S_N² = 0.000228971 (*individual sample variance for nitrocarburized pistons*)

S_C² = 0.11127484 (*individual sample variance for carbonitrided pistons*)

S_P² = 0.020419129 (*sample variance*)

t₀ = -5.657556462

Since t₀ < t_{0.5, 11}, we fail to reject the null hypothesis at 95% confidence interval

REFERENCES

1. J. Dosset, "Carbonitriding," ASM Handbook, Vol. 4, Heat Treating, S.R. Lampman *et al.* (Editors), ASM International, Materials Park, OH U.S.A., 1991, pp. 376-386.
2. J.R. Davis (Editor), Surface Hardening of Steels: Understanding the Basics, ASM International, Materials Park, OH U.S.A., 2002, pp. 127-139, 195-212.
3. G. Krauss, Steels: Heat Treatment and Processing Principles, ASM International, Materials Park, OH U.S.A., 1990, pp. 281, 310-315.
4. W.F. Smith, Structure and Properties of Engineering Alloys, McGraw-Hill, Inc., New York, NY U.S.A., 1993, pp. 26, 31, 69, 100, 599.
5. ASM Committee on Gas Carburizing, Carburizing and Carbonitriding, American Society for Metals, Metals Park, OH U.S.A., 1977, pp. 1-4, 18-25, 103-107, 125-147.
6. T. Réti, "Residual Stresses in Carburized, Carbonitrided, and Case-Hardened Components," Handbook of Residual Stress and Deformation of Steel, G.E. Totten, M. Howes, and T. Inoue (Editors), ASM International, Materials Park, OH U.S.A., 2002, pp. 189-208.
7. Kevin Sullivan's Autoshop 101, "Torque Converter", Toyota Series-Automatic Transmissions, Retrieved September 1 2008, from <http://www.autoshop101.com/forms/AT02.pdf>, pp. 12
8. P. Schobesberger, T. Streng, and S. Abbas, "Low-Distortion Heat Treatment of Thin Parts," Industrial Heating, Vol. 69, Issue 1 (2002), pp. 30-34.
9. M. Narazaki and G.E. Totten, "Distortion of Heat-Treated Components," Steel Heat Treatment Handbook: Metallurgy and Technologies, G.E. Totten (Editor), CRC Press, Boca Raton, FL U.S.A., 2007, pp. 608-637.
10. T. Bell, "Ferritic Nitrocarburizing," Source Book on Nitriding, ASM, Metals Park, OH U.S.A., 1977, pp. 266-278.
11. T. Bell, "Gaseous and Plasma Nitrocarburizing," ASM Handbook, Vol. 4, Heat Treating, S.R. Lampman *et al.* (Editors), ASM International, Materials Park, OH U.S.A. 1991, pp. 425-436.
12. P.D. Harvey (Editor), Engineering Properties of Steel, American Society for Metals, Metals Park, OH U.S.A., 1982, pp. 10.

13. G. Krauss, Principles of Heat Treatment of Steel, American Society for Metals, Metals Park, OH U.S.A., 1980, pp. 53, 130, 247, 269-271.
14. S. Lampman, "Introduction to Surface Hardening of Steels," ASM Handbook, Vol. 4, Heat Treating, S.R. Lampman *et al.* (Editors), ASM International, Materials Park, OH U.S.A., 1991, pp. 259.
15. A.K. Rakhit, Heat Treatment of Gears: A Practical Guide for Engineers, ASM International, Materials Park, OH U.S.A., 2000, pp. 171-173.
16. J.R. Davis (Editor), Gear Materials, Properties, and Manufacture, ASM International, Materials Park, OH U.S.A., 2005, pp. 245-247.
17. G. Krauss, Steels: Processing, Structure, and Performance, ASM International, Materials Park, OH U.S.A., 2006, pp. 298, 417-426, 456-461.
18. C. Dawes, Nitrocarburising and its Influence on Design in the Automotive Sector, Heat Treatment of Metals, Vol. 18, No. 1 (1991), pp. 19-30.
19. C. Dawes and D.F. Tranter, Nitrotec* Surface Treatment-its Development and Application in the Design and Manufacture of Automobile Components, Heat Treatment of Metals, Vol. 9, No. 4 (1982), pp. 85-90.
20. D. Pye, Practical Nitriding and Ferritic Nitrocarburizing, ASM International, Materials Park, OH U.S.A., 2003, pp. 18-19, 193-200.
21. M.A.J. Somers and E.J. Mittemeijer, "Modelling the Kinetics of Nitriding and Nitrocarburizing of Iron," Proceedings of the 17th ASM Heat Treating Society Conference Including the 1st International Induction Heat Treating Symposium, 15-18 September 1997, Indianapolis, IN U.S.A., D.L. Milman *et al.*(Editors), ASM International, Materials Park, OH U.S.A., 1998, pp. 321-330.
22. J. Grosch, "Heat Treatment with Gaseous Atmospheres," Steel Heat Treatment Handbook: Metallurgy and Technologies, G.E. Totten (Editor), CRC Press, Boca Raton, FL U.S.A., 2007, pp. 432-440, 456-457.
23. A. Fry, Nitrogen in Iron, Steel, and Alloy Steels. New Method of Surface Hardening Metal Science and Heat Treatment, Vol. 16, No. 3, 1974, pp. 203-204.
24. Y.D. Kogan, Fifty Years of Nitriding: A Brief Historical Review, Metal Science and Heat Treatment, Vol. 16, No. 3, 1974, pp. 197-199.
25. D. Pye, "Nitriding Techniques, Ferritic Nitrocarburizing, and Austenitic Nitrocarburizing Techniques and Methods," Steel Heat Treatment: Metallurgy and

- Technologies, G.E. Totten (Editor), CRC Press, Boca Raton FL, U.S.A., 2007, pp. 475-538.
26. B.A. Becherer, T. Vasco, and L. Ryan, "Control of Distortion in Tool Steels," ASM Handbook, Vol. 4, Heat Treating, S.R. Lampman *et al.* (Editors), ASM International, Materials Park, OH U.S.A. 1991, pp. 761.
 27. A.K. Sinha, "Defects and Distortion in Heat-Treated Parts," ASM Handbook, Vol. 4, Heat Treating, S.R. Lampman *et al.* (Editors), ASM International, Materials Park, OH U.S.A., 1991, pp. 603-604, 612-613.
 28. M. Narazaki, G.E. Totten, and G.M. Webster, "Hardening by Reheating and Quenching", Handbook of Residual Stress and Deformation of Steel, G.E. Totten, M. Howes, and T. Inoue (Editors), ASM International, Materials Park, OH U.S.A., 2002, pp. 259-260.
 29. R.T. von Bergen, "The Effects of Quenchant Media Selection and Control on the Distortion of Engineered Steel Parts," Quenching and Distortion Control Conference Proceedings, Chicago, IL U.S.A., 22-25 Sept. 1992, G. Totten (Editor), ASM International, Materials Park, OH U.S.A., 1992, pp. 275-282.
 30. B. Hernández-Morales, O. Barba-Méndez, A. Ingalls-Cruz, and J.A. Barrera-Godínez, Mathematical Modelling of Temperature and Stress Evolution During Cooling of a Stainless Steel Navy C-ring Probe, International Journal of Materials and Product Technology, Vol. 24, Nos. 1-4 (2005), pp. 306-318.
 31. E. Essadiqi, "Tool Steels," Steel Heat Treatment: Metallurgy and Technologies, G.E. Totten (Editor), CRC Press, Boca Raton, FL U.S.A., 2007, pp. 667, 685.
 32. M.A.H. Howes, "Factors Affecting Distortion in Hardened Steel Components," Proceedings of the First International Conference on Quenching & Control of Distortion, 22-25 September 1992, Chicago, IL U.S.A., ASM International, Materials Park, OH, U.S.A., 1992, pp. 257.
 33. G.E. Totten and M.A.H. Howes, "Distortion of Heat Treated Components," Steel Heat Treatment Handbook, G.E. Totten and M.A.H. Howes (Editors), Marcel Dekker, Inc., New York, NY U.S.A., 1997, pp. 267-270, 283-288.
 34. H.W. Walton, "Deflection Methods to Estimate Residual Stress," Handbook of Residual Stress and Deformation of Steel, G.E. Totten, M. Howes, and T. Inoue (Editors), ASM International, Materials Park, OH U.S.A., 2002, pp. 91,94.
 35. H.J. French, The Quenching of Steels, American Society for Steel Treating, Cleveland, OH U.S.A., 1930, pp. 132-136.

36. D.O. Northwood, L. He, E. Boyle, and R. Bowers, Retained Austenite-Residual Stress-Distortion Relationships in Carburized SAE 8620 Steel, *Materials Science Forum*, Volume 539-543 No. 5 (2007), pp. 4464-4469.
37. E. Boyle, R. Bowers, and D.O. Northwood, The Use of Navy C-Ring Specimens to Investigate the Effects of Initial Microstructure and Heat Treatment on the Residual Stress, Retained Austenite, and Distortion of Carburized Automotive Steels, *SAE 2007 Transactions: Journal of Materials and Manufacturing*, Section 5, Vol. 116, (2007), pp. 253-261.
38. H. Webster and W.J. Laird, Jr., "Martempering of Steel," *ASM Handbook*, Vol. 4, Heat Treating, S.R. Lampman *et al.* (Editors), ASM International, Materials Park, OH U.S.A., 1991, pp. 143-144.
39. C.E. Bates, G.E. Totten, and R.L. Brennan, "Quenching of Steel," *ASM Handbook*, Vol. 4, Heat Treating, S.R. Lampman *et al.* (Editors), ASM International, Materials Park, OH U.S.A., 1991, pp. 99-100.
40. C.F. Jaczak, J.A. Larson, S.W. Shin, SP-453: Retained Austenite and Its Measurements by X-Ray Diffraction, Society of Automotive Engineers, Inc., Warrendale, PA U.S.A., 1980, pp. 1-55.
41. M. Cohen, Retained Austenite, *Metal Progress*, Vol. 54, No. 6 (1948), pp. 823-826.
42. A.V. Sverdlin and A.R. Ness, "Effects of Alloying Elements on the Heat Treatment of Steel," *Steel Heat Treatment Handbook: Metallurgy and Technologies*, G.E. Totten (Editor), CRC Press, Boca Raton, FL U.S.A., 2007, pp. 179-181.
43. D.P. Koistinen and R.E. Marburger, A General Equation Prescribing the Extent of the Austenite-Martensite Transformation in Pure Iron-Carbon Alloys and Plain Carbon Steels, *Acta Metallurgica*, Vol. 7, No. 1 (1959), pp. 59-60.
44. R.L. Banerjee, Effect of Room Temperature Aging on Low Temperature Transformation of Retained Austenite, *Journal of Heat Treating*, Vol. 3, No. 4 (1984), pp. 353-355.
45. B. Liščić, "Steel Heat Treatment of Steel," *Steel Heat Treatment Handbook: Metallurgy and Technologies*, G.E. Totten (Editor), CRC Press, Boca Raton, FL U.S.A., 2007, pp. 314, 384-388.
46. J. Pan, "Factors Affecting Final Part Shaping," *Handbook of Residual Stress and Deformation of Steel*, G.E. Totten, M. Howes, and T. Inoue (Editors), ASM International, Materials Park, OH U.S.A., 2002, pp. 178.

47. J. Durnin and K.A. Ridal, Determination of Retained Austenite in Steel by X-Ray Diffraction, *Journal of The Iron and Steel Institute*, Vol. 206, No. 1 (1968), pp. 60-67.
48. R.L. Miller, A Rapid X-Ray Method for the Determination of Retained Austenite, *Transactions of the ASM*, Volume 57, No. 4 (1964), pp. 892-899.
49. R. Lindgren, Measuring Retained Austenite by X-Ray Techniques, *Metal Progress*. Vol. 87, No. 4 (1965), pp. 102-104.
50. B.D. Cullity, *Elements of X-Ray Diffraction*, Second Edition, Addison-Wesley Publishing Company, Inc., U.S.A., 1978, pp. 447-477.
51. J. Grum, "Induction Heating," *Handbook of Residual Stress and Deformation of Steel*, G.E. Totten, M. Howes, and T. Inoue (Editors), ASM International, Materials Park, OH U.S.A., 2002, pp. 221.
52. H.C. Child, Residual Stress in Heat-treated Components, *Heat Treatment of Metals*, Vol. 8, No. 4 (1981), pp. 89-94.
53. J. Grum, Overview of Residual Stress After Quenching Part II: Factors Affecting Quench Residual Stresses, *International Journal of Materials and Product Technology*, Vol. 24, Nos. 1-4 (2005), pp. 53-56.
54. C.O. Ruud, "Residual Stresses and Their Measurement," *Proceedings of the First Conference on Quenching & Control of Distortion*, 22-25 September 1992, Chicago, IL, U.S.A., ASM International, Materials Park, OH U.S.A., 1992, pp. 193-198.
55. C.R. Brooks, *Heat Treatment of Ferrous Alloys*, Hemisphere Publishing Corporation, Washington, DC U.S.A., 1979, pp. 119.
56. Z. Kolozváry, "Residual Stresses in Nitriding," *Handbook of Residual Stress and Deformation of Steel*, G.E. Totten, M. Howes, and T. Inoue (Editors), ASM International, Materials Park, OH U.S.A., 2002, pp. 209-219.
57. I.C. Noyan and J.B. Cohen, *Residual Stress: Measurement by Diffraction and Interpretation*, Springer-Verlag, New York, NY U.S.A., 1987, pp. 4-7.
58. M. Belassel, J. Pineault, and M.E. Brauss, Review of Residual Stress Determination and Exploitation Techniques Using X-ray Diffraction Method, *Materials Science Forum*, Vols. 524-525 (2006), pp. 229-234.
59. J. Pineault, M. Belassel, M. Brauss, and J. Ladouceur, Mapping Residual Stress Gradients Via X-Ray Diffraction, SP-2094: Experiments in Automotive

Engineering, Paper No. 2007-01-0802, SAE International, Warrendale, PA U.S.A., 2007, pp. 23-26.

60. J.A. Pineault, M. Belassel, and M.E. Brauss, "X-Ray Diffraction Residual Stress Measurement in Failure Analysis," ASM Handbook, Vol. 11, Failure Analysis and Prevention, W.T. Becker and R.J. Shipley (Editors), ASM International, Materials Park, OH U.S.A., 2002, pp. 484-497.
61. G.E. Totten, C.E. Bates, and N.A. Clinton, Handbook of Quenchants and Quenching Technology, ASM International, Materials Park, OH U.S.A., 1993, pp. 483-486.
62. K. Carr and P. Ferreira, Verification of Form Tolerances Part I: Basic Issues, Flatness, and Straightness, Precision Engineering, Vol 17, No (2) (1995), pp. 135.
63. F.T. Farago and M.A. Curtis, Handbook of Dimensional Measurement, Industrial Press Inc., New York, NY U.S.A., 1994, pp. 371.
64. G.R. Cogorno, Geometric Dimensioning and Tolerancing for Mechanical Design: A Self-Teaching Guide to the ANSI Y14.5M-1994 Standards, McGraw-Hill Professional, (2006), pp. 78.
65. S.Y. Chou and C.W. Sun, Assessing Cylindricity for Oblique Cylindrical Features, International Journal of Machine Tools and Manufacture, Vol. 40, No. 3 (2000), pp. 327-341.
66. N. Ohwada, T. Sampei, and K. Tezuka, Distortion in Heat-Treatment by Using the Navy C Type Test Piece, Transactions of Iron and Steel Institute, Japan, Vol. 24, No. 9 (1984), pp. B312.
67. D.D. Wackerly, W. Mendenhall III, and R.L. Scheaffer, Mathematical Statistics with Applications, Duxbury, Pacific Grove, CA U.S.A., 2002, pp. 793.
68. C. Gu, B. Lou, X. Jing, and F. Shen, Mechanical Properties of Carburized Cr-Ni-Mo Steels with Added Case Nitrogen, Journal of Heat Treating, Vol. 7, No. 2 (1989), pp. 87-94.
69. E. Boyle, R. Bowers, D.O. Northwood, X. Sun, and P. Bauerle, Microstructural Effects on Residual Stress, Retained Austenite, and Case Depth of Carburized Automotive Steels, SP-2192: Experiments in Automotive Engineering, Paper No. 2008-01-1422, SAE International, Warrendale, PA U.S.A., 2008, pp. 77-88.
70. M.J. Korwin, M.J., Morawski, C.D., Tymowski, G.J., and Liliental, W.K., "Design of Nitrided and Nitrocarburized Materials," Handbook of Metallurgical Process Design, G.E. Totten, K. Funatani, and L. Xie, Eds., Marcel Dekker, Inc., New York, NY U.S.A., 2004, pp. 555.

71. N. Krishnaraj, K.J.L. Iyer, and S. Sundaresan, Scuffing Resistance of Salt Bath Nitrocarburized Medium Carbon Steel, *Wear*, Vol. 210, No. 1-2 (1997), pp. 237-244.
72. T.R. Watkins, R.D. England, C. Klepser, and N. Jayaraman, Measurement and Analysis of Residual Stress in ϵ -Phase Iron Nitride Layers as a Function of Depth, *Advances in X-ray Analysis*, Vol. 43 CD ROM, T.C. Huang *et al.* (Editors), ICDD, Newtown Square, PA U.S.A., 2000, pp. 31-38.
73. V. Leskovšek, B. Podgornik, and D. Nolan, Modelling of Residual Stress Profiles in Plasma Nitrided Tool Steel, *Materials Characterization*, Vol. 5, No. 4 (2008), pp. 454-461.
74. A. Wells, Metallographic Analysis of Compound Layers on Ferritic Nitrocarburized Plain Low Carbon Steel, *Journal of Materials Science*, Vol. 20, No. 7 (1985), PP. 2439-2445.

PUBLICATIONS AND PRESENTATIONS

Publications

1. V. Campagna, R. Bowers, D.O. Northwood, X. Sun, and P. Bauerle, The Nitrocarburizing of Plain Carbon Steel Automotive Components, Proceedings of the 24th ASM Heat Treating Society Conference, 17-19 September 2007, COBO Center, Detroit , MI, U.S.A., ASM International, Materials Park, Ohio U.S.A., 2007, pp. 239-244.
2. V. Campagna, R. Bowers, D.O. Northwood, X. Sun, and P. Bauerle, Distortion and Residual Stresses in Nitrocarburized and Carbonitrided SAE 1010 Plain Carbon Steel, SP 2192: Experiments in Automotive Engineering, Paper No. 2008-01-1421, SAE International, Warrendale, Pennsylvania U.S.A., 2008, pp. 69-75.
3. V. Campagna, R. Bowers, D.O. Northwood, X. Sun, and P. Bauerle, A Comparison of Carbonitriding and Nitrocarburising on the Size and Shape Distortion of Plain Carbon SAE 1010 Steel. Submitted on 31 October 2007 for publication in Materials Forum.
4. V. Campagna, D.O. Northwood, R. Bowers, X. Sun, and P. Bauerle, The Analysis and Control of Distortion in Carbonitrided and Nitrocarburized Thin-Shelled Plain Carbon Steel Automotive Powertrain Components. Submitted on 24 April 2008 for publication in the Journal of ASTM International.

Presentations

1. V. Campagna, R. Bowers, D.O. Northwood, X. Sun, and P. Bauerle, The Nitrocarburizing of Plain Carbon Steel Automotive Components, ASM Heat Treating Society Conference, COBO Center, Detroit, Michigan U.S.A., 17-19 September 2007.
2. V. Campagna, D.O. Northwood, X. Sun, A Comparison of Carbonitriding and Nitrocarburizing on the Size and Shape Distortion of Plain Carbon Steel Automotive Components, 2007 National Manufacturing Week, Assembly Technology, and Quality Expo Conference, Rosemont, Illinois U.S.A., 24-27 September 2007.
3. V. Campagna, R. Bowers, D.O. Northwood, X. Sun, and P. Bauerle, The Nitrocarburizing of Plain Carbon Steel Automotive Components, 16th International Federation for Heat Treatment and Surface Engineering Congress, Brisbane, Queensland Australia, 30 October – 1 November 2007.

4. V. Campagna, R. Bowers, D.O. Northwood, X. Sun, and P. Bauerle, Distortion and Residual Stresses in Nitrocarburized and Carbonitrided SAE 1010 Plain Carbon Steel, SAE 2008 World Congress, Detroit, Michigan U.S.A., 14-17 April 2008.

VITA AUCTORIS

NAME: Victoria Nerina Campagna

PLACE OF BIRTH: Windsor, Ontario

DATE OF BIRTH: April 7, 1983

EDUCATION: Ontario Secondary School Diploma
St. Thomas of Villanova Catholic Secondary School
LaSalle, ON
1997 – 2002

Bachelor of Applied Science
Honours Mechanical Engineering – Materials Option, with Co-op
University of Windsor
Windsor, ON
2002 – 2006

Master of Applied Science
Engineering Materials
University of Windsor
Windsor, ON
2006 – 2008